INCREASING SUSTAINABILITY OF THE PAPERMAKING PROCESS VIA FORMULATION OF CELLULOSE NANOFIBERS AND POLYELECTROLYTE COMPLEXES

A Dissertation
Presented to
The Academic Faculty

by

Nasreen Khan

In Partial Fulfillment
of the Requirements for the Degree
Doctor of Philosophy in the
School of Materials Science and Engineering

Georgia Institute of Technology
August 2022

INCREASING SUSTAINABILITY OF THE PAPERMAKING PROCESS VIA FORMULATION OF CELLULOSE NANOFIBERS AND POLYELECTROLYTE COMPLEXES

Approved by:

Dr. Blair Brettmann, Advisor
School of Chemical and Biological Engineering and School of Materials Science and Engineering
Georgia Institute of Technology

Dr. Paul Russo
School of Chemistry and School of Materials Science and Engineering
Georgia Institute of Technology

Dr. Christopher Luettgen
School of Chemical and Biological Engineering
Georgia Institute of Technology

Dr. Meisha Shofner
School of Materials Science and Engineering
Georgia Institute of Technology

Dr. Carson Meredith
School of Chemical and Biological Engineering
Georgia Institute of Technology

Dr. David Cale Reeves
School of Public Policy
Georgia Institute of Technology and
LBJ School of Public Affairs, University of Texas, Austin

Date Approved: July 8, 2022

This thesis is dedicated to my grandmother: Naseem Firdos.

ACKNOWLEDGEMENTS

I would first like to thank my advisor, Dr. Blair Brettmann for her guidance, encouragement, and the opportunity to have a very enriching experience during these past 5 years both in and outside the lab. I am truly grateful to have been given the time to try many different things and become a better researcher.

I would like to express my gratitude to all my committee members: Dr. Meisha Shofner, Dr. Carson Meredith, Dr. Chris Luettgen, Dr. Paul Russo, and Dr. Cale Reeves. I had the unique and privileged opportunity to spend a lot of time learning from so many of them. An extra big thank you goes to Dr. Chris Luettgen for all of his encouragement and support for the many endeavors that I attempted related to paper and sustainability, both in and outside that lab during the past 5 years. Thank you for being the biggest *Talk Green to Me* podcast fan and our first and favorite interviewee. Thank you to Dr. Paul Russo for the support with OPALL and your time showing me different techniques in your lab. I would also like to thank Dr. Cale Reeves for taking the unexpected chance to both mentor and learn with me on how to think outside the box.

I would like to thank and acknowledge the financial support from the Renewable Bioproducts Institute and the Center for the Study of Women, Science, and Technology at Georgia Tech. I would additionally like to thank Dr. Mary Lynn Realff for giving me the opportunity to run the GEMS club. It was an extremely rewarding experience.

It is important that I thank my labmates, Manali, Elena, and Hannah. We have had some truly interesting times together and I am grateful to have spent them with you all.

Thanks goes to Alex, Jon, Mona, Jaehyun, Alexa, and Haley as well. An extra special thanks goes to Manali for all the fun podcast, sustainability, and recycling adventures we have had together. I am glad that we all made our lab and space into such an enjoyable environment.

I must acknowledge and give a huge thank you to all my talented, dedicated, and hardworking undergraduate students: Carly, Nadia, Anna, Heather, Petra, and Lexi. Thank you for your contributions to my research, this thesis, and your time. It was my privilege to get to work with you. Thanks to all the many other graduate students in MSE, Chemistry, ChBE and RBI that were willing to lend a hand and give insight.

Finally, thank you to my family and friends. Thank you to my parents. I would especially like to express my gratitude to my sister and brother-in-law for always believing in and being there for me. Thanks to all my many wonderful friends in GA and elsewhere who have kept me sane and provided encouragement and emotional support throughout the years. Thank you also goes to my MSE friends and study buddies, specifically, Sarah, Nithin, and Mike. I could not have gotten this far without you. You all are inspirations to me.

TABLE OF CONTENTS

LIST OF TABLES

LIST OF FIGURES

LIST OF SYMBOLS AND ABBREVIATIONS

CNC	Cellulose nanocrystals
CNF/CNFs	Cellulose nanofibrils
CNMs	Cellulose nanomaterials
DI	Deionized
DIC	Differential interference contrast
DIP	Deinked pulp
EPA	Environmental Protection Agency
f	Molar fraction of polycation
F_P	Post-consumer cellulose fibers
FENE	Finite Extensible Nonlinear Elastic
FITC	Fluorescein isothiocyanate isomer
HCl	Hydrochloric acid
LAMPS	Large-scale Atomic/Molecular Massively Parallel Simulator.
LBL	Layer by layer
LCA	Life cycle assessment
LJ	Lennard-Jones
MC_{PC}	Marginal cost of post-consumer fibers
MC_V	Marginal cost of virgin fibers
MD	Molecular Dynamics
MSD	Mean square displacement
MW	Molecular weight
NaCl	Sodium chloride

NaOH	Sodium hydroxide
OCC	Old-corrugated cardboard
O_P	Other non-cellulosic material
PAA	Polyacrylic acid salt
PAH	Polyallylamine hydrochloride
PC	Post-consumer
PCF	Post-consumer fiber
PDADMAC	Polydiallyldimethylammonium chloride
PDMAEMA	Poly[2-(dimethylamino)ethyl methacrylate
PEC	Polyelectrolyte complex
PEI	Polyethyleimine
PEM	Polyelectrolyte multilayers
PVAm	Polyvinyl amine hydrochloride
RDF	Radial distribution function
R_P	Recycling rate
SBSK	Southern bleached softwood kraft
TM_P	Total manufactured product
USD	United States Dollar
VF	Virgin fiber
VP	Virgin product
WRV	Water retention value
WVT	Water vapor transmission (WVT)
α	Virgin fiber content
β	Recycled fiber content
δ_{PC}	Recycling disposition rate

ε	Permittivity
η	Fiber recovery efficiency
σ	Monomer bead diameter
$\$_P$	Minimum per-unit cost to produce product

SUMMARY

Sustainability is multifaceted. The paper industry is centered around the use of a renewable and biodegradable material: cellulose. However, the sustainability of paper is not only reliant on the material itself, but on the process used to produce paper. A trade-off when processing cellulose into paper, compared to production of materials from fossil fuel-based polymers, is the inherent hydrophilicity of cellulose and consequently the requirement of large amounts of energy to dry the water during production. More recent advancements introduce cellulose nanofibrils (CNFs) as additives in papermaking to improve properties and potentially replace plastics for multi-layer packaging applications. The trade-off is that their micron and nanosized features require even greater amounts of energy to produce and to dry compared to typical cellulose fiber pulps. To achieve greater sustainability of CNFs and products made from them, methods to reduce the energy needed to dry are necessary and one strategy is to design the chemicals in the cellulose slurry to improve drainage prior to evaporative drying.

This thesis explores formulation decisions to make paper manufacturing more sustainable through increasing percent solids with the use of CNFs and polyelectrolyte complexes (PECs). By increasing the percent solids of the wet paper web that enters the evaporative dryer, the sustainability and energy efficiency of the paper-making process can be improved. Going through the thesis formulation decisions were explored from small to larger scales, starting from studying molecular interactions between cellulose and polyelectrolytes and ending with consumer decisions and policy implications.

At the molecular scale, this thesis aims to determine how electrostatic interactions and the selection of solid-like precipitate or liquid-like coacervate forming PECs enhances the interactions of the PECs to cellulose fibers and how this improves water retention and increases percent solids. This work specifically studies the effects of mixing order and the selection of polyamine polycations of differing hydrophobicity on the rate of assembly, flocculation and morphology in suspension, and phase-dependent interactions of PEC and CNFs and how these affect the water retention values when they are added to CNF slurries. The findings are then applied to the formation of handsheets at a larger bench scale and realistic CNF and PEC loadings that are typically used in paper formulation with the overall aim to improve standard pulp and paper properties including: percent solids, tensile strength and opacity.

Finally, the role of manufacturing decisions and consumer behavior on increasing sustainability through increasing the flow of CNF and polyelectrolyte packaging is explored. Because sustainability is becoming an increasingly important issue to consumers, they want to know that their actions, particularly through their purchasing decisions and disposition behaviors, are not negatively affecting the environment. Increasing solids in this case means achieving the highest useable post-consumer material through a circular economy with manufacturing and consumer behavior.

The results of this thesis show how appropriate polyelectrolyte selection and experimental parameters give insights into molecular interactions and can be scaled up to useful properties and outcomes to improve the sustainability of papermaking.

CHAPTER 1. BACKGROUND

Parts of this chapter were adapted from publications in Polymers and ACS Omega.

Khan, N. Zaragoza, N. Travis, C. Goswami, M., Brettmann, B.K., Polyelectrolyte complex coacervate assembly with cellulose nanofibers. ACS Omega 2020, 5, 28, 17129-17140. https://doi.org/10.1021/acsomega.0c00977

Khan, N., Brettmann, B. Intermolecular interactions in polyelectrolyte and surfactant complexes in solution. MDPI Polymers, 2019,11(51). https://doi.org/10.3390/polym11010051

The information in this chapter is the background related to the sustainability of paper manufacturing. Specifically, this chapter focuses on the current state of research related to papermaking formulations with cellulose nanofibers and polyelectrolyte complexes (PECs) and the interactions of the materials with each other and with water.

1.1 Papermaking

The pulp and paper industry is one of the largest in the world. The United States produces more than 70 million tons of paper and paperboard in a year and is the second largest producer in the world [1]. The market value of the paper mills in 2021 amounts to 34.6 million dollars [1]. Consequently, paper is a technology that is both personally and societally important. In 2019 Americans consumed 73 million tons of paper and board in the United States[2].

The pulp and paper industry aims to improve its sustainability particularly with respect to its energy usage [3,4]. In the US, it is one of the largest manufacturing users of

energy, using 400 trillion Btu of energy for paper drying in 2010 to produce 83 million tons of paper and paperboard [3]. Consequently, the Alliance for Pulp & Paper Technology Innovation (APPTI) has a goal of reducing purchased energy in the paper-making process [3].

Because the dryer section uses about 20% of the total energy for the papermaking process, among many approaches to decreasing energy usage is to increase the percent solids in the paper web going into the dryer section [3,5]. The industry has specifically set a goal to increase solids from 45-55% to 65% by 2030 to improve the energy efficiency of the process [3].

Figure 1-1 depicts a typical paper-making machine setup. Starting from the wet end, first a pulp slurry or suspension is dispensed from the headbox onto a wire mesh in the forming section. Here water is drained out by gravity or vacuum. The resulting wet fiber web moves to the press section, where additional water is pressed out from the fibers and into an absorbent felt, resulting in a percent solids of approximately 45-55% of the paper web [3,4]. After this, the web goes through a dryer section where steam-heated rollers dry the web and increase solids to around 90- 95% [3,4]. Additional sizing or coating steps can be applied before calendaring and rolling up of the dry paper web [6,7]. There are many areas for improvement in this process but the largest energy demand in the paper-making process is at the dryer section [3,4].

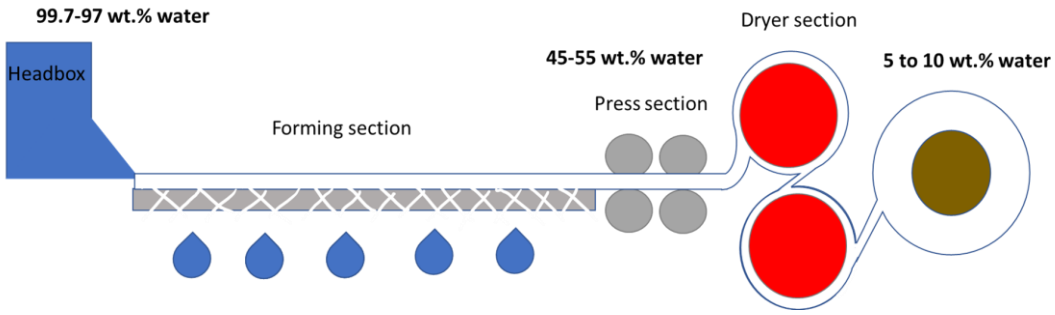

Figure 1-1 Simplified papermaking setup showing typical percent water through the sections in the papermaking process.

One approach to increase percent solids before the dryer section is to better formulate the paper furnish in the wet end of the process. A formulation can be defined as the components of a mixture that serve a specific purpose relating to processability or function of the final processed mixture. The basic components of a paper furnish include cellulose fibers and water [7]. Additionally, additives such as polyelectrolytes and fillers are often included and are responsible for imparting various properties such as strength, drainage, bulk, etc. [7–9].

1.2 Cellulose fibers in papermaking

Cellulose fibers are the major component in paper and paper-based products. Cellulose fibers come in pulp form after they are separated from biomass such as wood or crops or wastepaper by mechanical or chemical processing. Cellulose fibers from chemical and mechanical pulps have different physical features such as longer fiber lengths from chemical pulping and the processes result in different yields, non-cellulosic content, energy for consumption, and costs [7]. Additional processing to obtain fibers from recycled and post-consumer streams also lead to physical and chemical changes of the fibers including reduced fibrillation [7,10]. These physical and chemical differences can be utilized to make

paper-products of different grades and provide various functions. The different attributes of various pulp types such as surface area, porosity, and chemical functional groups on their surface also dictate their behavior during the papermaking and for the final paper properties [11]. Particularly important for sustainable water and energy consumption is how these attributes result in the retention of water and drainage during sheet formation.

The characteristic features of cellulose fibers at different length scales explains their affinity and high retention of water [12,13]. Starting from the molecular level, cellulose is composed of a repeating monosaccharide beta-d glucose unit [14,15]. The hydroxyl groups on the ring structure make it highly hydrophilic, as it can easily hydrogen bond with water [15,16]. Next, the cellulose chains form microfibrils and then several microfibrils together form microfibril bundles [13,15,17]. Amphiphilicity of the cellulose molecule leads to structured crystalline and disordered amorphous areas that form twists in the microfibrils. These then dictate the distribution of water molecules near the surface of and inside accessible hydrophilic portions of the microfibril bundles [17]. Finally, microfibril bundles make up the bundle networks that then form the lamellae of the layered cell wall [17]. The cell wall also accounts for pores that retain water and allow for swelling of the fibers.[15,18]

Besides structure, other factors also contribute to the adsorption of water in cellulose fibers, including the presence of chemical components left from residual wood and biomass, such as water-soluble hemicelluloses and ligno-cellulosics [16,19,20]. These can contribute negatively charged species such as xylan and gluconic acid which are solvated by water [21]. Additional processing, chemical refining with Kraft or sulfite extraction and bleaching can contribute charged species like carboxylic acid and sulfonic groups, which also contribute to the attraction of water [16,20]. Mechanical pulping and increased refining,

including homogenization, create highly fibrillated fibers with a large surface area, which then swell and retain more water [22–24].

During the formation of a paper web, components of the paper formulations and pulps affect dewatering and the retention of water. The presence of high surface area and small fibers called fines in the slurry or present on the surface of larger fibers adds significant processing challenges in terms of retaining water, drainage during web formation, and drying of the sheet. Fines are defined as the fraction of pulp able to pass through a mesh screen having a hole diameter of less than 76 μm [25,26] . These can be fibers, particles, or fillers that are added to pulp slurry [26]. Fines have their own morphology, surface area, and consequently their own intrinsic water retention capacity [22,23,27]. Figure 1-2 depicts how compared to fibers, fines alone or with fibers decrease dewatering and can densify fiber pads, while some fillers can allow for open structure and less dense fiber mats that allow water to drain [28,29].

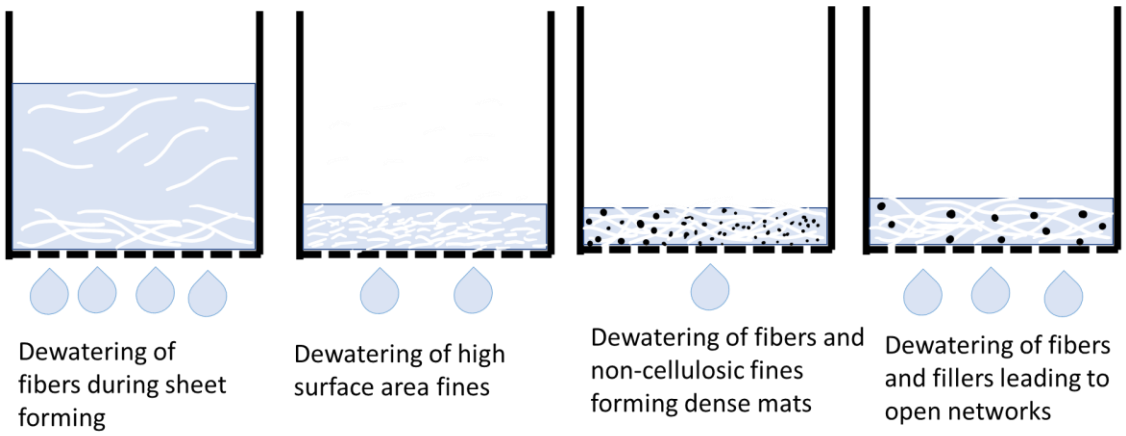

Figure 1-2. Features of cellulose fibers, fines and additives that reduce water expelled during the formation of a paper web in the forming section. The number of droplets in the image represent volume drained during formation.

Several mechanisms have been proposed to explain how fines block drainage during fiber mat formation. These include the Kozeny-Carman model, the Choke-point model, or fiber mat densification. The Kozeny-Carman model describes the resistance to flow of a liquid through a packed-bed [28,30]. For paper web formation, it highlights that the resistance of water through the forming web is influenced by the void fraction and size and shape of the bed material. Specifically, it indicates that fibers with the highest specific surface area will dewater the least [30–32]. In the Choke-Point model, initially fines are free from the fiber surface and can move or have mobility but become stuck at points during the formation of a mat and then block or slow down water moving through the voids in the overall fiber network [30,33]. Finally, the fiber mat densification model expands on the ideas of the Choke-point model by considering how the location of fines in a mat of paper can affect its overall structure [30,34]. Here fines can act as spacers or fillers that either "bridge" or "fill" spaces between fibers respectively [30].

1.3 Cellulose nanomaterials in papermaking and properties

Cellulose fibers used for paper-making depend on the fiber source, but are generally in the millimeter (100s of microns) scale for length and micron for width (10s of microns) [7,35]. These can be further broken down and processed to create cellulose nanomaterials (CNMs) [12,14,36]. CNMs have sizes on the submicron scale (1 to 100 nanometer width and 100 to 1000 nm length) and high aspect ratios (>1000 for CNFs [36,37]). Their small size gives them advantageous properties not realized by other cellulosic additives previously [12,38], but they are also energetically expensive to manufacture and convert into marketable products [36,39–41].

CNMs can be made from chemical, mechanical, or recycled pulps, and are subjected to additional significant mechanical or chemical processing beyond typical paper pulps as depicted in Figure 1-3 [36,42]. CNFs and cellulose microfibrils (CMFs) are formed from strong mechanical shearing that breaks down pulp fibers until they are in the micron and nanoscale [12,43,44]. They can also be referred to by their percent fines content or amount of energy imparted on the fibers in kWh/T into producing fines [36]. Refining up to 90 to 95% fines is typical to achieve micron and nanoscale fibrils [45]and requires large amounts of gross energy with each pass in a homogenizer [36,45]. It has been found that energy costs increase with increasing fines content and are in the thousands of kWh/MT [36,45]. However, the amount of homogenization and percent fines needed can be optimized for the desired final paper properties and 90 to 95% fines is not always necessary [45]. Still, the appropriate minimum content of CNF to achieve desired properties will also have implications on the amount of energy needed to dry CNF-containing paper.

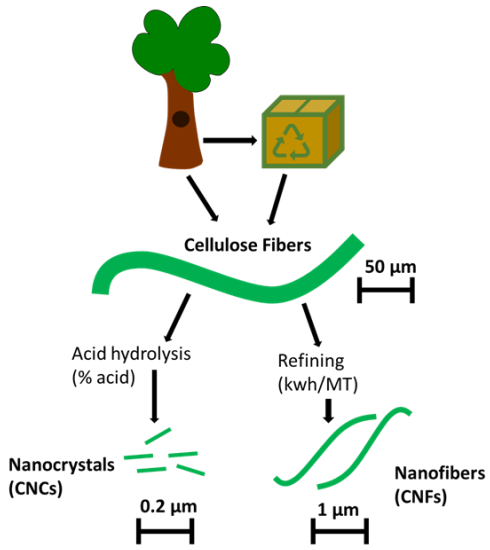

Figure 1-3. Cellulose nanocrystals and cellulose nanofibers from virgin or recycled cellulose sources can be made from acid hydrolysis or refining, respectively.

CNFs can be further modified and subjected to pretreatments including enzymatic [12,46,47], sulfonation [48], and TEMPO oxidization [49,50]. The addition of carboxyl [38,51] or charged groups to the surface of CNFs can further enhance properties and functionality needed for a required product performance [38] but the incorporation of these hydrophilic and charged species means more attraction to water and therefore will make functionalized CNF more difficult to dry [5,52]. Alternatively, the incorporation of hydrophobic species or modification is possible but is primarily done to increase compatibility with hydrophobic components or for specific properties such as increasing softness, because they otherwise interfere with the bonding of hydrophilic fibers and additives [7]. Overall, the combination of physical modification to high surface area and high fines content and chemical modification both increase the processing challenges of draining and removing water.

Despite the processing challenges and costs related to making and using CNFs, their high surface area and ability to be functionalized offer many advantageous qualities

in terms of product functionality include increased strength to weight ratio and barrier properties [53]. Their high strength to weight ratio has been cited to be above that of metals such as titanium or aluminum alloys [41,54]. Decreasing the weight of composites compared to other inorganic fillers to get the same properties is advantageous because lighter composites can reduce cost of transportation and decrease fuel consumption [41], which can lower the costs passed on to the consumer. The strength also implies stronger more durable products, which consumers can keep for longer before needing to waste.

Consequently, CNFs are already used in several products including non-durable paper items such as bath tissue, diapers, and durable such as sports equipment, electronics, tires, and cement. Furthermore, their use in new value-added consumer products beyond current forest products is expected to grow by 3% in GDP of Finland by 2030 [41]. This coupled with the continuous increase in US personal consumption expenditure of all goods from 3.6 trillion USD in 2012 to 4.5 trillion USD in 2019 [55] implies that the value CNFs will provide in terms of enhancing product performance and their impact on the economy will be large.

CNFs and CNCs also offer advantages for improving sustainability despite the initial energetic costs. CNFs, like most paper and paper-based products, are largely obtained from forest products i.e., trees and other lignocellulosic biomass, making them bioderived [12,43]. Given that CNFs and cellulose are made of beta-d-glucose, they are also biodegradable [56]. This is advantageous as an alternative to fossil-based plastics, particularly in single use items such as plastic packaging [43]. For multi-layer packaging, CNF and CNCs can be an alternative to plastic when used as a coating or a layer that has the ability to improve both water vapor transmission (WVT) and oxygen transmission properties [43,57,58]

. Low oxygen and moisture barriers are key barrier property parameters to ensure the products within the packaging stay intact and shelf-life is maximized [43,58].

Their potential to be an alternative to plastic to achieve barrier properties in multi-layer and container packaging is particularly promising for waste management and the circular economy [59]. With the smaller size of CNMs comes significant processing challenges that that require high energy inputs and are costly. Also, with size comes the potential to use and extract CNMs from various and new waste streams, while obtaining the same properties as those extracted from virgin materials [41].

While CNMs can be made from a variety of virgin and recycled sources, particularly for CNFs, fibers that can achieve higher fibrillations through mechanical refining are needed obtain the required morphology and size for improved properties. Fibers from recycled sources can have collapsed fibers and reduced swelling capacity that can make high fibrillation through mechanical refining more difficult to achieve [60]. Consequently, virgin bleached kraft softwoods or bleached chemical softwoods, are often preferred because they give higher yields or better-quality CNFs [61]. CNMs from waste and agricultural residues such as old corrugated boxes, empty fruit bunch, tobacco, and cane straw can also obtain similar final properties such as strength compared to virgin sources [45,60,62]. Therefore, the potential to make CNMs from alternative pulp sources exists and may be a more sustainable option.

CNFs are incorporated into or with paper of typical virgin or recycled pulp fibers in at least three ways, all of which require formulation from a wet slurry [63]. CNFs can be formed into free-standing nanopaper [45,50,64], forming a barrier coating on another substrate

with a method like a slot-die coating [38], or being mixed with pulp fibers in a slurry [65]. CNFs are typically added to pulps concentrations of 1 to 10 wt.% [23,37,53,65,66], although less than 5 wt.% is more common. The use of higher concentrations is limited because CNFs become more viscous and gel-like with increasing concentrations [38,67], making them difficult to flow and consequently process.

Increasing the loading of CNF in paper has been shown to enhance properties, in particular tensile strength [53,65,66] but the processing trade-off is that it also increases water retention [23,65,66] and drainage times [27,38,66]. To improve drainage and water retention, polyelectrolytes and PECs are commonly used in papermaking and can be used with CNFs [68] as well.

1.4 Polyelectrolytes and their molecular interactions

Polyelectrolytes are polymers with charged or ionizable monomeric units [69]. Polycations are positively charged and can act as bases, while negatively charged polyanions can act as acids [69,70]. These charged polymers have several different features that can affect their behavior in solution and how they interact with other species [69,7069,70]. Figure 1-4 illustrates the key polyelectrolyte properties including charge density, structure, specific functional groups, hydrophobicity of the backbone and pendants, and weak and strong behavior of the polyelectrolytes, which all play a role in the structures formed when mixing oppositely charged polyelectrolytes together. Weak polyelectrolytes are those that are charged at certain pH values, while strong ones are charged independently of the pH of the solution [69–71].

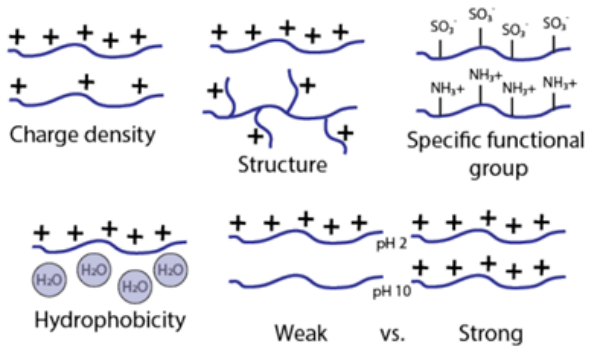

Figure 1-4. Schematic of different polyelectrolyte characteristics.

The performance and behavior of polyelectrolyte-containing formulations and products start from their underlying intermolecular interactions. Manipulating these through formulation leads to property changes at larger macroscopic scales. The primary governing molecular interaction of polyelectrolytes are electrostatic [70,72], where the two components attract (opposite charge) or repel (like charge) due to the presence of charges on the chain. Hydrophobic interactions can also contribute [73,74], where molecules attract due to low compatibility with water [75].

1.4.1 Electrostatic interactions

Electrostatic interactions are described by Coulomb's law, Equation 1, which gives the magnitude of the force (F) created by the repulsion or attraction of two charged points (q_1 and q_2) over the squared distance (r) between them. Coulomb's constant (K_e) accounts for the dielectric permittivity of the medium (Dill & Bromberg, 2011)

$$F = \frac{K_e q_1 q_2}{r^2}. \quad (1)$$

The local charge density and the local counterion concentration can be taken into account by the Debye-Hückel model to calculate the Debye length ($\boldsymbol{\kappa}^{-1}$) as described in Equation (2).

$$\kappa^{-1} = \sqrt{\frac{\varepsilon_r \varepsilon_0 k_B T}{2 N_A e^2 I}}. \quad (2)$$

where ε_r is the dielectric constant, ε_0 is the permittivity of free space, k_B is the Boltzmann constant, T is the temperature, N_A is Avogadro's number, e is the elementary charge, and I is the ionic strength of the electrolyte solution. The Debye length is the distance from a charge surrounded by other point charges that the interaction potential is screened. This is accepted for simple salts, but the model is limited for polyelectrolytes because it treats the ions as a point charge. For polyelectrolytes the charges are on functional groups that are periodic on the backbone or pendant off of the main chain [69,76]. Despite the simplicity of the model, the Debye length is often used in theoretical treatments to model the interaction between charged chain segments [69,77].

The Bjerrum length (λ_B) is also used to describe electrostatic interactions and is defined as the distance between two charges at which the interaction strength is comparable in magnitude to the thermal energy, k_BT. This is commonly used to describe the strength of the electrostatic interaction [69,78,79]. Other theoretical treatments extended from the Debye-Huckel approximation, such as the Manning parameter and counter-ion

condensation theory, can be used to further describe the behavior of charges and counter-ions on a polymer chain.

The most important factors that affect electrostatic behavior are ionic strength [69,80], pH [81–83], and counterion valency [69,80,84,85]. Because polyelectrolytes have charges along the length of the polymer chain, the electrostatic interaction is significant, especially when they are fully charged. [70,86–88].

In terms of solution ionic strength, increasing the concentration of salt weakens the coulombic potential energy between charges [78]. At low-salt concentrations, the electrostatic interactions are reduced. At high-salt concentrations they can be significantly reduced such that polyelectrolytes behave more like neutral polymers in solution [80,89–91].

Electrostatic interactions of polyelectrolytes can be manipulated by the pH. If the pH is not sufficiently acidic or basic, which depends on the functional group, the dissociation of the charge may be reduced or eliminated, resulting in a polymer that is essentially neutral and eliminating electrostatic interactions. This has been seen for weak polyelectrolytes including poly(methacrylic acid) (PMA) [74,92,93] and polyacrylic acid (PAA) [74,92,94]. If ionization is significantly reduced with a change in pH, then the chain can phase-separate out of solution due to low solubility in water [95–97].

Increasing the charge density by increasing the number of charged monomer units on a polyelectrolyte chain can increase electrostatic interactions given that distance between charges decreases. [87,95,96,98].

1.4.2 Hydrophobic interactions

Hydrophobic interactions are driven by the repulsion between a non-polar solute, such as hydrocarbons, and the surrounding polar solvent, usually water. Water molecules are thought to behave as a network of polar molecules in which the hydrogen bonding between molecules excludes other solutes [99–101]. Consequently, hydrocarbons in particular have low solubility and prefer to aggregate with non-polar molecules. These interactions are understood from the solubility of a non-polar species in water or a water mixture [102–104].

Charged polyelectrolytes are water soluble and stay in an extended chain conformation (rigid rod) in an aqueous or polar solvent due to the favorable interactions between the charged monomers and water and repulsion between neighboring charged monomers [103]. In an uncharged state, the polyelectrolytes can collapse depending on the hydrophobicity of the uncharged polymer backbone. In a good or theta solvent, the polyelectrolyte will be in a less extended random coil conformation. In a poor solvent, such as with a hydrophobic backbone in water, it will be in a collapsed conformation (Figure 1-5). The thermodynamic change from extended to coil state is driven significantly by hydrophobic interactions [102–104].

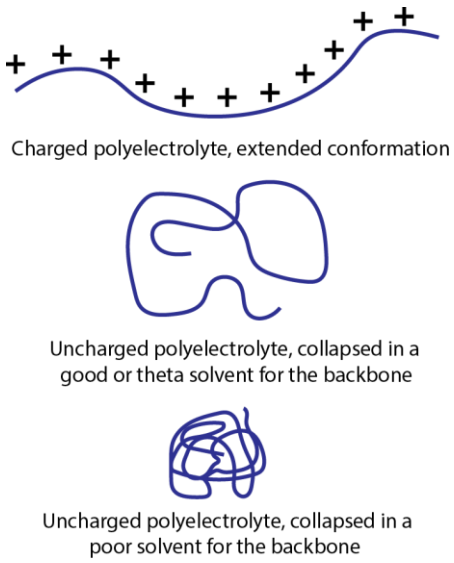

Figure 1-5. Schematic of charged polyelectrolyte conformation in good, theta, or poor solvents.

The strengths of the hydrophobic interactions are sensitive to many material and solution properties, and these can be used to tune parameters in many systems. Briefly, some factors that affect hydrophobic interaction strength include temperature [105], co-solvents/co-solutes [106,107] and alkane chain length [108].

Some of these parameters, such as temperature, influence both electrostatic and hydrophobic interactions. Additionally, electrostatic interactions can compete with the hydrophobic effects. These drive morphology and phase behavior [109–111] when polyelectrolytes are complexed with surfaces [71], surfactants [72], or with each other [73,112].

1.5 Polyelectrolyte complexes

When oppositely charged polyelectrolytes are combined, they spontaneously form PECs driven by the release of their counter-ions [113,114]. These are thought to have various configurations including a ladder or scrambled-egg structure, depending on the

polyelectrolyte characteristics [70]. The complexes can also form different phases, solid or liquid and gel-like, depending on experimental conditions as seen in Figure 1-6. For example, when one or both oppositely charged polyelectrolytes are strong, they typically form a more solid-like and kinetically trapped precipitate phase when combined, whereas when weak polyelectrolytes are combined, they can form liquid phase complexes [115].

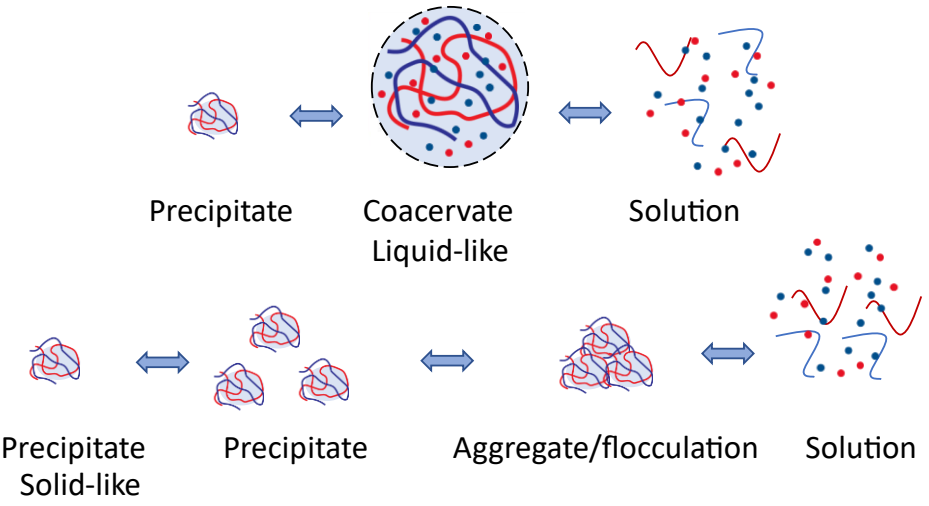

Figure 1-6. Schematic of the transition of precipitates to coacervate and solution phases (top) and precipitates to aggregates and solution phases (bottom) with decreasing electrostatic interactions. Red lines, blue lines, red dots, dark blue dots, and light blue represent polycations, polyanions, free cation, free anion, and water, respectively.

Various phases of PECs can be achieved with the selection of individual polyelectrolytes to be complexed and other experimental parameters that manipulate the electrostatic interactions. Strong polyelectrolytes are fully charged in most pH ranges and favor the precipitate phase, which favors transitions to a solution phase with weakened electrostatic interactions. Weak polyelectrolytes can form a precipitate phase when they are fully charged, whereas coacervate phase is preferred when there are fewer charged groups with lower ionization through pH [116,117]. Similarly the coacervate or solution phases

for both strong and weak polyelectrolytes can be achieved by reducing the electrostatic interactions between the oppositely charged groups by adding salt [116,118,119] and changing the molar ratio away from 1:1 charge-match of the charged groups [120,121]. Reducing concentration of the polyelectrolytes also favors a coacervate or solution phase due to reduced number of intrinsic ion pairs [117,120,122]. Finally, increasing the temperature reduces electrostatic interactions and increases hydrophobic interactions. These can have competing effects on the interactions between polyelectrolyte chains and the preference of a particular phase depends on the other experimental conditions already described [119,123–125].

Smaller coacervates coalesce into large complexes and will undergo liquid-liquid phase separation over time [126,127]. As can be expected, the coacervates have large water contents, from 50 to 80 wt.% water [127,128] which indicates a high degree of swelling. Illustrations and microscope images of solid-like and liquid-like PECs are shown in Figure 1-7, respectively.

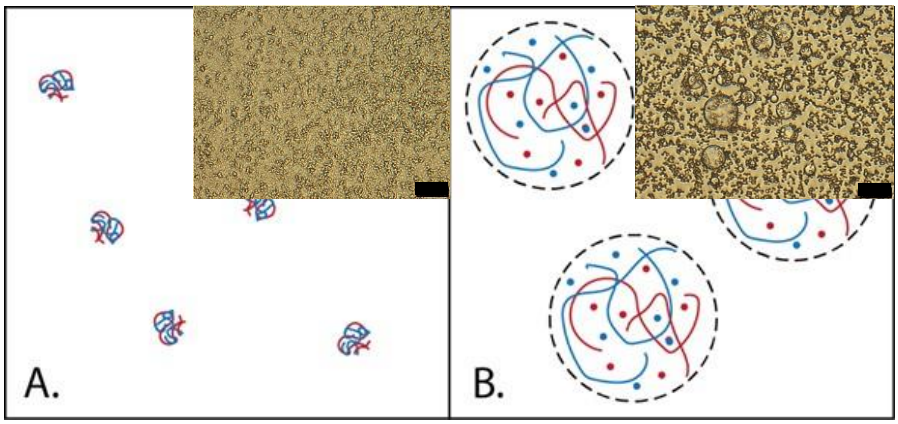

Figure 1-7. Illustration and images (inset) of (A) Solid-like precipitate phase and (B) Liquid-like viscous coacervate phase of polyelectrolyte complexes. Scale bars are 25 µm. Colored lines represent polymer chains and dots represent salt ions but do not represent actual size of the chains or salt relative to the size of the complexes.

Precipitate properties can also be manipulated using solution composition. Typically with precipitates, it is believed that a polyelectrolyte in excess forms a charged corona on the outside of complex [129]. Added salt can neutralize the charges on the surface, which then causes smaller precipitates to aggregate and flocculate together [69,80]. The salt can also allow for some rearrangement and screening of the chains, which can initially increase the size of the complexes before decreasing them to solution phase [130]. In some cases, it is possible to have both a combination of precipitate, coacervate, and polyelectrolytes free in solution [131].

Specific experimental factors can be controlled to utilize both electrostatic and hydrophobic interactions to binding, structures, and phases of PECs. As mentioned, electrostatic interactions are influenced by pH [117,132], charge density [133], and salt concentration [132,134]. Hydrophobic interactions are influenced by chain length, molecular weight or structure of the polyelectrolyte chains [74]. Other experimental parameters, such as polyelectrolyte concentration [122], stoichiometry [123,135], and mixing procedure [129,136] also

impact the formation and properties of the PECs and PEC-containing formulations. In altering these parameters, changes in the resulting measured properties of the structures and phases include surface charge [137], turbidity (from concentration of PECs) [117,138], particle size and aggregation [139].

The salt concentration in PEC complex solution is particularly useful for balancing electrostatic interactions and achieving a desired coacervate phase. By increasing the concentration of salt in a given system, the PEC can transition from a solid precipitate, to a gel or liquid-like coacervate phase, and then to a solution phase given a strong enough mono or multivalent salt [116]. This is because the added salt electrostatically screens the intrinsic ion pairs between the oppositely charged chains allowing the chains to become more mobile and the liquid-like [124].

1.6 Polyelectrolytes in papermaking

Polyelectrolytes and PECs have been used in paper-making formulation as additives to increase strength, improve drainage, act as retention aids, change flocculation, and more [7,121,140–142]. Wet chemistry approaches that lead to flocculation and aggregation or coating of the cellulose can decrease water binding and increase the percent solids in the web by improving drainage of excess allowing the drying process to be more energy efficient [140,143] . Challenges remain in designing these systems to maximize solids content while also considering manufacturability.

Figure 1-8 shows the three ways that polyelectrolytes interact with cellulose fibers during the papermaking process. These are charge neutralization, bridging and flocculation, and retention of fines during the forming process. Polycations in particular

help with charge neutralization by complexing with negatively charged groups on the fiber surface [7,144,145]. This helps dewatering by reducing the number of available charged groups that water can form around. Additionally, when the concentration of counterions increases in the nearby solution as the polyelectrolytes adsorb, an osmotic pressure difference is created between the solution and the water inside cellulose pores, driving water to leave the pores and leading to pore collapse[21]. Depending on the polyelectrolyte properties, especially the charge density and molecular weight, the flocculation and aggregation of fiber networks can be changed through bridging or charge-patch mechanisms [7,146,147]. With the charge-patch mechanism, a polycation adsorbs locally onto the surface of a negatively charged particle and can completely coat that section of the cellulose fiber. Patches such as these cover the entire surface but can attract to and bind uncovered areas on other negatively charged particle surfaces [148]. In bridging, the polyelectrolyte extends outward from one or more tethered points on the surface in the form of loops or tails and can be attracted to another surface [148]. Appropriate flocculation of fibers can allow excess free water to pass through by changing the overall open structure of the fiber bundles and can help improve other properties such as strength. Finally, polyelectrolytes can also be used as retention aids, in that they allow for small fines or negatively charged particles to attach to the fiber surface and allow bridging between fibers or fines [30,140,147,149].

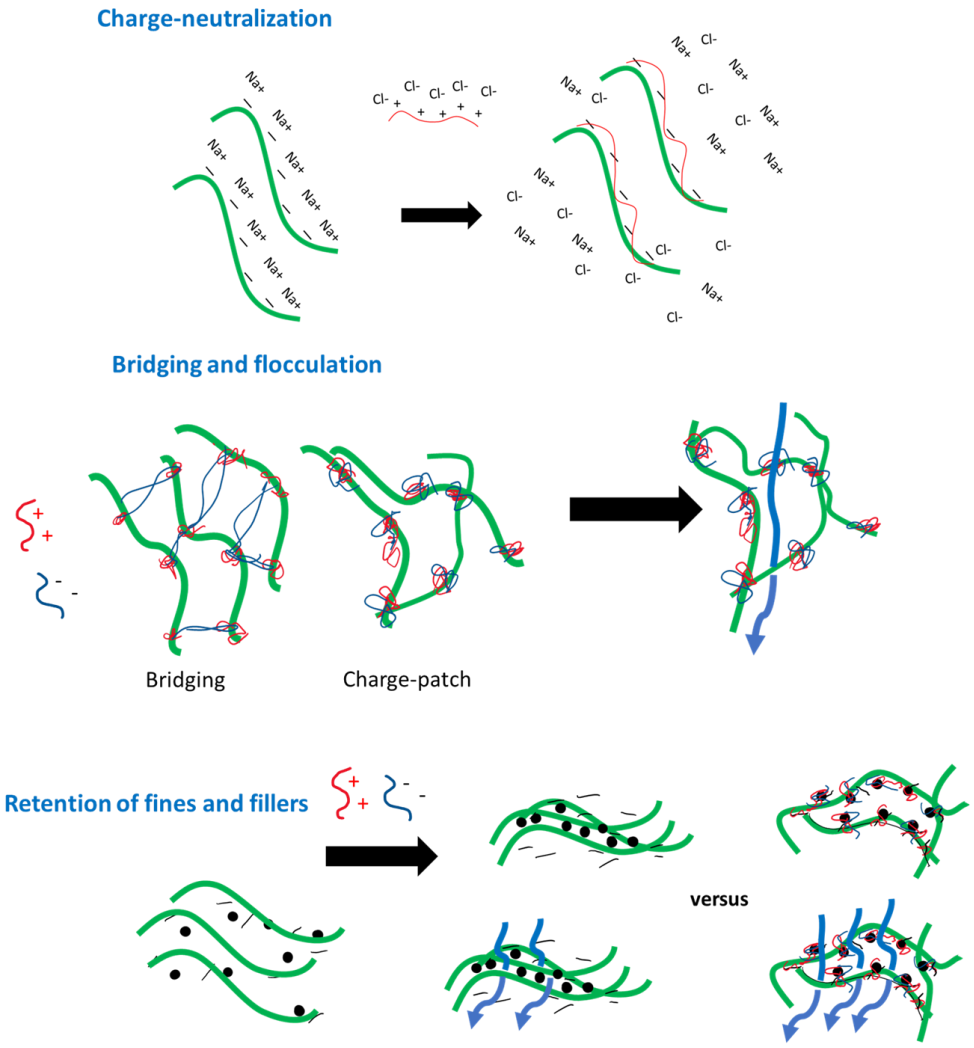

Figure 1-8. Polyelectrolytes or PECs can interact with cellulose fibers (green lines) in multiple ways leading to charge neutralization, bridging or flocculation, and retention of fines and fillers to the fiber surfaces. These improve the flow through of water (blue arrows) during fiber mat formation. The red and blue lines represent polycations and polyanions, respectively.

Typical polycations used in papermaking include cationic starches [3,143,150], polyvinyl amines [3,143,151], polyacrylamide [3,140,143,150], polyethyleneimine[7] and more. Despite negative charge repulsion, anionic polyelectrolytes have also been reported to show some

interaction with cellulosic material, particularly in the presence of salt, which screens the negative charges [143] . They also tend to create larger flocs of fibers compared to cationic ones [143,146] , which in turn change formation of the fiber mat and the time it takes for it to drain and forming lab tests [29].

CNMs can also be chemically modified to have cationic species on its surface and can be used for a number of applications. Cationic CNCs have been proposed to be used as flocculants for waste-water treatment [152] , CNFs modified to be used as strength and bulking additives in papermaking [153], and positively-charged nanopaper filters [154], and can be modified with various chemistries to have different positively charged functional groups [152,153,155].

While polycations are important in papermaking, the use of both polycations and polyanions together with cellulose has been shown to have improved properties for improving drainage and retention of water and for physical properties of paper. Much of the work done on PECs in papermaking is focused on either layer-by-layer interactions (LBL) on particle surfaces or forming pre-formed PECs, where the polyelectrolytes are mixed separately and the resulting complexes are added to the cellulose particles [121,145,151,156–160].

Pre-formed PECs have been shown to be retained at fiber interfaces [121,157,159], increase mechanical properties of bulk paper systems [121,156,161] and flocculate charged clay particles at high settling velocities [145]. Despite these improved properties, pre-formed PECs have also been shown to plug up channels in the fiber network that would allow water to pass through during drainage and wet pressing [30,162]. Additionally, more recent studies have

shown that instead of adding pre-formed complexes, forming complexes in the presence of charged particles (cellulose and others), can further increase adsorption of the polyelectrolytes and retention of the complexes on the fibers [21,121,157,159]. In both cases, distinctions of phase behavior of PECs have not been thoroughly studied.

Appropriate formulation and selection choices of polyelectrolytes and experimental parameters is critically important for every aspect of papermaking, including increasing sustainability through reducing the water retained and drained during the process. A major strategy in applying PECs to fibers is the concentration of polyelectrolytes used. This determines if the surface achieves charge neutrality and if PECs are in a layer-by-layer regime on the surface of the fibers or are in excess in solution. Formulation strategies include the addition of polyelectrolytes in excess [146,147], the application of oppositely charged polyelectrolytes with a layer-by-layer method [163,164] or use of PECs (PECs) [136,140,145].

The formulation strategy to add polyelectrolytes in excess is based on increasing the concentration of the polyelectrolyte such that the surface charge on the fiber changes from negative to neutral and then positive, depending on the desired outcome. It has been shown that the closer a fiber is to zero zeta-potential, the greater the dewatering and drainage [30,165]. Surfaces can still accommodate and adsorb on more polyelectrolyte past the charge neutral point until it takes on the same charge as the adsorbed polyelectrolyte [166]. Initially, the charge increases and eventually plateaus at a given surface charge (zeta potential), after which increased concentration of polyelectrolyte does not change the charge [166]. Here excess chains can attach and extend out into the solution in the form of loops and tails [167]. The excess chains in the charge reversal or overcharging regime can

allow for complexation with oppositely charged polyelectrolytes or creating layer-by-layer (LBL) or polyelectrolyte multilayers [137].

In LBL, layers of polyelectrolytes are formed by dosing in excess, washing off residual unattached polyelectrolyte, and then creating a new layer by soaking the existing layer in polyelectrolyte of the opposite charge in excess. The layer-by-layer (LBL) literature has shown that both weak and strong polyelectrolytes effectively adsorb onto an oppositely charged surface forming multi-layers [168–170]. Similarly, adding polyelectrolytes sequentially in the presence of charged surface or colloid leads to the formation of PECs at the surface. These are different than LBL films in that excess polyelectrolyte on the surface or in solution is not washed away in between polyelectrolyte addition steps [170,171]. Many of the same factors apply in the adsorption of polyelectrolytes to form PECs on charged surfaces as polyelectrolyte adsorption on an oppositely charged surface and colloids [170,172].

Overall, PECs can be directly added to fibers in a variety of strategies including the addition of the polyelectrolytes directly to the fibers in solution or as pre-mixed PECs [140,162,171]. The majority of these studies evaluate look at adsorption behavior of the PECs [159,173], the morphology of the pre-formed PECs [174,175] , and improvements in strength as related to adsorption behavior [159,173], for flocculants and drainage of inorganic particles such as silica [140,170].

1.7 Methods for measuring dewatering of fibers

There are several standard methods to measure dewatering of pulps and wet end formulations, many of which have standards recommended by the Technical Association

of the Pulp and Paper Industry (TAPPI). These include water retention value (WRV), drainage using a dynamic drainage (Britt) Jar, and Canadian standard freeness (CSF) tests [31,34,176]. These are interrelated but elucidate slightly different behaviors in terms of interactions with cellulose fibers and water, additives, and the formation of fiber mats [176]. Overall, they are valuable for comparative studies to understanding dewatering behavior of pulps and paper formulations.

While these methods are standardized and work well for pulp fibers of typical sizes, they do not necessarily work well for CNFs. This is primarily because many of the filters designed for use in these apparatuses have large mesh sizes. For example, the support screen of a Britt jar consists of a metal sheet with holes that are a minimum of 76 µm in diameter [29]. Consequently, fines and CNFs would largely pass through the apparatuses without other filters [25]. There are no standard testing methods for CNFs but variations of lab-scale methods for WRV and drainage of CNFs exist [22,27,177].

1.7.1 Water retention values

WRV testing physically measures how much water a fiber pad retains after excess water is centrifuged out of it. These tests capture changes to fibers and fiber pads due to the presence of water in a number of ways. Because water can exist in fibers and a fiber pad through many mechanisms, only broad correlations can be made, but as seen in (Figure 1-9), the WRVs for fibers are believed to account for free and bulk non-bound water in a fiber network [29,178], freezing bound water on the surface and in pores [178] and in the inter-fibril bundle spaces for CNFs and CMFs [22,23,178]. These have been elucidated by the response of WRVs to experimental changes such as amount of refining of fibers [22,177,179]

which indicates it responds to surface area changes and shifting pH and ionization which indicates that the fibers swell due to the presence of charged groups [24,51,52,180]. WRVs also correlate to the structural properties of the resulting fibers and fiber pad [21,23,178].

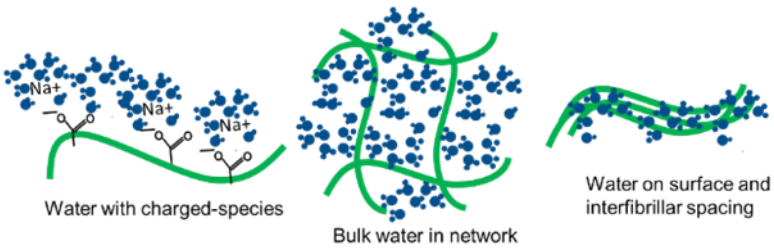

Figure 1-9. Water retention values of CNF represent water in fibril network, surface and interfibrillar spacing, and with swelling from charged species

WRVs are influenced by the behavior of the individual components in the network. A few studies have evaluated WRVs of CNFs alone or mixed in larger pulp fiber slurries and found that they greatly increase with the addition of fibrils or fines (including small particles) [22,23,27,177,179]. Consequently, strategies to reduce the WRV of CNFs or CNF containing slurries are needed to improve dewatering.

As discussed, adding polyelectrolytes to cellulose fibers is one strategy to improve dewatering and have been shown to improve WRVs of various wood pulps in some cases [34,181], but the addition of polyelectrolytes have not always shown to improve WRVs significantly when compared to a reference fiber sample [21,163,164,164,171,182,183]. Consequently, there is still no clear relationship between the addition of polyelectrolytes applied to CNFs and their resulting WRVs for these approaches previously used, this motivates further study to focus on what factors can improve these.

1.7.2 Correlation of drainage and water retention values of cellulose nanofibers

While many studies suggest that WRVs and dewatering as measured by drainage are correlated [26,29], even with the presence of CNFs [27,34,66], the tests provide different information in terms of dewatering. In general drainage methods measures the amount of water removed over time as a fiber mat is forming, whereas WRVs have primarily been used to understand the capacity of fiber network and pad to retain water at particular time and pressure [26,29].

As WRVs increase, drainage time typically also increases and it has been suggested that relationship with CNF concentration may be linear in some cases but this changes with presence of additives such as polyelectrolytes [34,66]. Relating WRV to drainage in the case of CNFs and other fine types, it has been found that the rate of water removal from CNF slurries significantly decreased with the addition of higher specific surface area particles, but that the final WRV did not change [27]. Furthermore, the use of polycations to neutralize charges on fibers and retain fines are known to improve drainage [29,184] but do not necessarily correlate to water retention values in the same way [181,184]. This suggests that a combination of factors influence and play a role in dewatering, particularly in measuring WRVs.

CHAPTER 2. ORDER-OF-ADDITION AND COACERVATE INTERACTIONS WITH CELLULOSE NANOFIBERS AS A FORMULATION STRATEGY TO REDUCE WATER RETENTION VALUES

This chapter was adapted and reprinted with permission from:

Khan, N. Zaragoza, N. Travis, C. Goswami, M., Brettmann, B.K., Polyelectrolyte complex coacervate assembly with cellulose nanofibers. ACS Omega 2020, 5, 28, 17129-17140. https://doi.org/10.1021/acsomega.0c00977.

In this chapter the interactions between CNFs and polyelectrolyte complex (PEC) coacervates of weak polyelectrolytes, polyacrylic acid salt (PAA) and polyallylamine hydrochloride (PAH) were studied. CNFs are a model system for understanding cellulose/polyelectrolyte interactions and their effect on dewatering because they retain water more than larger pulp fibers. Furthermore, the effect of the choice of mixing sequence on the rate of assembly of PECs with cellulose nanofibers (CNF) and water retention value was explored. Molecular dynamics simulations paired with experimental techniques were used understand the molecular interactions at the nanoscale and understand how they tie to observed properties for paper formulation. This study focuses on the fundamental aspects of PEC coacervate formation, assembly, and agglomeration of PEC with CNF as the sequences of mixing of PAH, PAA and PEC coacervates with negatively charged CNFs are altered.

By changing the of the polyelectrolytes to CNFs, the interactions between the materials can be tuned, which in turn changes the degree of association of the coacervates to the CNFs and the rate at which they aggregate. Importantly for the papermaking process, the lowest water retention values were found when adding the polycation to the CNFs first, compared to the other cases and significantly lower values than those of CNF by itself. Coarse-grain molecular dynamic simulations further illuminate the fundamental mechanism of aggregation by taking into consideration the interaction between cellulose and the complexes at the molecular level. The simulations corroborate the experimental observations by showing the importance of strong electrostatic interactions in aggregate formation.

2.1 Materials and Methods

To represent a paper, furnish system while allowing for fundamental experimentation and approximately representative simulations, a model system containing CNFs was selected. CNFs are extensively mechanically refined fibers with nano to micron scale dimensions (lengths of 130-225,000 nm and widths of 5-200 nm [185]) and therefore large aspect ratios [3,38,186,187]. The surface charge and chemistry of cellulosic materials are determined by their processing, including pre-treatment and mechanical shearing [16]. Residual lignin, hemicellulose, and extractive components from the cellulose source and chemical modification such as from bleaching can also have an influence on the surface charge and properties of the material, so there is not one consistent model system [16,188]. Additionally, while the fiber charge depends partly on the amount of acid functional groups, it is affected by the pH, ionic strength, and swelling of the fibers [16,157,189].

The high aspect ratio and surface area of CNFs lead to greater water retention than other pulps, making them among the highest users of energy for drying and providing a good basis for evaluation of the water retention and phase behavior with PECs [14,37,190]. CNFs have also been previously studied using molecular simulations [191–194], though their interactions with polyelectrolytes and complexation behavior have not been examined, so there is a need to understand the full system, which includes CNF and polyelectrolytes, for further improving the materials design principles.

The polyelectrolyte complex coacervate system was designed using weak polyacrylic acid salt (PAA-, MW 15,000 g/mol, degree of polymerization in number of repeat units N= 160, PDI not available or measured) and polyallylamine hydrochloride (PAH+, MW 17,500 g/mol, N=186, PDI=1.28). Polyelectrolyte solutions were prepared at pH 6.5 and were mixed in a 1:1 molar ratio. At this pH, they are both highly charged and at this molar ratio have the highest formation of complexes (S. Perry et al., 2014; Spruijt et al., 2010). These parameters have been shown to form the coacervate phase with increasing sodium chloride (NaCl) concentrations [116,120,122]

2.1.1 Cellulose nanofibers characterization

CNF was received in 3 wt.% stock slurry solutions from the University of Maine Process Development Center and kept refrigerated. The cellulose source material is from bleached softwood pulp and refined using a mechanical homogenization process. The product specification reports the surface charge to be in the range of -48 to -5 mV [185]. The slurry was dialyzed in a semi-permeable regenerated cellulose membrane from Ward's Science for a minimum of 2 days while stirring in deionized water. The weight percent of

the resulting slurry was determined gravimetrically. This slurry was used as a stock solution. A density of 1 g/mL was assumed for all CNF solutions. Stock dialyzed CNF solutions were sonicated for 10 minutes and vortexed prior to all sample preparation and testing to minimize aggregation.

The dialyzed CNF was titrated to determine the charge density on the stock. The method was based on procedures for determining total and surface charge density of CNFs using conductivity measurements described elsewhere [14,195]. Briefly, conductivity titrations were conducted on dialyzed CNF based on methods suggested for CNFs with weak acid groups [14,195]. Approximately 240 mg from stock CNF solutions was titrated in a total 400 mL initial solution volume. Fresh 0.1 M HCl and 0.1 M NaOH stocks were prepared and used within 24 hours to titrate CNF. Nitrogen gas was bubbled for at least 30 minutes before titrating and during the procedure to reduce conductivity effects from dissolved carbon dioxide. Linear equations were fit to the three linear portions of the graphs.. From the volume calculated at the intercept of these lines, the weak acid equivalence point volume (V1) and strong acid equivalence point (V2) were determined. The difference between the two represents the volume it takes to titrate the weak acid groups on the surface of the fibers with 0.1 M HCl. The resulting charge density was calculted for the three repeats as shown below in Figure 2-1. The average charge density of the CNF from these repeats was measured to be 0.367± 0.067 mmol/g.

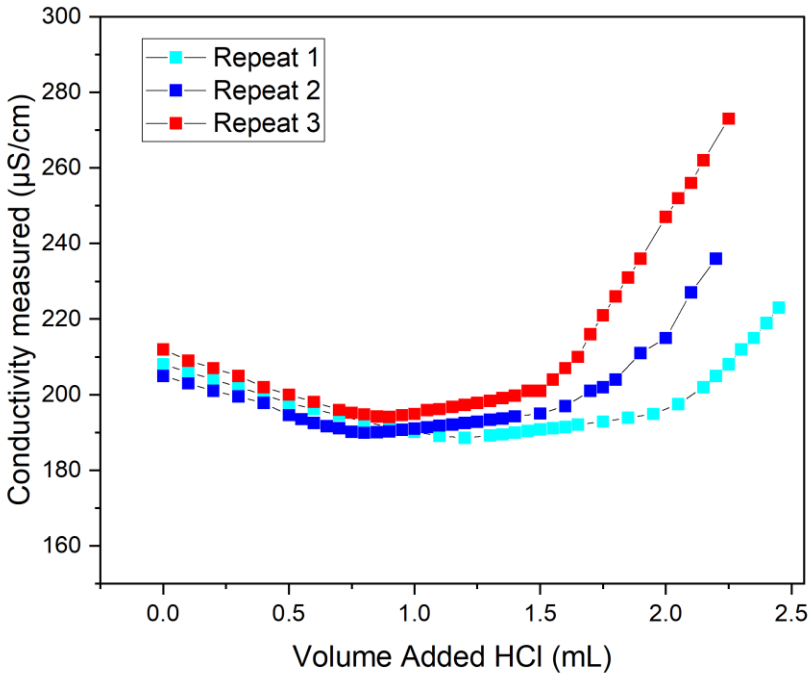

Figure 2-1. Conductivity titrations of dialyzed CNFs used to calculate the average charge density of the fibrils used.

2.1.2 Polyelectrolyte complex composition

PAA sodium salt (degree of polymerization, N=160, molecular weight=15,000 g/mol) in a 35 wt.% aqueous solution was purchased from Sigma Aldrich. PAH was purchased as a powder from Sigma Aldrich (N= 186, molecular weight=17,500 g/mol). They were used without further purification. Stock solutions of 0.5 M or 10 mM polyelectrolytes were prepared with respect to moles of monomer. Solutions were made in nanopure water from the Milli-Q water system at a resistivity of 18.2 MΩ*cm and adjusted to pH ~6.5, where both polyelectrolytes are highly charged, using small volumes of hydrochloric acid (HCl) or sodium hydroxide (NaOH) and continuing to account for the overall concentration. The ionic strength changes from the pH adjustment of the stock

solutions were calculated to be less than 0.05 M total ions for the 0.5 M stocks and less than 3 mM total ions for the 10 mM stock.

2.1.2.1 Mixing Preparation of PECs

Precipitates, coacervates or solution phases were achieved by mixing the stock solutions of the polycation or polyanion with appropriate amounts of 5 M NaCl solutions and water, which were also adjusted to pH ~6.5 using HCl or NaOH. Final mixtures were prepared in 1.5 mL Eppendorf tubes with pre-calculated concentrations to achieve final salt concentrations between 0 and 4 M NaCl in the experimental mixtures. The final mixtures were at 1, 5, 110 mM total polyelectrolyte concentrations equimolar by degree of polymerization (N). After each addition, the sample was vortexed for 30 seconds. Polycation was added first, followed by the polyanion unless otherwise specified. These were prepared in 1.5 mL Eppendorf tubes. For the timed studies, the first four components (CNF, water, salt, and polyelectrolyte) were vortexed in a centrifuge tube and then placed in a 96 well plate. The final component (either the polycation, polyanion, or pre-formed coacervates) was then added to the rest of the mixture in the 96 well plate using a pipette and no further mixing was performed.

Three different total polymer concentrations were examined in this study, 1 mM, 5 mM and 110 mM. The 1mM total polyelectrolyte concentration was chosen based on a procedure for PAH and PAA coacervation described in Perry et al [116]. A 5 mM total polyelectrolyte concentration was sufficient for the microscopic and electrophoretic mobility studies described below. The 110 mM total polyelectrolyte concentration was chosen as an extreme high concentration case.

The purpose of these studies was to identify salt concentrations that result in coacervate formation of PAA and PAH for the wide range of polymer concentrations that are used throughout the studies. It was important to test higher concentrations, as they are not reported in the literature, but the larger weight percentages of polyelectrolyte or other additives are frequently used in the paper industry [196]. Given that the critical salt concentration needed for the transition to coacervate phase increases with increasing total polyelectrolyte concentration [123], it was important to establish a range where coacervates exist even when high polyelectrolyte concentrations are used. To confirm this here, a combination of turbidity analysis, optical microscopy, and visual inspection were used to distinguish the two phases.

2.1.2.2 Fluorescent Labeling of PAH

PAH was fluorescently labeled with fluorescein isothiocyanate isomer (FITC). FITC purchased from Sigma-Aldrich (CHEM IMPEX INT'L INC- MW: 389.39 g/mol). was prepared at a 1 mg/mL concentration in DMSO. PAH was prepared at a 2 mg/mL concentration in freshly prepared 0.1 M sodium bicarbonate solution at pH 9. FITC solution (50 µL) was added dropwise to the PAH solution while stirring using a micropipette. The FITC-PAH solution was kept in dark at 4ºC overnight and then transferred to dialysis tubing with a molecular weight cut-off of 6-8 kDa. The solution was dialyzed in water for 4 days and the water was changed 7 times. UV Visible Spectroscopy was run on an Agilent Cary 60 system to determine the ratio of FITC to PAH from absorbance values at 280 and 495 nm. The ratio was calculated based methods given in Sigma-Aldrich product literature for FITC labeling of a primary amine protein because PAH also has a primary amine. The

ratio was estimated to be 0.26 FITC to PAH. This solution was freeze-dried and then a 10mM stock solution adjusted to a pH 6.5 was made.

Samples made for microscopy were adjusted so that the total polyelectrolyte concentration accounted for the 0.26 degree of substitution by monomer unit of PAH-FITC. Immediately after the samples were prepared, a drop was placed on a clean glass slide and a coverslip was added. Images were taken right after this. Fluorescence imaging was conducted on a Zeiss AxioObserver Z1 Fluorescent Microscope, 20X / 0.8 NA Plan Apochromat (wd = 0.550mm) objective lens, and Zeiss AxioCam color camera or Hamamatsu Flash 4.0 CMOS camera.

2.1.2.3 Turbidity

Samples of 325 μL were prepared and plated in triplicates of 100 μL each. Three samples were run and averaged. All samples were prepared with the same polyelectrolyte (0.5M), salt, and deionized water stock solutions. For 1 mM total polyelectrolyte samples, 650 μL of sample was prepared. Water and salt were added together first and vortexed for 15 seconds at 3200 rpm. PAH was always added first to the NaCl solution and vortexed for 30 seconds at 3200 rpm. PAA was added last and vortexed for 30 seconds at 3200 rpm. Samples were run on the plate reader immediately after preparation. Corning ultra-low attachment surface 96-well plate microplates were used.

Semi-quantitative assessment of phase regimes was based on the haze of suspended PEC particles with increasing salt concentrations (precipitate, coacervate, solution regimes). Turbidity is a measure of the haziness of a suspension based on the scattering of the colloids in solution as light in the visible wavelengths is transmitted through the sample

[14,70]. Consequently, this is a common technique used to understand the presence of PECs and is used often used in paper-making to understand flocculation behavior [157,197]. A plate reader equipped with a UV spectrophotometer (BioTek Synergy H4 micro plate reader) was used at a wavelength of 550 nm for the turbidity measurements. The polyelectrolytes do not absorb at this wavelength. Turbidity was calculated from $T = \ln(I/I_0)$, with I=intensity of light passed through sample volume and I_0= incident light intensity. Samples of 350 μL were prepared and plated in triplicates of 100 μL each. Samples were run within half an hour of preparation. Corning ultra-low attachment surface 96-well plate microplates were used.

2.1.3 Cellulose nanofibers and polyelectrolyte complex mixing procedure

Because the effect of CNF and PEC mixing procedure was to be tested in this study, this will be discussed more explicitly in the characterization of CNFs and PEC interactions section and in the discussion section. Briefly, dialyzed CNF stock was mixed with deionized water, NaCl, PAH, and PAA, as appropriate to achieve the concentration of CNF and PECs needed and with what type of order-of-addition desired (types illustrated in Figure 2-2). Solutions with 0.05 and 0.5 wt.% CNF and 5 mM or 50 mM total PEC concentration were prepared. Mixing steps involved vortexing for 30 seconds at 3200 rpm on a vortex mixer.

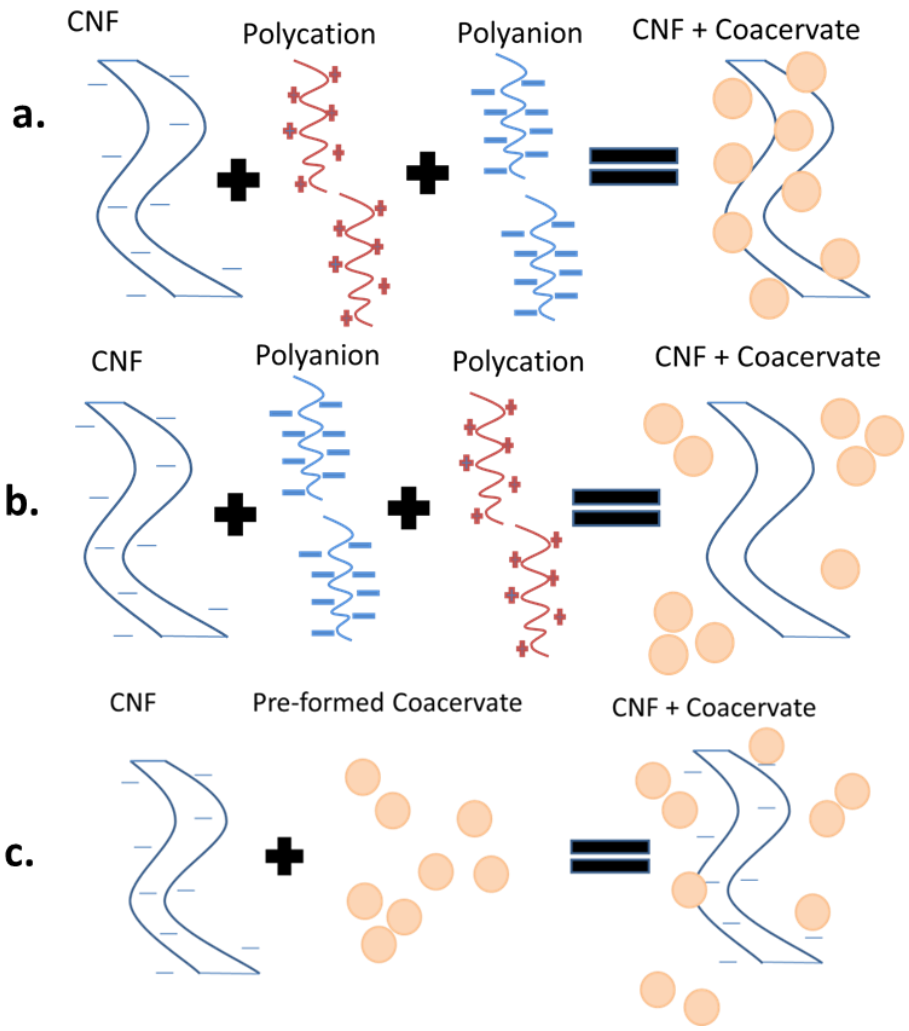

Figure 2-2. Schematic of three different order-of-addition variations of polyelectrolytes to CNFs tested in this study. Polycation was either added sequentially to CNF first (a), added sequentially second after polyanion was added (b), or pre-formed separately then added to CNF (c).

2.1.4 Characterization of cellulose nanofibers and polyelectrolyte complex interactions

2.1.4.1 Electrophoretic Mobility

Electrophoretic mobility was used to understand the surface charge behavior of CNFs with and without polyelectrolytes. Electrophoretic mobility values were measured using a

Zetasizer Nano Z (Malvern Instruments, Ltd., Worcestershire, UK) with a dip-cell setup. The instrument temperature was equilibrated to 25ºC for 2 minutes.

CNF were prepared at 0.05 wt.% in a 1 mM NaCl solution and adjusted to the appropriate pH using small volumes of HCl and NaOH. Typically the electrophoretic mobilities of CNFs are tested with small amounts of salt [14], motivating the selection of 1 mM NaCl. The CNF-only samples were sonicated for at least 10 minutes and re-agitated before running. Analysed data was an average of at least three measurements.

CNFs with polyelectrolytes were prepared at 0.05 wt.% CNF with 1 mM NaCl and up to 5 mM total polyelectrolyte concentration in solution. The samples were vortexed for 30 seconds after each addition. The pH values were recorded after sample preparation. Samples were re-mixed immediately before running samples. CNFs with PECs were prepared at a total polyelectrolyte concentration of 5 mM with 1mM NaCl in nanopure water. The polycation was added first followed by polyanion unless otherwise specified. The same method of preparation was carried out as with the turbidity samples. Samples were tested the same day as they were prepared and agitated immediately before running the samples.

Timed zeta-potential studies were also performed to examine the rate of assembly. The samples were prepared in a similar manner to the timed studies for the microscopy studies explained below. The CNF, water, salt, and first polyelectrolyte were vortexed together. The electrophoretic mobility of this mixture was then measured. A pre-determined amount of the final component was then added to the same cuvette using a pipette without further mixing and measurements were immediately taken. An initial one-

minute temperature equilibration time was set and then 40 sub-runs were taken per measurement. A 30 second wait time was set between measurements and 14 measurements were made per sample. After this time point, the values do not significantly change. Aggregation can occur at long times, so this test was not capable of going to the very long times examined in the microscopy studies. Each sample type was prepared and tested in triplicates of 800 µL. The measurements at any given time point were averaged from all three samples. For the zero-time point, three measurements were taken per sample for each of the 3 samples and averaged.

While the CNF surface charge is primarily reported as the zeta-potential in the literature using the Henry equation with Smoluchowski or Hückel approximations [14,36,198], electrophoretic mobility is a more accurate measure of surface charge character, because it requires fewer assumptions [14]. CNFs have high aspect ratios and can aggregate, so assumptions from Smoluchowski equations, which treat the particles as spherical, may not be appropriate [14,70]

2.1.4.2 Microscopy and Videos

For both PECs and CNFs with PECs, approximately 50-100 µL of samples were imaged in optically clear Corning ultra-low attachment surface 96 well microplates using a Leica DMi8 inverted microscope using transmitted light mode, HC PL FLUOTAR 20 or 50x objective lenses, and Leica DMC2900 camera.

To better visualize the behavior of the interactions of CNF with polyelectrolytes or coacervates added with different mixing orders, still micrographs at different time points and time lapse videos were taken after the last component was added. First the CNFs, salt,

and first polyelectrolyte were added sequentially and vortexed for 30 seconds between the addition of each component and then the final polyelectrolyte was added to a 96 well plate on the microscope stage without further mixing or agitation. For the pre-formed case, the coacervates were made with PAH, PAA, water, and salt vortexed together and that mixture was added to CNF by themselves. Figure 2-3 shows the representative procedure for the case where PAH is added first, followed by PAA.

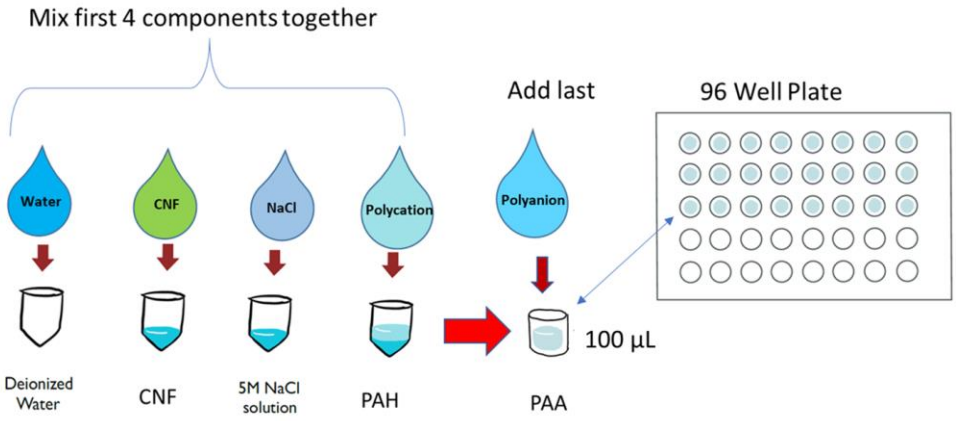

Figure 2-3. Representative schematic of mixing procedure of CNF with PAH first and PAA second for taking timed microscope images and videos.

The videos were taken for approximately 2 hours and 10 minutes after the last addition for the 5 mM total polyelectrolyte concentration scenarios. A video showing the mobility of PAH PAA coacervates at 110 mM total polyelectrolyte and 2 M NaCl concentration is also provided.

The videos are available by the publisher ACS Omega at:

https://pubs.acs.org/doi/10.1021/acsomega.0c00977?goto=supporting-info

- Video 1: CNF 1 M NaCl 5 mM PAH 1st PAA 2nd (AVI)
- Video 2: CNF 1 M NaCl 5 mM PAA 1st PAH 2nd (AVI)
- Video 3: CNF 1 M NaCl 5 mM Pre-formed PAH PAA (AVI)
- Video 4: Coacervates 2 M NaCl 110 mM PAH PAA (AVI)
- Video 5: Precipitates 0 M NaCl 110 mM PAH PAA (AVI)

2.1.5 Water retention values

The CNF stock was first sonicated for 10 minutes and then vortexed before using. The required amount of water was added to the CNF, then vortexed for 30 seconds, followed by the required amount of 5 M NaCl, and then vortexed for 30 seconds. The first 0.5M polyelectrolyte was added dropwise to CNF mixture while on the vortex mixer at 1500 rpm, then vortexed for an additional 30 seconds at 3200 rpm. This was then pipetted in and out 20 times for full mixing. The last polyelectrolyte was also added dropwise on the vortex mixer, vortexed for another 30 seconds and pipetted in and out 20 times. For the pre-formed samples, the CNF was added last, vortexed 30 seconds and pipetted in and out 20 times.

Immediately after preparation, 500 µL of sample was pipetted into Milli-Q Ultrafree-MC centrifugal filter tubes with 0.22 µm pore size Durapure hydrophilic PVDF membrane. The samples were then centrifuged at 12,000 g for 30 minutes. These conditions are more stringent than compared to typical standards in terms of the force used [199] and comparable to methods in the literature on other CNF systems [22,177]. These adequately reach the asymptote of minimized WRVs for the time and force used. Immediately after centrifugation, the samples were removed and weighed, and then put in an oven at 25ºC. The oven was set and ramped to 110ºC, then the samples were dried for an additional 30

minutes at this temperature, before turning the oven back down to 25ºC. The weights were measured after the samples reached room temperature again.

Water Retention Value is calculated as shown in Equation 3:

$$Water\ Retention\ Value\ \% = \frac{w_w - w_D}{w_D} \times 100 \quad (3)$$

Where w_w is the weight of the wet sample immediately after centrifugation and w_D is the weight of the sample after it is oven dried.

2.1.6 Molecular dynamics simulations

Molecular dynamics simulations were designed to mimic the mixing procedures and based on the formulation of the PEC system chosen to interact with CNF in the experimental procedures. This was done in collaboration with Dr. Monojoy Goswami at Oak Ridge National Labs who constructed and carried out the simulations. The simulation procedures are described briefly here, and further details can be found in the publication [136].

The experiments were designed to examine how the order-of-addition of the polyanion (PAA), polycation (PAH), or pre-formed complexes affects their interaction with CNFs. To complement these, 3 sets of simulations were performed; (1) polycation and polyanion complexation, (2) CNF, polycation and polyanion coacervate formation with polycation (PAH) added first and (3) CNF, polycation and polyanion coacervate formation with polyanion (PAA) added first. The pre-formed coacervates added to CNF simulations were not performed due to limited computational time.

Coarse-grained (CG) molecular dynamics (MD) simulations were performed using Large-scale Atomic/Molecular Massively Parallel Simulator (LAMMPS) MD package [200] on the Titan supercomputer. A Kremer-Grest bead-spring polymer model was used, where the monomer beads of the polymer are connected by Finite Extensible Nonlinear Elastic (FENE) bonds. In LAMMPS, non-bonded short-range repulsive Lennard-Jones (LJ) interactions between the beads are embedded in FENE potential that ensures no overlapping between two monomer beads. Explicit electrostatic interactions were computed using the Coulomb potential, and positive or negative charges were assigned appropriately to the monovalent charged beads.

The coarse-graining is done at the monomer level following bead-spring polymer model [201] as shown in Figure 2-4 (a) and (b). Each monomer of PAA and PAH is represented by spherical beads. In MD simulations, chain lengths and salt concentrations can influence the self-assembly process. The CNF and chain concentrations that would lead to coacervate formation were estimated based on prior simulations on PECs [202–204]. Concentrations of 0.75% CNF concentration, 1.2% PAA and PAH coarse-grained monomer concentration and 9% salt concentration (both positive and negative ions) were chosen. The PAA and PAH backbones have 80% charges each and are modeled as polyanion and polycation, respectively. The percentage of negative charges on the CNF backbone is 25%. The concentrations used here are much higher than the experimental concentrations, which was done because there is a minimum limit of overall number of monomers in MD simulations that is needed to form coacervate. Additionally, the simulating system is much smaller than the experimental system such that following the exact experimental system would mean that the simulating system's total number of

monomers would become appreciably low and a physically meaningful effect would not be observed. The CG CNF, PAA and PAH molecules are all randomly put in a box of size $100\times100\times100\ \sigma^3$, where σ is the monomer bead diameter.

The chain length of PAA and PAH are 60 monomer units, which is below the entanglement length of polymers in coarse-grained simulation [205]. The polymer chains are generated by repeating each monomeric unit 60 times, i.e., degree of polymerization of the PAA and PAH coarse-grained chains are 60. The PAA and PAH chains contain negative and positive unit charges on the side chain. To understand the coacervate formation driven by strong Coulombic interactions, the chain length was chosen to be less than the entanglement length. The energy parameter, ε, for the LJ interaction was kept at 1.0 for the interactions between different monomer beads, except for the charged beads. For the charged beads a strong interaction parameter was used, i.e., $\varepsilon = 2.0$.

The CNF is modeled as a stiff long chain of 75 monomers with side chains containing negative unit charge. While this CNF model is simplistic, this model in the CG simulations adequately serves the purpose of understanding the assembly of coacervate formation with CNFs. The stiffness of the CNF is specifically controlled.

The same number of positive and negative counterions are randomly added to neutralize the CNF, PAA and PAH charges. Salt ions are incorporated as single bead positive and negative charges. Explicit 90,000 salt ions and counterions to balance electroneutrality are added to the system. This refers to 9% salt concentration. The simulations are performed in the implicit solvent condition, i.e., no explicit water is used.

It is a common practice in bead-spring polymer simulation to use 'implicit solvent' method to avoid large computational costs associated with 'explicit' water molecule simulation.

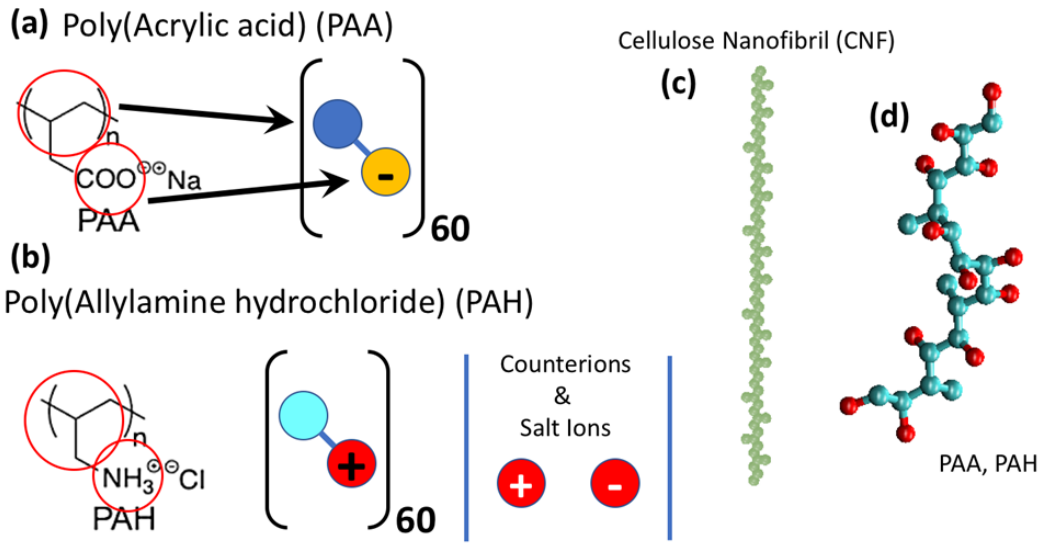

Figure 2-4. Parameters used to model CNF, PAH, PAA, and NaCl system in coarse-grain molecular dynamic simulation model (a) and (b) coarse graining of PAA and PAH respectively. The salt and counterions are shown at the bottom. The CNF and polymer chain models are shown in (c) and (d).

Two sets of simulations were performed as shown in Table 2-1 for the coacervate-only system and CNF-with-coacervate system. In the first set of simulations, polyanion-polycation complexation were performed to understand coacervate formation. Thereafter, two sets of simulations were performed. For Set I, the polycation (PAH) interacts with the CG CNF monomers first and then polyanions (PAA) are introduced in the system. For Set II, the polyanion (PAA) interacts first with the CG CNF and then PAH is introduced in the system. The construction of the MD model is such that both the polycations and polyanions are simultaneously present in the initial system. The experimental condition is mimicked by allowing interactions between CNF and polyanions and polycations to begin at different

simulation timesteps, while the experiments are performed by physically adding PAA and PAH in two different orders. Therefore, the order-of-addition behavior is achieved by effectively introducing zero interaction of all types between CNFs and polycation or polyanion in Set I and Set II, respectively. While this approach allows the other type of polyelectrolyte to be present in the system, the other polyelectrolytes do not contribute to any interaction except occupying their respective spaces. In simulations, addition of large macromolecules, in this case the polycations and polyanions, separately become difficult and computationally intractable and hence the method chosen is described here.

Table 2-1. Coarse-grain molecular dynamics simulations performed with or without CNF and in first or second order-of-addition.

Set	*CNF*	*First add*	*Second add*
I	-	PAH (polycation first)	PAA
II	-	PAA (polyanion first)	PAH
I	CNF	PAH (polycation first)	PAA
II	CNF	PAA (polyanion first)	PAH

2.2 Results and Discussion

2.2.1 Formation of PAH/PAA coacervates

To understand the interaction between PECs and CNFs, the precipitate and coacervate regimes with the PAH and PAA in the presence of NaCl was identified. The formation and appearance of these regimes at various concentrations and molecular weights of PAH and PAA with NaCl and other salts have been previously reported [116,117,120,122]. This was verified and higher concentrations were tested to select conditions for coacervate formation with CNFs at polymer concentrations important for the remaining studies in this work. Through a combination of microscopy and turbidity analysis, the transition from precipitate to coacervate occured at salt concentrations of 0.1 M, 0.2-0.4 M, 0.4-0.5 M and 0.7-0.8 M NaCl for 1 mM, 5 mM, 50 mM and 110 mM total

polyelectrolyte concentrations, respectively. A salt concentration of 1 M was selected to move forward with for the remaining studies, as coacervate formation is established at those conditions, even for higher concentrations of polyelectrolytes.

Figure 2-5 shows that the turbidity changes as the concentration of NaCl is increased for 1, 5, 50 and 110 mM total polyelectrolyte concentrations. In all four cases at no salt, precipitates readily form, as has been seen previously for variations of experimental conditions with PAH and PAA [116,120,122]. The initial turbidity is relatively low because the precipitates that form are large, solid-like, and tend to sediment or flocculate out of solution to the bottom of the well plate [80,129]. Once a small amount of salt (0.1-0.2 M) is added, a large jump in turbidity is observed due to formation of smaller complexes that do not settle out. The increase in the suspended PECs leads to a maximum in the turbidity curves. This maximum also increases with increasing total polyelectrolyte concentration, as the amount of material present to scatter light is higher. At the lower salt concentrations, the precipitate phases are unstable and start to flocculate or aggregate resulting in large variation and standard deviations in turbidities. This can be observed at lower salts concentrations in other studies as well [120,122]. As the salt concentration is further increased and the precipitates transition into the coacervate regime, the coacervates are more stable, turbidity values become more consistent and begin to plateau. This behavior is accentuated at higher polyelectrolyte concentrations (50 and 110 mM).

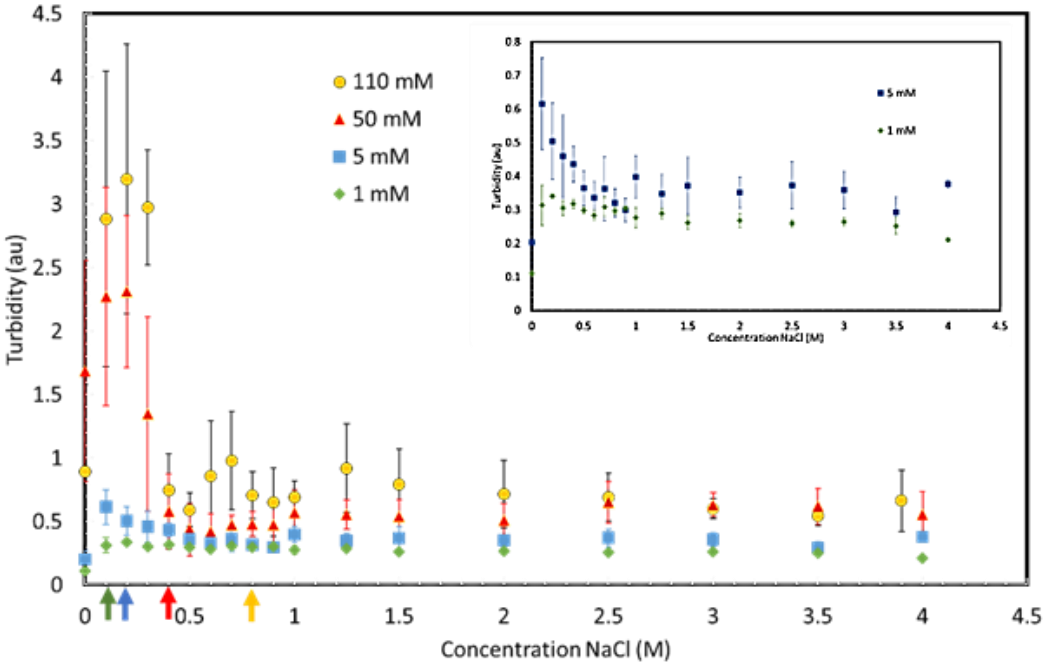

Figure 2-5. Turbidity plots of 110 mM (yellow circles), 50 mM (red triangles), 5 mM (blue squares), 1 mM (green diamonds) total polyelectrolyte concentration with 0 to 4 M NaCl concentration. The inset shows the 5 and 1 mM total PEC concentrations. The arrows indicate a transition from precipitate to coacervate phase.

Generally, as the salt concentration increases, the resulting electrostatic screening leads to the precipitates transitioning to coacervate and solution phases [116,123,129]. As seen in Figure 2-5, for all four total polyelectrolyte concentrations tested here, the turbidity is seen to increase and then decrease at around 0.4 to 0.5 M NaCl. However, for the 1 and 5 mM total polyelectrolyte concentrations, after the initial maximum is reached, the turbidity steadily decreases with increasing salt concentration. These findings are similar to the observations by Perry et al. for the 1 mM PAH, PAA, and NaCl system [116]. The decrease they observed with increasing salt concentration was more pronounced and was dependent on the type of salt that was used [116]. From these results the transitions from precipitate to coacervate were determined to occur at salt concentrations of 0.1 M, 0.2-0.4 M, 0.4-0.5 M

and 0.7-0.8 M NaCl for 1 mM, 5 mM, 50 mM and 110 mM total polyelectrolyte concentrations, respectively. These are marked with arrows on the x-axis in Figure 2-5.

Figure 2-6 A-C show the macroscopic phase behavior and D-F show the micrographs of the 110 mM total polyelectrolyte concentration PECs after centrifugation. From the macroscopic visual inspection of the samples prepared in centrifuge tubes and the optical micrograph, the precipitate form was confirmed at 0 M NaCl. The liquid coacervate phase was clearly seen at 1 M and 2 M NaCl for the 110 mM total polyelectrolyte concentration samples in the macroscopic images and corresponding well to the turbidity measurements. The coacervates are small in the 2 M NaCl case, so they are difficult to distinguish from precipitates in the micrograph. A video of the mobile coacervates is available (Video 1 Coacervates 2 M NaCl 110 mM PAH PAA.avi), demonstrating that they are, indeed, liquid phase separated coacervates with our previous paper [136]. This can be compared to another video showing the behavior of precipitates (Video 2 Precipitates 0 M NaCl 110 mM PAH PAA.avi). By combining the turbidity results and observations in microscopy (Figure 2-6), a salt concentration of 1 M for 5 mM total polyelectrolyte concentration was chosen to move forward with for the remaining studies, as coacervate formation is established at those conditions.

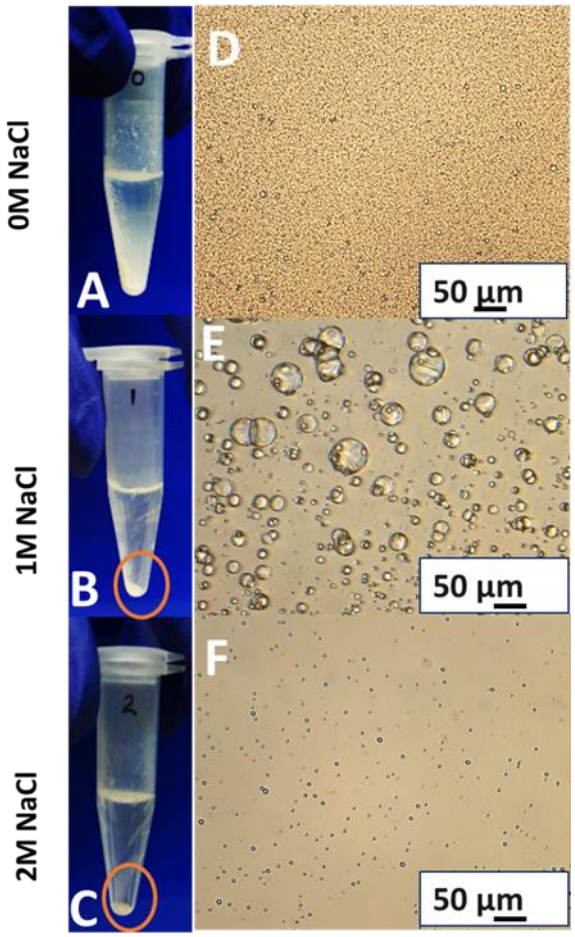

Figure 2-6. Images of 110 mM total PAH PAA concentration after centrifugation with (A) 0 M NaCl (B) 1 M NaCl (C) and 2 M NaCl. Coacervate phase is circled (B&C). Micrograph of 110 mM PAH PAA with 0 M NaCl, 1 M NaCl, and 2 M NaCl after centrifugation (D-F).

2.2.2 Polyelectrolyte complex coacervate interactions with cellulose nanofibers over time

Once the salt concentrations at which coacervates are formed were established, 0.05 wt.% CNF were introduced into the 5 mM total polyelectrolyte system. Using microscopy to observe the interactions, how the order-of-addition of PAH and PAA affected their coacervation and association with CNF while varying the order-of-addition of the components was tested. In the first scenario, PAH (+) is added to the fibers and salt solution

first, then PAA (-) added last. The second scenario is the opposite, where PAA (-) is added to the fibers and salt solution first, and PAH (+) is added last. Finally, in the third scenario, salt was added to PAH and PAA when forming the initial pre-formed coacervates, which were then added to fibers. The coacervates form and are left to move and coalesce over time without additional agitation.

The micrographs in Figure 2-7 show the differences between the three scenarios when the third component is added to the well plate. Adding the polycation or the polyanion first shows different aggregation to the fiber than the pre-formed first case. Between the polycation and the polyanion first cases, the time of attachment to the fibers varies. In the first scenario (Figure 2-7 A, D, G, J, M and P), when (PAH (+) is added first), the coacervates form in solution and move from the solution to the fibers. The formation of the coacervates occurs almost immediately upon addition of the last component and the association of the coacervates to the fibers starts to occur around 4 to 5 minutes and continues over approximately the next 20 to 30 minutes. As the coacervates become localized near the fibers, they become less mobile than those in the bulk and are primarily attached to the particles and not exchanging with the coacervates dispersed in the solution The fibers are mostly covered by the 40 minute mark (Figure 2D) and almost completely covered at 70 minutes (Figure 2-7 G), when a dense aggregation of coacervates can be observed. In scenario two (Figure 2-7 B, E, H, K, N and Q), where PAH was added last (PAA (-) already present), many coacervates form in the bulk solution and eventually move to the fibers as well, but it takes longer than in the first case. Fibers and coacervates are more disperse in this PAA first case. At the 40-minute mark (Figure 2-7E), significantly less of the fibers are covered with coacervates and they are primarily seen in the bulk. By

70 minutes, the coacervates are localized to the fibers and both orders of addition show similar amounts of association and form a tighter network (Figure 2-7 G and H). At 100 minutes (Figure 2-7 J and K), the aggregation of coacervates to the fibers looks similar to that at 70 minutes. After 24 hours (Figure 2-7 M and N), the fibers in both cases are covered with coacervates that are tightly bound and after approximately 3 days (Figure 2-7 P and Q), the coacervates have started to coalesce into larger coacervates with the fibers still attached.

In the pre-formed coacervate scenario (Figure 2-7 C, F, I, L, O, and R), the coacervates are already well dispersed in the bulk solution. They also move to the fibers, similar to the other cases, but the association has only begun at the 40 minute mark, with many coacervates still in the bulk even up to 70 minutes, and significant coverage only occurs at 100 minutes and beyond (Figure 2-7 F, I, and L). It is not until after 24 hours that there is large amount of coacervates on the fibers (Figure 2-7 O) and they do not form the same close aggregation as the first two scenarios, which is still evident 3 days later (Figure 2-7 R). As discussed in the introduction, pre-formed coacervates have been used to improve paper strength properties in paper formulation. These results suggest that their interaction is weaker than in the case where positively charged polyelectrolytes are added first, at least at short time frames. Over time, the pre-formed coacervates continue to move to the fibers and adhere along the surface.

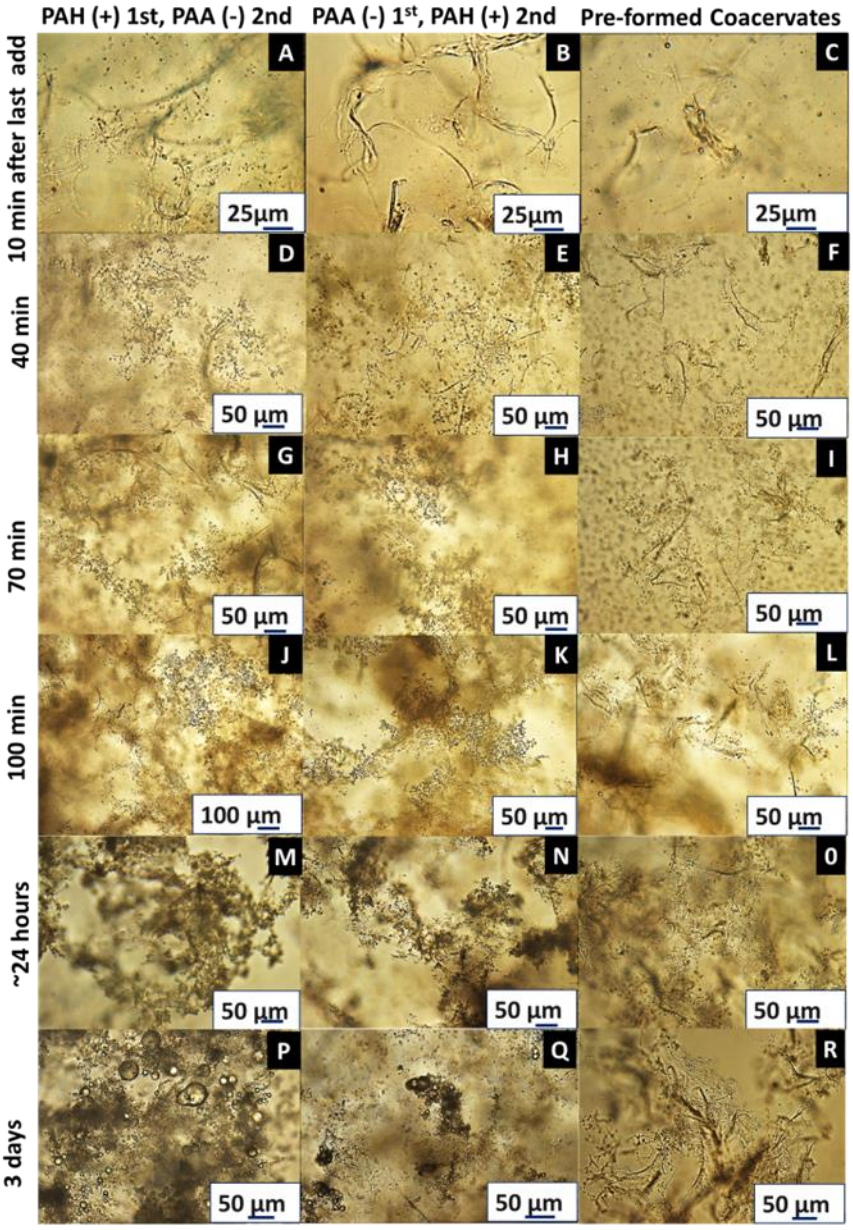

Figure 2-7. Microscope images of CNF and coacervates after 10, 40, 70, 100 minutes, ~24 hours, and 3 days after adding the last component on the microscope while varying the order-of-addition of 5 mM total polyelectrolytes to CNF solutions. In (A,D,G,J,M, P) PAH (+) was added first, then PAA (-), in (B,E,H,K,N,Q) PAA(-) was added first, then PAH (+), and in (C,F,I,L,O,R) pre-formed coacervates were added to the CNF. The rows are the time points.

Overall, the differences between the three scenarios of mixing order are the relative time it takes for the coacervates to be immobilized and the association with the fibers with the coacervates. The behavior is illustrated in the schematic in Figure 2-8. When adding the polyelectrolytes to the CNF and salt solution, coacervates form and become immobilized on the fibers. The coacervates seen in the bulk solution move to the fibers and become relatively scarce in the bulk over time.

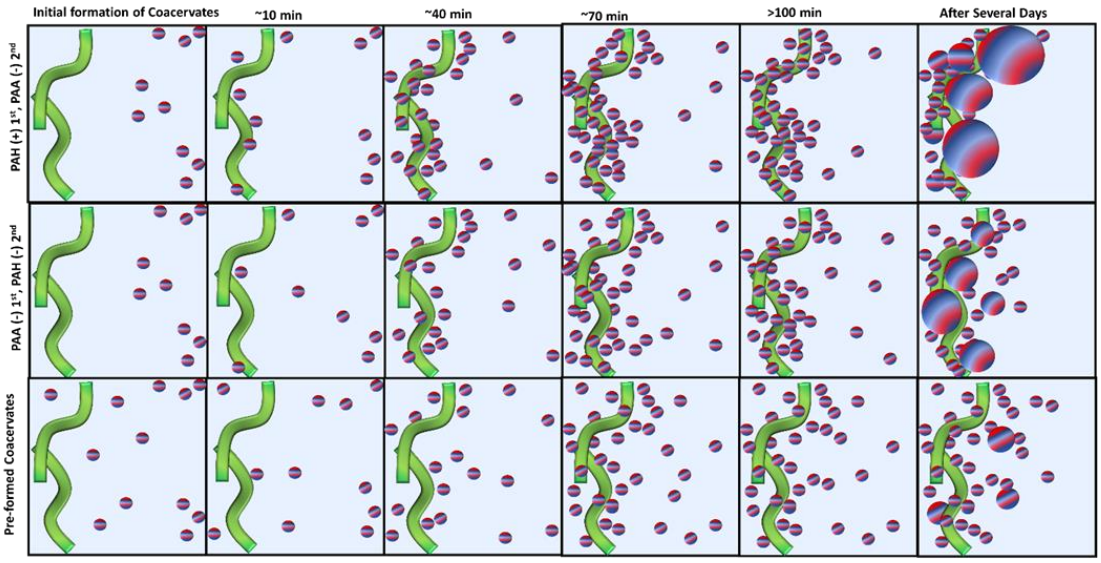

Figure 2-8. A schematic representation of the association of the coacervates with fibers over time in varying the mixing order for 5 mM total polyelectrolytes.

2.2.3 Cellulose nanofibers and polyanion interactions with fluorescent labeled polycation

To better visualize the interaction between coacervates and CNFs while changing order-of-addition of the polyelectrolytes, fluorescent labeled PAH was used to prepare the coacervates. Figure 2-9 shows 0.05 wt.% CNF 1 M NaCl and 5 mM total polyelectrolytes

with the three different order-of-addition scenarios. Unlike the previous images where the last component was added directly to the well plate and allowed to move on their own, the samples in Figure 2-9 were vortexed immediately after the addition of the last polyelectrolyte in the centrifuge tube. They were then placed on glass slides and covered with a coverslip. Figure 2-9 A, C and E show differential interference contrast (DIC) images with fluorescence overlay (where the CNF can be seen) and Figure 2-9, B, D and F show just the fluorescent images.

These results further confirm that even with complete mixing, there is a difference in the attachment of the coacervates to the fibers with the order-of-addition. When the PAH-FITC is added first (Figure 2-9 A and B), the coacervates largely cover the fibers in large droplets with few coacervates in the free space in the solution. The PAH coats the fibers and the free PAH-FITC and PAA form large coacervates that have coalesced together. While coacervates are also attached with the PAA first case (Figure 2-9 C and D), these are small, disperse, and many still in the bulk solution. Here, the added PAH will complex with PAA preferentially, but some of the PAH is electrostatically attracted to the negatively charged fibers and coats them as well. In the pre-formed coacervates case, the fibers are difficult to distinguish in the fluorescent image (Figure 2-9 F) because PAH-FITC has not significantly adsorbed to their surface. The PAH-FITC that would electrostatically attract to the fibers are already complexed with the PAA. Consequently, significantly fewer coacervates are seen to be attached to the fibers and the majority of them remain in solution instead.

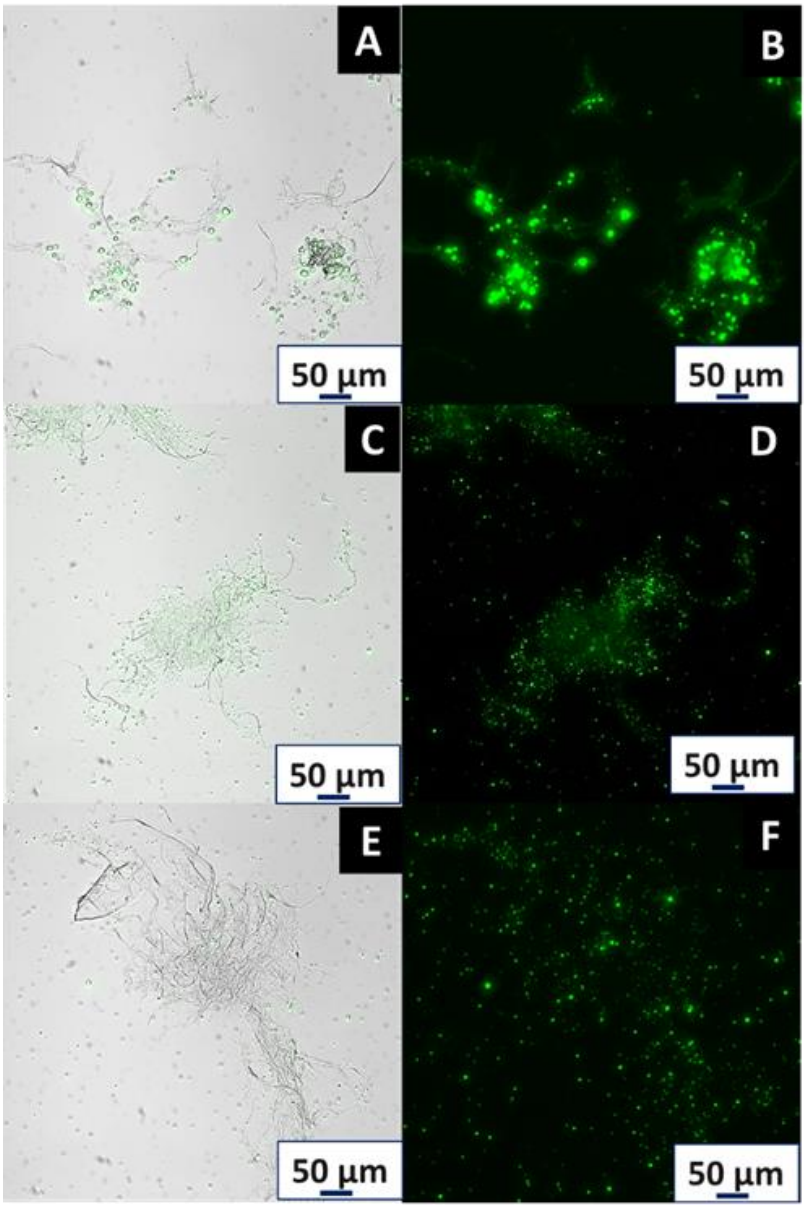

Figure 2-9. Microscope images of 0.05wt% CNF, 1 M NaCl, and 5 mM total polyelectrolyte concentration of labeled PAH and PAA were completely vortexed together. The left column is an overlay of the DIC image and fluorescence image, while the right column is the fluorescence filter alone. In A and B, PAH-FITC (+) was added first, then PAA (-), in C and D PAA(-) was added first, then PAH-FITC (+), and in E and F Pre-formed PAH-FITC and PAA coacervates were added to the CNF.

These results are consistent with Zhao and Zacharia who showed that the mixing order of PAH followed by PAA led to greater encapsulation of negatively charged Bovine

Serum Albumin than PAA followed by PAH [206]. Additionally, previous studies with PECs and negatively charged surfaces showed that the adsorption of pre-formed PECs to negative charged surfaces increases with increasing salt concentration (0 to 100 mM NaCl) for both strong [121,159] and weak [159,207] polyelectrolyte systems. These results suggest that even with higher salt concentrations (1M NaCl), attachment of the PEC coacervates to the negatively charged CNF is less in the pre-formed case as compared to when the coacervates are formed in the presence of the fibers.

2.2.4 Cellulose nanofibers and polyelectrolyte complexes interaction videos

Real-time videos of the three orders of additions were taken under the microscope in well plates to support the still-frame timed micrographs. Time-lapse videos up to approximately 130 minutes were taken and available with the SI in our publication [136]. These are Video 1: CNF 1 M NaCl 5 mM PAH 1st PAA 2nd.avi, Video 2: CNF 1 M NaCl 5 mM PAA 1st PAH 2nd.avi and Video 3: CNF 1 M NaCl 5 mM Pre-formed PAH PAA in the supporting information. Comparing Video 1 and 2, in the case where PAH was added first (Video 1), there is more coverage at earlier times of the fibers with coacervates as compared to case where PAA was added first (Video 2) at around 30-40 minutes. When pre-formed coacervates (PAH PAA and salt) were added to the CNF in Video 3, by 40 minutes, appreciably less attachment of the coacervates to the fibers is seen and coacervates are present more in the bulk. This is true even at the 2 hour and 10-minute time point but the coacervates near the fibers are far less mobile in each case.

2.2.5 Cellulose nanofibers and polyelectrolyte complex mixture surface charge analysis

The interactions of CNF with the complex coacervates are supported by the surface charge of the CNFs with and without the polyelectrolytes, as measured using electrophoretic mobility. As expected, and shown in Figure 2-10A, CNFs with 1 mM NaCl are negatively charged at pH values between 4-10. This includes a negative charge at a pH value of 6.5, which is the value used for the polyelectrolyte solutions for the coacervation experiments (electrophoretic mobility here is between -0.86 and -1.4 $\mu m \cdot cm \cdot V^{-1} \cdot s^{-1}$. Because these electrophoretic mobility values correspond to zeta-potential values of approximately -10 to -20 mV, these can be considered slightly negatively charged.

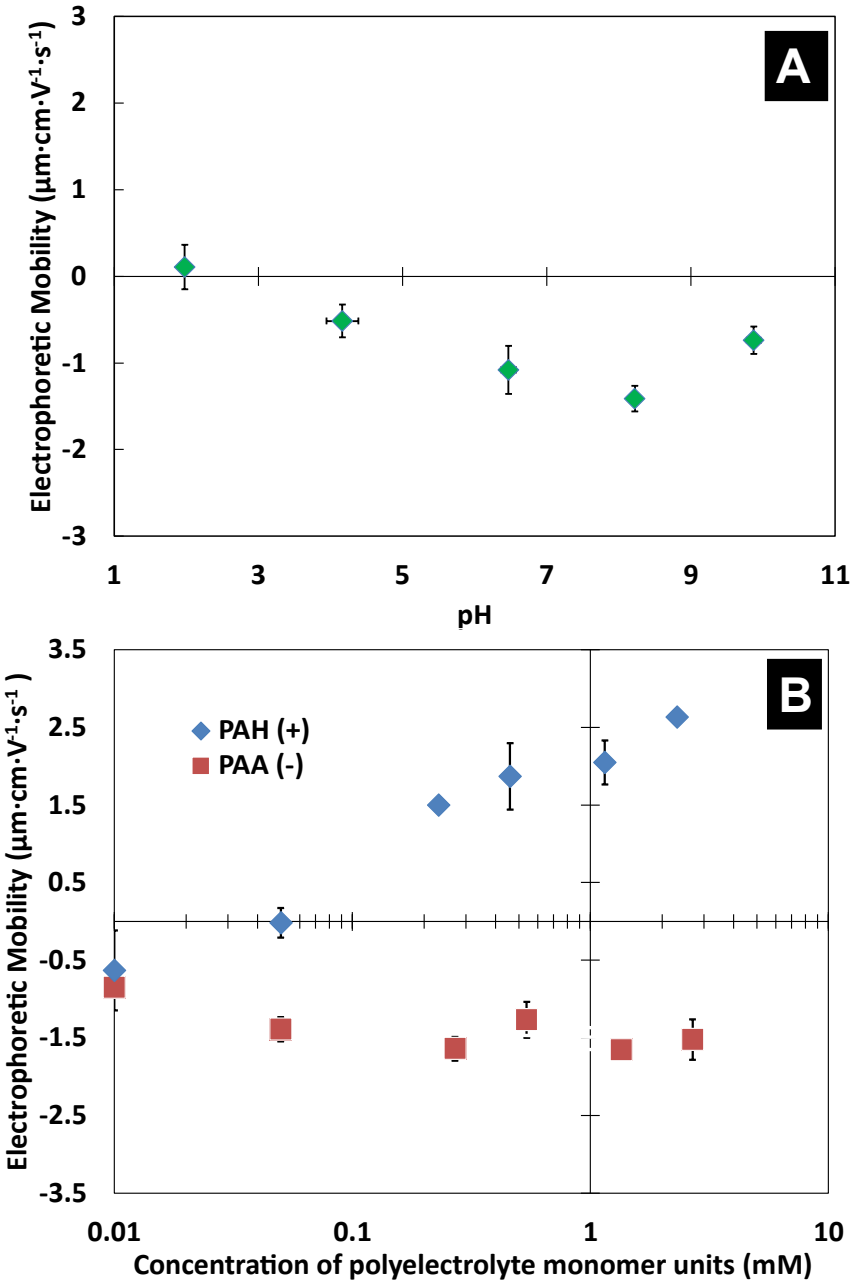

Figure 2-10. Electrophoretic mobility of 0.05 wt.% CNF and 1 mM NaCl: (A) at various pH values (each point is an average of 3 samples), (B) with increasing concentrations of PAH (+) or PAA (-) at pH 6.5 (each point is an average of 3 samples).

Because these CNFs are negatively charged, it can be expected that the oppositely charged polyelectrolyte will adsorb to the surface of the particles and neutralize the surface charge, while the negatively charged polyelectrolyte will repel and the particle surface

charge will not change. It has been reported that low molecular weight and highly positively charged polyelectrolytes readily adsorb onto the surface of cellulose fibers in flat configurations within seconds to minutes [208]. The adsorption was confirmed by adding increasing concentrations of either PAH (+) or PAA (-) to a 0.05 wt.% CNF and 1 mM NaCl dispersion at pH 6.5 and measuring the electrophoretic mobility at each concentration. Figure 2-10 B shows that the electrophoretic mobility increases linearly with PAH concentration on a semi-log scale. The surface charge switches from negative to positive at a PAH concentration of 0.05 mM (charge neutral) and is positive at higher PAH concentrations, which correspond to the minimum polyelectrolyte concentrations used in this study. This also confirms that for the 5 mM total polyelectrolyte concentration scenario, adding PAH first results in excess polycation at the surface. As expected, increasing the concentration of PAA did not appreciably change the surface charge of the CNFs. At all concentrations of added PAA tested, the electrophoretic mobility stayed between -0.85 and -1.5 $\mu m \cdot cm \cdot V^{-1} \cdot s^{-1}$ and did not significantly change when compared to CNF with 1 mM NaCl at pH values near 6.5, which have electrophoretic mobility values between -0.86 and -1.4 $\mu m \cdot cm \cdot V^{-1} \cdot s^{-1}$.

Finally, timed electrophoretic mobility experiments were conducted that measured the three order-of-addition scenarios at pH 6.5 (Figure 2-11) over time in minutes. Interestingly, for the case where PAH (+) was added first, upon addition of the PAA (-), the electrophoretic mobility appreciably shifted from a positive mobility to a negative one. This change of sign was not seen when PAA (-) was present first and PAH (+) was added. Similarly, the electrophoretic mobility did not significantly change in the case where fibers were added to pre-formed complexes. This, when taken in context with the 2-system

mixtures in Figure 2-10, indicates that the PAH absorbs onto the fibers when mixed, unlike the PAA and pre-formed coacervates. This may increase the local PAH concentration near the fibers or provide a position for new coacervates to form after the initial rapid bulk formation, leading to the faster kinetics for aggregation of coacervates onto the fibers. These results further support the importance that the order-of-addition plays to the overall system.

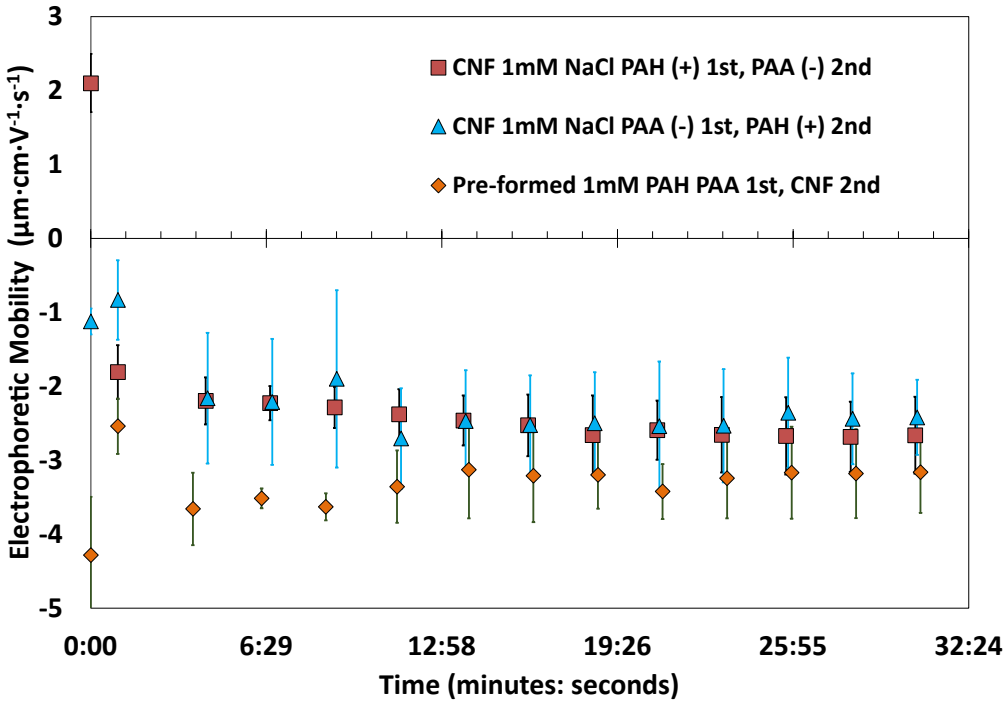

Figure 2-11. Electrophoretic mobility over time in minutes of 0.05 wt.% CNF with 1 mM NaCl with PAH (+) first, then PAA (-) added (red squares), PAA (-) first and then PAH (+) added (blue triangles), pre-and formed coacervates first, then CNF added (orange diamonds). Each curve is an average of 3 samples.

2.2.6 Molecular dynamic simulations

To enhance the understanding of coacervate formation and their interactions with CNF at the molecular level, CG MD simulations for three different systems were

performed. System-I for is for the coacervate formation of just the polycation (PAH) and polyanion (PAA) at 9% salt concentration as seen in the snapshot in Figure 2-12 A. The other two systems are in the presence of CNF and are affected by the order of polyanion and polycation addition. These are polycation-first (PAH-first) in Set 1 and polyanion-first (PAA-first) in Set 2. The snapshots of these two sets of simulations without salt and counter-ions and showing the two different orders are shown in Figure 2-12-B and C.

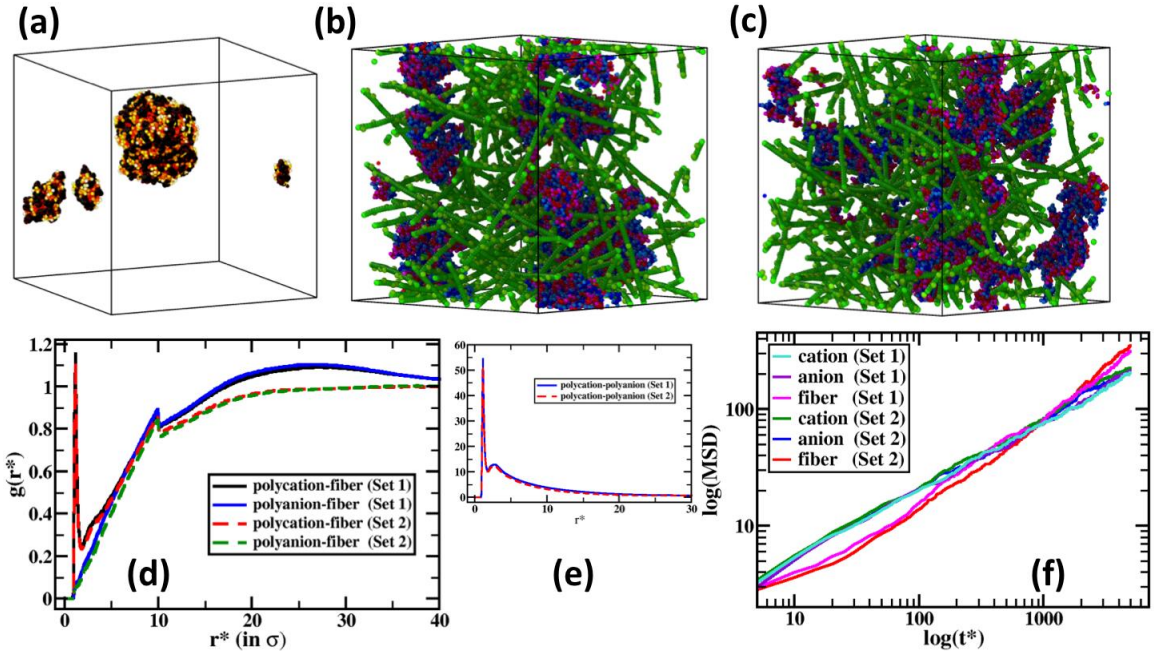

Figure 2-12. Molecular dynamics simulation results. (a) Polyanion-polycation complex formation without CNF. The light colors are polyanions and black colors are polycations. (b) Simulation snapshots of polycation-first added then polyanion. (c) Simulation snapshot for polyanion-first, then polycation. Green represents CNF CG molecules. Blue represents polyanion and red represents polycation. For clarity, counterions and salt ions are not shown. (d) Radial distribution function (RDF) between polycation-fiber and polyanion-fiber. The black and red curves represent polycation–fiber RDF for polycation-first (Set 1) and polyanion-first (Set 2) systems respectively. Blue and green curves represent polyanion – fiber RDF for polycation-first (Set 1) and polyanion-first (Set 2) systems respectively. (e) RDF between polycation and polyanion for polycation-first (blue) and polyanion-first (red) systems. (f) Mean-square-displacement (MSD) versus time (t*) for charge species coming from fiber, polyanion and polycation.

In the polycation-first case (Figure 2-12 B), due to the strong, oppositely charged electrostatic interactions between the polycations and the CNF, the PAH form complexes with the CNF. While the majority of the polycation charges are attached to the negatively charged CNF, some amount of residual polycation charges is free in solution, attributed to excluded volume interactions arising from the chain conformation. Larger coacervates form after the addition of polyanions that complex with the residual positive charges on

the polycations on the CNF surface. Consequently, in the polycation first case a large number of smaller PEC coacervates that are attached to the CNF surface can be observed, which is similar to the experimental observations in Figure 2-7 and Figure 2-9. In the polyanion-first case (Figure 2-12 C), the negative charged CNF and polyanions experience strong repulsive electrostatic interactions and therefore the polyanions do not attach to the CNF. Consequently, when the polycations are subsequently added, the majority of them form PECs with the polyanions that are already present in solution but because of their attraction towards negatively charged CNF, some of the polycations attach to the CNF. This drags a few polyanions to the CNF surface. Therefore, in the polyanion-first case mostly large PEC coacervates form with very few polycations attached to the CNF. Similar morphology is observed in the experiments in Figure 2-7 and Figure 2-9.

To further understand the interactions between the CNF and polyelectrolytes in the two orders of additions, the radial distribution function (RDF) was determined. RDF represents how the density of a given object varies with distance from a reference point [193,201]. The RDF, g(r*), was calculated near the CNF for both sets in Figure 2-12 D and the results show sharp peaks for fibers with polycation charges for both of the order-of-addition cases (black and red lines). This indicates stronger electrostatic affinity of polycations to the CNFs. The first peak in polycation-first case (black line) is little higher than the polyanion-first case (red line) suggesting higher agglomeration in PAH-first case. In the experiments, the PAH-first (polycation) case shows rapid coacervate formation with CNFs, while in the PAA-first (polyanion) case show slow attachment of coacervates to the CNFs. Similarly, the g(r*) from the MD simulation shows enhanced polycation and CNF agglomeration due to strong electrostatic interactions between oppositely charged

polycations and CNFs. This can be attributed to the faster coacervate formation in the PAH-first case in experiments. The simulations show a strong polycation-fiber first peak for both the polycation-first and polyanion-first case. This is due to strong electrostatic interactions between oppositely charged (polycation and CNF) molecules. They do not represent differences in coacervate size as were seen in the snapshots. In both Set 1 and 2, the PAA-fiber (blue and green lines) for both order-of-additions show no agglomeration. This can be attributed to the repulsion between polyanion with negatively charged CNF.

In Figure 2-12 E shows the g(r*) between polyanion and polycation charges near the CNF. The g(r) shows two peaks, indicating two layers of charges near the CNF surface. The large peak heights of these g(r) show strongly agglomerated polycation-polyanion coacervate. The g(r) along with the snapshots show agglomeration mechanisms that depends on order-of-addition of the polyelectrolytes. This phenomenon may also play a role in how CNFs interact with PECs during processing in solution.

In Figure 2-12 F, the mean-square-displacement (MSD) of the different charged species coming from polycation, polyanion and CNF for both the systems was determined. MSD represents a measure of the change of the position of a particle from a reference point over time and can represent diffusivity [209]. Specifically, the diffusive motion can be analysed by the long-time MSD. MSD for CNF shows it has faster motion than the polyelectrolytes in both order-of-addition cases. In the diffusive regime of the MSD plot, long time MSD show higher diffusivity for the fibers indicating that there is a greater number of mobile CNF that are weakly attached to the polyanions. For polycation-first case (magenta line), the MSD is slightly lower as most of the CNF is complexed with the coacervate that restricts their motion. For both systems, the diffusivity of the polyanions

and polycations are slower because they are part of coacervate agglomeration as observed in Figure 2-12 E.

2.2.7 Water retention values of cellulose nanofibers with polyelectrolytes

Measurement of the WRV is a standard technique used in paper manufacturing and research to evaluate the water retained by pulps [23,30,176,199]. Given the high surface area and fibrillation, CNFs are expected to have high measured WRVs [30,177,183]. The PEC in this work were selected to decrease the water retention in cellulose fiber materials in the papermaking process, so in addition to the fundamental studies on the PEC phase behavior and surface interactions the WRV of PECs mixed with CNFs were also measured.

The WRVs obtained for the CNF by themselves (262 ± 29.0 %) are consistent with the values that have been reported in the literature for other CNF sources with functional group modifications or additional refining [22,177,210], as well some larger pulps [23,159,211,212]. As seen in Figure 2-13 for all three PEC-CNF mixtures (PAH first, red, PAA first, yellow, and pre-formed, green), the WRVs are lower than CNF by itself. The pre-formed coacervates had the highest WRV (212 ± 13.0 %) of the three PEC cases. This was not appreciably different than CNF with 1 M NaCl control WRVs (216.7 ±14.7%) (not shown). Consequently, the interaction between pre-formed coacervates and CNF at 1M NaCl is minimal and does not impact the water retention of the fibers in this scenario. This is consistent with the microscopy results that showed coacervates formed primarily in the bulk and are not closely associated with the CNFs. Likely, this will limit the polyelectrolytes from closing available spaces on the surface of CNF fibril bundles and allow the fibers to retain their water [21,23,208]. Between the PAH first (140 ± 10.5 %) and

PAA first cases (149 ± 12.1 %), the average of the PAH first case is slightly lower. The averages of the two scenarios were compared by performing a t-test with the null hypothesis that PAA first has a higher WRV. With a one-tail distribution, the PAA first case is higher with 94% confidence. Again, these results are consistent with the observations from microscopy, simulations and surface charge measurements that show closer association of the PECs to the fibers when the PAH is added first.

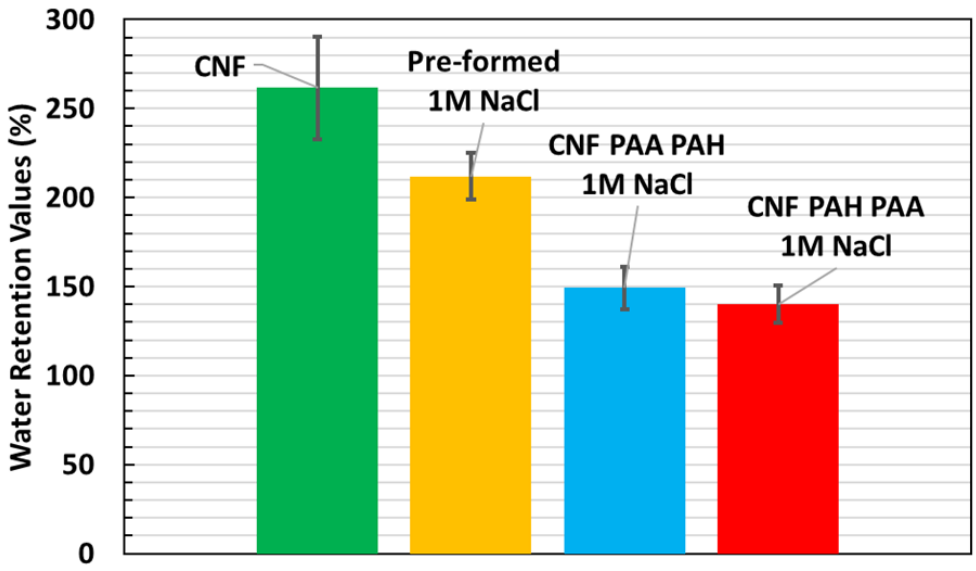

Figure 2-13. Water retention value data for 0.5 wt.% CNF, 1 M NaCl, and 50 mM total polyelectrolyte concentration. The order-of-addition of the polycation first (PAH), polyanion first (PAA), or pre-formed coacervates was varied. WRVs of 0.5 wt.% CNF samples with and without 1 M NaCl are shown for comparison.

2.3 Conclusions

In this study the coacervate formation between the PAA and PAH PECs and negatively charged cellulose nanofibrils were investigated. Optical microscopy, fluorescence microscopy, surface charge analysis and simulations, showed that the order-of-addition of the PAA and PAH to the CNFs affects the association of the PECs to the

fibers, both the extent of the association and the time it takes for the coacervates to fully associate with the fibers. Specifically, when pre-formed coacervates were used, there was a loose association to the fibers, and it took up to 3 days for full agglomeration. In contrast, when the polycation was added to the slightly negatively charged CNFs first, there was significantly more association of the coacervates to the fibers and they were mostly fully associated by the 40-minute timepoint. This behavior is driven by the electrostatic interactions between the polymers and the surface of the CNFs, as shown using electrophoretic mobility measurements and MD simulations.

The relevance of this to the paper industry is related by the measurement of the water retention values for CNFs mixed with PECs and showed that the WRV was not significantly different for pre-formed coacervates compared to the control sample and was lowest for the case where the polycation was added first. This is consistent with the experimental examination of coacervate association with the CNFs, as the WRVs are expected to be lower when the polyelectrolytes can interact with the cellulose fibers in a way that allows for decreasing available surface area in terms closing pores in the form of interfibrillar spacing and increasing free space that water can drain through with appropriate flocculation of the fibrils. These studies on the interactions between polyanions, polycations and CNF will have impact on formulation design thinking for improving drainage and water retention in paper manufacturing. More broadly, this work improves the understanding how order-of-addition as a formulation decision to tune interactions, not just polyelectrolyte charge and structure, plays a significant role in polyelectrolyte complexation and interactions with particles from the molecular scale.

CHAPTER 3. SELECTION OF POLYCATIONS AND IONIC STRENGTH IN POLYELECTROLYTE COMPLEXES AS A FORMULATION STRATEGY TO OPTIMIZE WATER RETENTON VALUES

This chapter is adapted from a manuscript submitted for publication:

Khan, N., Renfroe, A., Von Grey P., Witherow, H., Brettmann, B.K., The influence of electrostatic interactions of polycations in polyelectrolyte complexes on water retention values of cellulose nanofibers. Manuscript submitted.

This study utilizes the WRV technique developed in the previous chapter, where the technique was used to tie the results of the molecular scale effects of order-of-addition of PAH and PAA on PEC coacervate phase association to CNFs to testing that is more relatable to the paper industry. Besides order-of-addition, the selection of polycation in a PEC system is important in tuning properties of a slurry formulation for improved water retention. Because individual polyelectrolytes have unique characteristics based on their chemical structure that influence the properties they impart to cellulose slurries, examining a broad range of polyelectrolytes is valuable for designing formulations for improved drainage and WRVs.

In this work, three readily available polyamine polycations were complexed with the polyanion polyacrylic acid (PAA) to show reductions in water retention values (WRVs) of CNF mats related to electrostatic interactions. The relative hydrophobicity of the polycations was also determined and ranked using turbidity testing. Furthermore, PECs

can form in two phases (solid precipitates and liquid coacervates) and the phase behavior needs to be understood in the context of how it influences the WRV. Finally, how the selection of polycation and the electrostatic interactions influence the retention of water in cellulose nanofibers (CNFs) has not previously been studied. Consequently, the salt concentration was varied to test regimes where electrostatic interactions dominate and regimes where charges are screened so that other molecular interactions such as hydrophobicity control the polymer behavior. The WRVs were tested with PECs away from charge-match ratio (4:1) to reduce the number of intrinsic ion pairs that can form between PECs and with fibers.

For a further comparison, a known coacervate-forming polycation: Poly[2-(dimethylamino)ethyl methacrylate (PDMAEMA) was also complexed with PAA and the WRV was tested. A combination of attributes makes this polyelectrolyte different than the other three polyamines tested here, including the structure of its pendant groups, the presence of oxygen in the functional group, and a choice of a larger MW. The larger MW would likely favor a bridging, rather than a charge-patch mechanism, when added to CNF fibers. This is known to influence the flocculation and aggregation behavior of fiber networks. It can also form coacervates at low-salt concentrations, unlike the other polycations tested here so was included in the study. This will be discussed separately from the other three polycations.

By studying these different PECs under changing experimental parameters, how PEC formulations can improve WRV with CNFs for better design of cellulose slurries can be evaluated.

3.1 Materials and Methods

3.1.1 Cellulose nanofiber selection

The same CNF lot (90% fines) used in Chapter 2 was used for this study and prepared in the same way including a two-day dialysis. All CNF was taken from the same lot (Lot#U35), from the same storage conditions, and dialysis time to minimize variability between sources. Because variability is a significant challenge in the use of natural products [12,49], further discussion and characterization of these CNFs can be found in Chapter 2.

3.1.2 Polyelectrolyte selection

Weak polyamine polycations of low molecular weight with tunable ionization with pH were used in this study (Figure 3-1). Polyacrylic acid (PAA) sodium salt (degree of polymerization, N≈638, molecular weight (MW) ≈60,000 g/mol and PDI=2.4) in a 35 wt.% aqueous solution and polyvinyl amine hydrochloride (PVAm) powder (N≈314, MW=25,000 g/mol) were purchased from Polymer Sciences, Inc. The PDI was not available for PVAm from the supplier and not separately measured. Complexation in this study was conducted at measured maximum turbidity for "charge-match" and greatly deviated at 4:1 polycation to polyanion monomer units for "away-from-charge-match" to minimize influences of large MW differences between oppositely charged chains. However, based on reported synthesis routes for PVAm [213–216], the PDI may be expected to be greater than 1.28 [215,216]. Polyallylamine hydrochloride (PAH, N≈ 186, MW=17,500 g/mol and PDI=1.28) and polyethyleneimine hydrochloride (PEI, linear, N≈251,

MW=20,000 g/mol and PDI ≤1.4) were purchased as powders from Sigma Aldrich. Poly[2-(dimethylamino)ethyl methacrylate (PDMAEMA, N≈157, MW≈75,500 g/mol and PDI=1.12) was purchased from Polymer Source, Inc and used as is. Molecular weights are average values listed by the vendor in the Table 3-1 below. The use of low molecular weight polycations favors a charge-patch mechanism in terms of adsorption to the fibrils [146,147]. PEI and PAH were used as received. PVAm was dissolved in DI water and filtered using a 0.22-micron Milli-Q hydrophilic PVDF filters to remove visible particulates. The filtered solution was dried and used to prepare solutions for testing.

Stock solutions were prepared in 0.5 M or 10 mM polyelectrolyte concentrations based on the concentration of the monomer unit. Solutions were made in deionized water from a Milli-Q water system at a resistivity of 18.2 MΩ*cm and pH was adjusted as necessary, using small volumes of hydrochloric acid (HCl) or sodium hydroxide (NaOH).

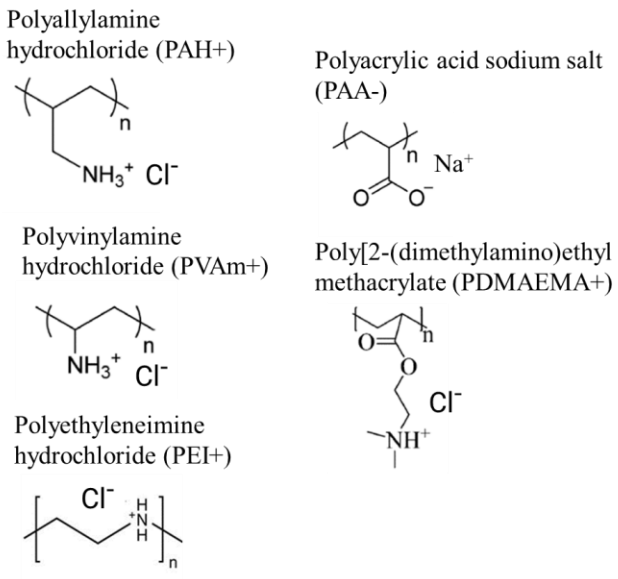

Figure 3-1. Structures of polyelectrolytes used to for polyelectrolyte complexes in this study. Individual polycations were complexed with the polyanion polyacrylic acid salt.

Table 3-1. Polyelectrolytes used to study WRV behavior and their key characteristics.

Polycation	**Characteristic**	**Molecular Weight**	**Calculated % ionization (pH value at which ionization was determined)**
Polyallylamine hydrochloride (PAH+)	Primary amine	17.5 kg/mol	99% (pH 6.5)
Polyvinyl amine hydrochloride (PVAm+)	Primary amine	25 kg/mol	99% (pH 6.5)
Polyethyleneimine hydrochloride (PEI+)	Secondary amine	20 kg/mol	99% (pH 5.3)
Poly[2-(dimethylamino)ethyl methacrylate (PDMAEMA+)	Tertiary amine	75.5 kg/mol	95% (pH 6.3)
Polyacrylic acid sodium salt (PAA-)	Carboxylic acid	60 kg/mol	99% (pH 6.5)

3.1.3 Cellulose nanofibers and polyelectrolyte complex mixing procedure

3.1.3.1 Polyelectrolyte complex samples

PECs were prepared by mixing the stock solutions of the polycation and polyanion with appropriate amounts of 5 M NaCl solutions and water, which were also adjusted to

pH ~6.5 using HCl or NaOH. The final mixtures were either 5 mM total polyelectrolytes for PEC turbidity studies and electrophoretic mobility testing or 50 mM total polyelectrolyte concentrations for WRVs and microscope images. PEI was adjusted to a pH of 5.3, where it is fully ionized. It has been shown that for the formation of PECs, the ionization of the polycation at a given pH is more important than the differences of the pH between the oppositely charged polyelectrolytes [114,120,122]. For all the studies the order-of-addition was CNF, water, salt solution (if needed), polycation and then polyanion. As shown in chapter 2 that this sequence of addition with polycations added first gives the lowest WRVs [136].

When preparing samples with PECs, the polycation and polyanion were added in terms of their mixing molar ratio, which is expressed by the molar fraction of polycation:

$$f = \frac{n\,(polycation)}{n\,(polycation) + n\,(polyanion)} \tag{4}$$

where *n* represents the molar amount of monomer units of either polycation or polyanion. Similarly, charge ratio is defined as *n* (polycation): *n* (polyanion). Therefore, samples prepared "away-from-charge-match" were done at 4:1 charge ratio and mixing molar ratio (*f*=~0.8). Specifically, the samples prepared at 4:1 charge ratio were prepared at *f*=~0.77 PAH/PAA, *f*=0.8 PVAm/PAA, and *f*=0.8 PEI/PAA. Samples prepared at "charge-match ratio" were prepared based on the results of turbidity testing where the ratio at maximum turbidity indicates a 1:1 polycation: polyanion monomer interaction.

3.1.3.2 Cellulose nanofibers and polyelectrolyte complex samples

The CNF stock was first sonicated for 10 minutes and then vortexed before using. The required amount of water was added to the CNF, then vortexed for 30 seconds, followed by the required amount of 5 M NaCl, and then vortexed for 30 seconds. The first 0.5 M polyelectrolyte was added dropwise to CNF mixture while on the vortex mixer at 1500 rpm, then vortexed for an additional 30 seconds at 3200 rpm. This was then pipetted in and out 20 times for full mixing. The last polyelectrolyte was also added dropwise on the vortex mixer, vortexed for another 30 seconds and pipetted in and out 20 times. For the pre-formed samples, the CNF was added last, vortexed 30 seconds and pipetted in and out 20 times.

3.1.4 Turbidity testing

3.1.4.1 Turbidity testing for identification for maximum complexation polycation to polyanion ratio

Turbidity testing was used to identify which ratio of the polycation to PAA led to maximum turbidity Figure 3-2 , which has been shown previously to indicate maximum complexation [138,169]. These ratios of polycation to polyanion were then used for WRV studies after confirming a neutral electrophoretic mobility of the PECs with CNFs, also indicative of maximum complexation. Samples of 325 μL and 5 mM total PEC concentration were prepared and plated in triplicates of 100 μL each. All samples were prepared with 10 mM polyelectrolyte solution, salt, and deionized water stock solutions. Water and salt were added together first and vortexed for 15 seconds at 3200 rpm. PAH was always added first to the saltwater solution and vortexed for 30 seconds at 3200 rpm. PAA was added last and vortexed for 30 seconds at 3200 rpm. Three samples were run and

averaged. Corning ultra-low attachment surface 96-well plate microplates were used. A plate reader equipped with a UV spectrophotometer (BioTek Synergy H4 micro plate reader) was used at a wavelength of 550 nm for the turbidity measurements following methods of other reported studies [136,138]. Samples were run on the plate reader immediately after preparation. Turbidity was calculated from $T = \ln(I/I_0)$, with I=intensity of light passed through sample volume and I_0= incident light intensity.

3.1.4.2 Turbidity for ranking hydrophobicity of polycations

Turbidity measurements were also used to rank polycation hydrophobicity in the uncharged state. Approximately 3.5 mg of solid polycations were dissolved in DI water and the volume of water was adjusted to vary the concentration in mg/mL. The initial pH of the starting solutions was acidic (< pH 5) and not turbid. Then 100 μL of 5 M NaOH solution was added twice (total of 200 μL) and vortexed at 1500 rpm for 10 seconds, leading to solutions of pH>12 where polyelectrolytes are uncharged. The final concentration reported in mg/mL includes the volume of NaOH. Samples at multiple concentrations of polycation were prepared until the solution was turbid, indicating insolubility. The solutions were plated and read in the plate reader at a wavelength of 800 nm where higher concentrations of polycation do not absorb. Samples were prepared in triplicates. The absorbance values were converted to turbidity units. Microscope images were taken in an inverted Leica DMi8 microscope using transmitted light mode, HC PL FLUOTAR 20 or 50x objective lenses, and Leica DMC2900 camera.

3.1.5 Electrophoretic mobility

Electrophoretic mobility testing was used to confirm the concentration at which the CNF was beyond the fiber saturation point and the surface is saturated from the adsorption of the polycations. Samples were prepared at 0.05 wt.% CNF in a 1 mM NaCl solution and appropriate concentration of polyelectrolytes. For CNF+PEC samples a total of 5 mM PECs were used. The method was also used to confirm the charge of the CNF+PECs at polycation: polyanion ratio of 1:1 and 4:1.

Electrophoretic mobility values were measured using a Zetasizer Nano Z (Malvern Instruments, Ltd., Worcestershire, UK) with a capillary cell setup. The instrument temperature was equilibrated to 25°C for 30 seconds before running samples. Data was an average of six measurements per sample. A maximum of 100 sub-runs were taken per measurement. Each sample was 750 µL and three samples were averaged.

3.1.6 Water retention values

Water retention values were taken with the same method as described in Chapter 2. Samples were prepared with a total CNF concentration of 0.5 wt.% and 50 mM total polyelectrolyte concentration unless otherwise specified.

3.1.7 Microscopy and imaging

PEC samples were imaged in optically clear Corning ultra-low attachment surface 96 well microplates using a using a Leica DMi8 inverted microscope in transmission mode. For 50 mM PEI/PAA samples at 0 M NaCl, samples were centrifuged first to collect and pipette enough to visualize. Approximately 40 µL of the samples were pipetted into a 96 well plate. Images were taken at the center of the individual well.

CNF-PEC samples in slurry form were imaged with an optical scanner in a flow cell designed for imaging cells and bacteria. Samples were prepared at the same concentrations and method as the starting slurry for the WRV studies. Approximately 0.2 mL of sample was taken up by a 1mL disposable syringe and placed into a IBIDI µ-slide VI 0.5 glass bottom flow cell. Samples were scanned on an Epson Perfection 3490 Photo scanner in gray scale and reflective mode.

3.2 Results and Discussion

3.2.1 Determination of maximum complexation of polyelectrolyte complexes

Turbidity testing was used to assess the ratio at which the maximum complexation of polycation to polyanion is observed. Maximum complexation is marked by a maximum turbidity and occurs at polycation to polyanion monomer ratio of 1:1 [138,169,217,218] where insoluble complexes form [131]. Away-from-charge-match, the turbidity decreases from the formation of smaller complexes [169], a lower overall concentration by weight of insoluble complexes [120,122], the overall complex considered more soluble [219], or a change in phase of the complex which has been observed [122,131].

As can be seen in Figure 3-2 A, maximum turbidity was achieved at a ratio of 0.4 mol/total mol of polyelectrolytes for PAH/PAA (meaning that 0.4 moles of PAH based on monomer unit and the remainder 0.6 moles of PAA was added) and 0.5 mol PEI/total polyelectrolyte. PVAm/PAA formed large precipitates that tended to aggregate and settle to the bottom of the well plate as seen in Figure 3-2 A. Consequently, the ratio of maximum turbidity was not easily identified with this technique or microscopy. To ensure that ratios used were appropriate, electrophoretic mobility testing was performed with 0.05 wt.%

CNFs with the same concentration (5 mM total PEC) and ratio of polycation to polyanion as the turbidity testing. When both the turbidity is maximum and the electrophoretic mobility or zeta-potential are near or at a value of zero, maximum complexation is confirmed [72]. Electrophoretic mobility results are discussed in the section below. These ratios were used to further prepare samples for WRV testing.

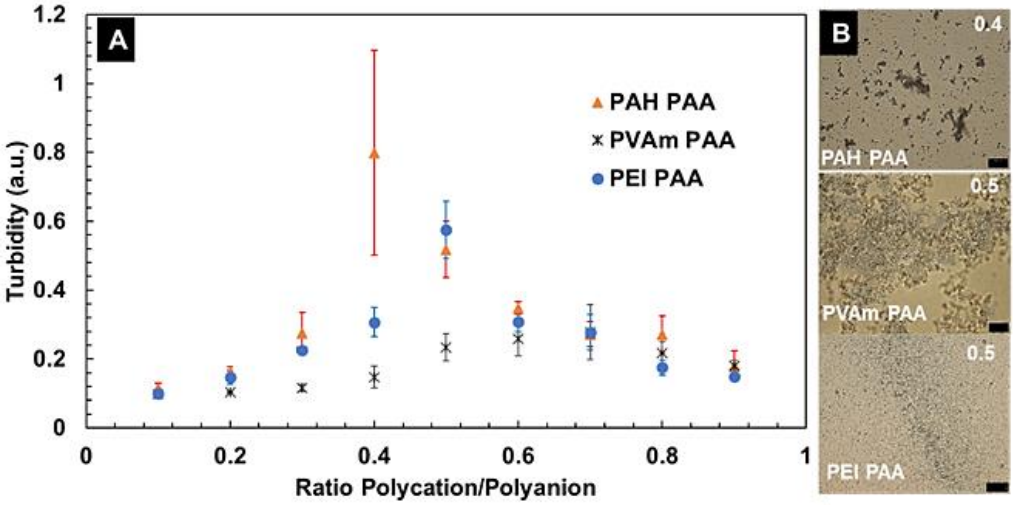

Figure 3-2. Turbidity of 5 mM PECs versus ratio of polycation to polyanion (PAA) (A). Micrographs of PECs at the polycation to PAA ratio corresponding to maximum turbidity (B).

3.2.1.1 Turbidity testing to determine polycation hydrophobicity

While each of the polyamine polycations here differ in the number of methyl groups in either their backbone or pendant group, the hydrophobicity of the polymer cannot be assumed based on functional groups. Consequently, turbidity testing was conducted to determine the hydrophobicity ranking of the polycations used here relative to each other. Turbidity indicates the presence of suspended particles in solution that can scatter light. For polymers, turbidity has been used evaluate macroscopic phase separation and to

understand hydrophilic to hydrophobic transitions of polymer systems that have LCSTs [220,221] and cloud point phase separations [73]. Furthermore, Li et al. measured the turbidity of polyacrylic acid (PAA) at an acidic pH and polyallylamine hydrochloride (PAH) at a basic pH (9) where the protonation of these were low, to understand their solubility in solution due to hydrophobicity of the chains [222]. In preparing polycation samples, the solutions had enough NaOH (pH >12) so that the polycations are no longer protonated and solubility in solution due to the presence of the charged amine group was eliminated.

As seen in Figure 3-3, PEI became turbid at the lowest concentration of 5.5 mg/mL and formed aggregates in solution. At 11.7 mg/mL, PVAm and PAH were still clear. From this, PEI can be considered the most hydrophobic in this study. At 12.5 mg/mL, PVAm had a slightly higher turbidity than PAH but by 14.6 mg/mL the turbidity for both were approximately the same. Consequently, PVAm can be considered slightly more hydrophobic than PAH. While PAH has another methyl in its structure than PVAm, it did not show a significance increase in hydrophobicity based on these results. This may be in part from the slightly higher average molecular weight of PVAm (25kg/mol) compared to PAH (17.5 kg/mol).

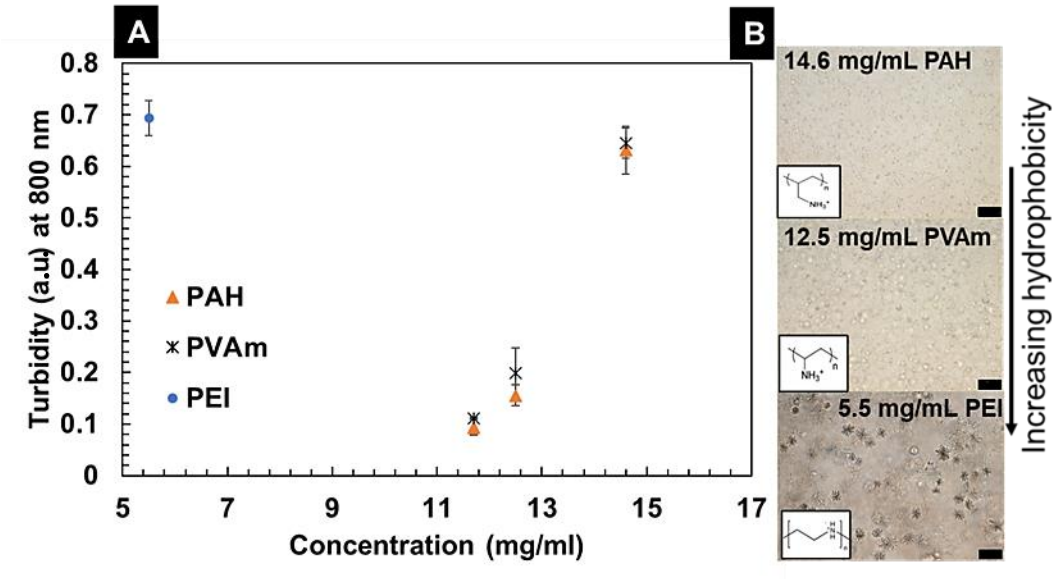

Figure 3-3. Turbidity versus concentration of polycations in mg/mL at pH >12 (A). Micrographs of PEI, PVAm, and PAH at corresponding polycation solution concentrations where they are turbid (B).

3.2.2 Electrophoretic mobility to determine polyelectrolyte complex concentrations and ratios

To confirm full adsorption of polycations to the CNF and that excess polycation would be available to form PECs in solution, electrophoretic mobility testing of 0.05 wt.% CNF with increasing polyelectrolyte concentrations was performed as in Chapter 2. Figure 3-4 shows the electrophoretic mobility with increasing concentration of the increasing polycations based on monomer units. As expected, increasingly negatively charged PAA did not further decrease the surface charge of negatively charged CNFs. Also, as expected, electrophoretic mobility increases with increasing polycation concentration [146,166,181]. The charge neutral concentration (neutral electrophoretic mobility) was achieved near 0.02 mM polyelectrolyte (0.015, 0.02, and 0.025 mM for CNF with PEI, PAH, and PVAm,

respectively). Beyond this, adsorption to the surface continues to increase logarithmically before plateauing at the saturation point [166]. As seen in Figure 3-4, at 2.5 mM polycation addition to 0.05 wt.% CNF, the fibers are well beyond charge neutral and saturation with the addition of all three polycations and the excess is in solution and would be able to form PECs with the addition of oppositely charged polyanion. Given that these measurements must be performed at a dilute CNF concentration, to scale the amount of polycation to be appropriately added to 0.5 wt.% CNF for WRV tests, 25 mM polycation was further added for polycation control tests and 50 mM for PEC samples. Therefore, the concentrations of polyelectrolytes and PECs for WRV testing to correspond the results of electrophoretic mobility data where the surface of the fibers are completely saturated and in excess.

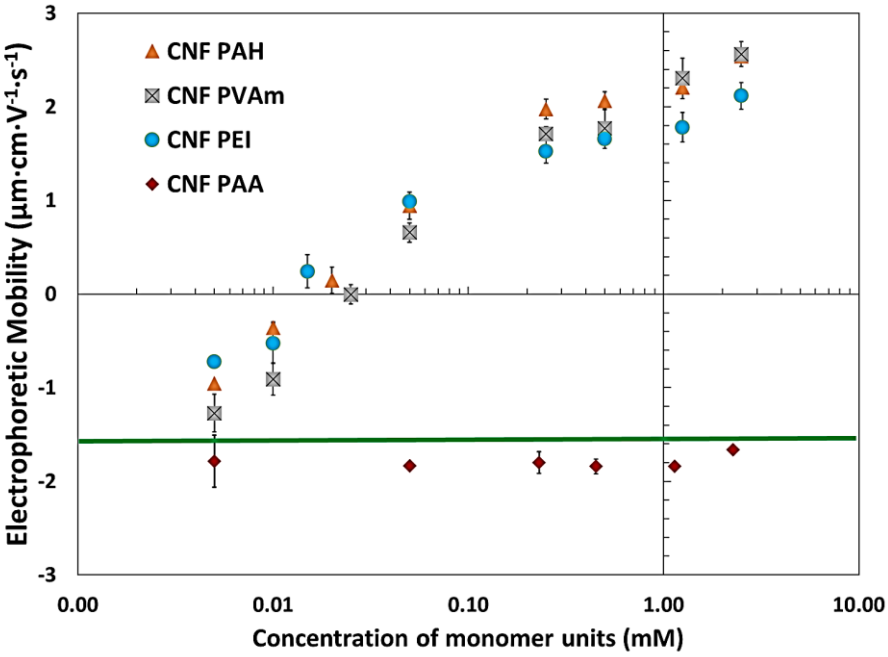

Figure 3-4. Electrophoretic mobility of 0.05 wt.% CNF, 1 mM NaCl, and increasing polyelectrolyte concentration in molar of monomer unit. The green line indicates CNF control.

As mentioned, WRV samples were prepared with PECs that correspond to both a maximum turbidity and a near zero electrophoretic mobility. The polycation to polyanion ratios where electrophoretic mobility was near zero (0.06 ± 0.91, -0.05 ± 0.67, 0.51 ± 0.04 µm·cm·V^{-1}·s^{-1}) were 0.5, 0.5, and 0.4 ratios for PAH/PAA, PVAm/PAA, and PEI/PAA, respectively. These ratios were used for WRV testing going forward unless otherwise specified. For "away-from-charge-match" samples made at 4:1 polycation: polyanion, the electrophoretic mobilities were for CNF with PAH/PAA, PVAm /PAA, PEI/PAA were 1.64 ± 0.02, 2.59 ± 0.05, and 2.22 ± 0.13 µm·cm·V^{-1}·s^{-1}, respectively.

3.2.3 Water retention values of cellulose nanofiber controls

Because these samples are multicomponent and WRV testing responds to different factors, several control experiments were necessary. First the WRV of CNF of increasing concentration was tested. Figure 3-5 showed that WRV decreases with increasing CNF slurry concentration. This behavior has been observed with partially-dried paper samples of pulps of larger fibers [178] and CNF [27] and is believed to be indicative of changes in the specific surface area within the slurry and overlap of the fibers [178]. While increasing the concentration of fibers in the solution also means increased initial mass of the fibers in the fiber pad, the increased concentration of fibers also allows for an increased number of contact points between the fibers upon drying [178]. This leads to densification and a collapse of interfibrillar pores [21]. Going forward, 0.5 wt.% CNF was chosen for the remaining testing with polyelectrolytes.

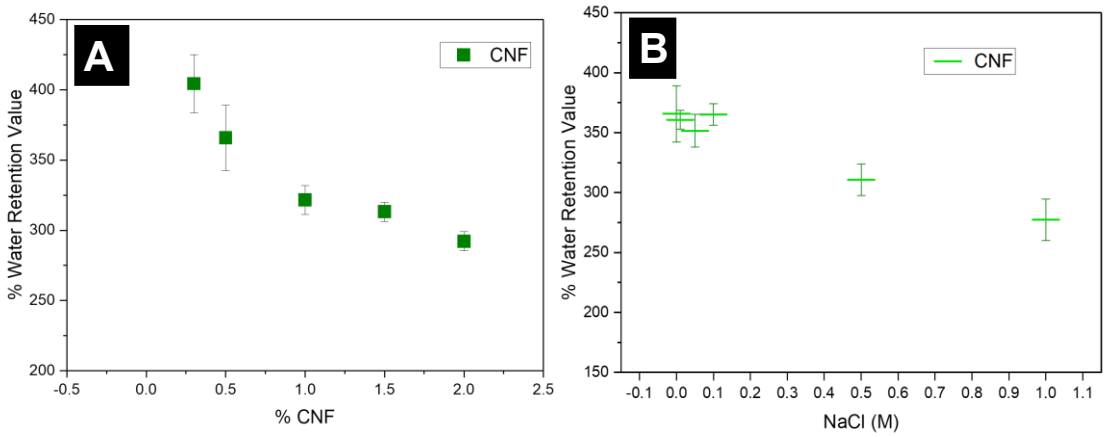

Figure 3-5. WRV of CNF slurries with increasing CNF concentration (A) and increasing sodium chloride concentration of 0.5 wt.% CNF slurries (B).

The influence of electrostatic interactions on the WRVs of 0.5 wt.% was tested with increasing salt up to 1 M NaCl, as seen in Figure 3-5. Here the WRVs are higher at low-salt concentrations and decrease with increasing NaCl, particularly at 0.5 and 1 M NaCl.

Given that the fibers are negatively charged, the electrostatic screening of negative surface charges on the CNF can allow for a reduced swelling [52] and consequently decrease the WRVs, which has previously been seen for pulps of larger fibers [180].

3.2.4 Water retention values of cellulose nanofiber with polyelectrolyte controls

The WRV of CNF samples were tested with single polyelectrolytes. As mentioned, the polycation concentration and adsorption was confirmed by electrophoretic mobility. The selected polyelectrolyte concentration, 25 mM polycation is significantly past the saturation point for 0.5 wt.% CNF concentration. As seen in Figure 3-6 B, the WRVs of 0.5 wt.% CNF with the PAA polyanion (25 mM) and the polycations PEI, PVAm, and PAH (25 mM) were measured. The WRVs with the individual polyelectrolytes decreased with increasing salt concentration in the same manner as the CNF-only samples with similar values. There was no appreciable improvement in the WRV at any salt concentration with any polyelectrolyte on its own. This is consistent with much of the WRV literature that has shown polycations alone [181] beyond charge reversal concentration or polyelectrolytes complexed in a LBL regime do not appreciably improve (decrease) WRV when dosed beyond charge neutral point. The results confirmed that the addition of polycations only did not improve WRV compared to the CNF alone.

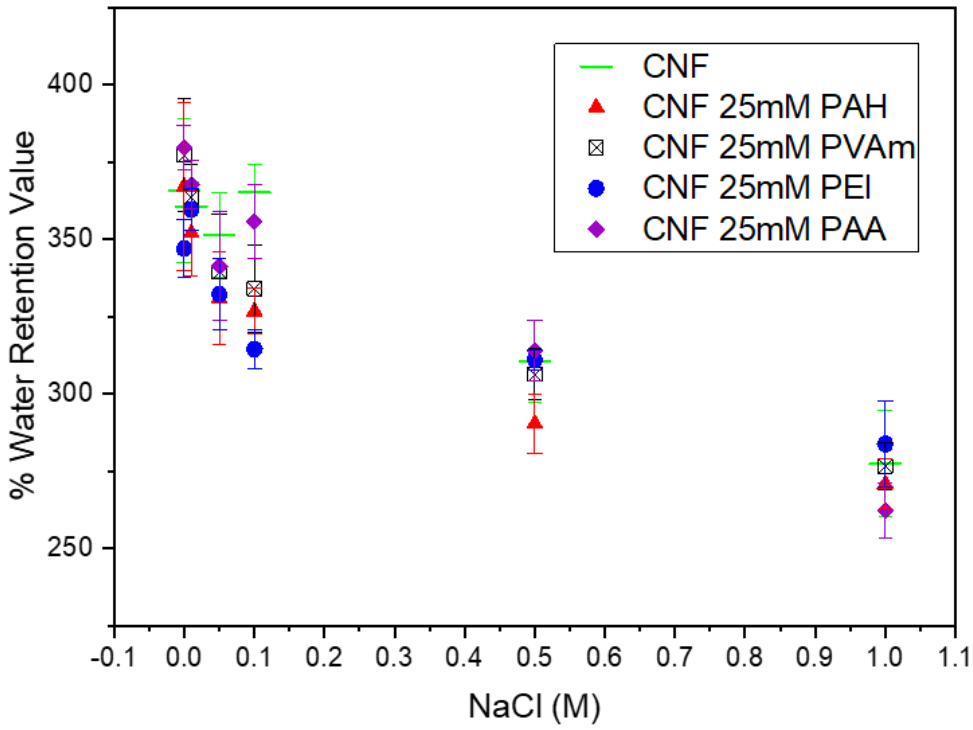

Figure 3-6. WRV of 0.5 wt.% CNF with 25 mM total polyelectrolyte concentration by unit with increasing NaCl concentration.

Because the purpose of this study was to understand the role of the PECs on WRVs, the concentration of polycations chosen had to be in excess. As a comparison, the WRVs of CNF with a total PEC concentration in the LBL regime was additionally measured. Here there are no excess PECs in solution (0.5 mM PECs) at 0 and 1 M NaCl and the concentration is slightly above the charge neutral point (electrophoretic mobility near zero). The results were 376.2 ± 8.2, 377.4 ± 12.6, and 367 ± 12.8 at 0 M NaCl and 259 ± 5.9, 258.2 ± 7.6, 259.9 ± 9.6 % at 1 M NaCl for PAH/PAA, PVAm/PAA, and PEI/PAA, respectively. These were similar to the CNF-only WRVs of 365.8 ± 23.4 % at 0 M NaCl and 277.3 ± 17.3 % for 1 M NaCl. This confirms that changes of WRVs of 0.5 wt.% and 50 mM PECs were due to the presence PECs in the network.

These control studies indicated that the 0.5 wt.% CNF slurries are a sufficient control for analysis during the remainder of this study and that any improvements are due to the PEC in the system, not the polyelectrolytes alone.

3.2.5 Water retention values of cellulose nanofibers with polyelectrolyte complexes at charge-match ratio at 1:1

To understand the influence electrostatic interactions and the selection of polycation within a PEC, WRV of CNFs with 50 mM total PECs were first tested at the polycation to PAA ratio with maximum turbidity and near zero electrophoretic mobility. Figure 3-7 shows the WRVs of 0.5 wt.% CNF with 50 mM total PEC for PEI: PAA, PVAm: PAA, and PAH: PAA with increasing NaCl concentration from 0 to 1 M NaCl (plot is split into 0-0.1 M and 0.5-1 M to show detail). Figure A. 1 in the appendix shows all data on a single plot. As was seen with the control samples, the WRVs with PECs decrease with increasing salt concentration. The WRVs are either lower or higher than the controls depending on the salt content. Consequently, the results can be further discussed in two regimes: low-salt regime from 0 to 0.1 M NaCl (Figure 3-7 A) and a high-salt regime at 0.5 and 1 M NaCl (Figure 3-7 B).

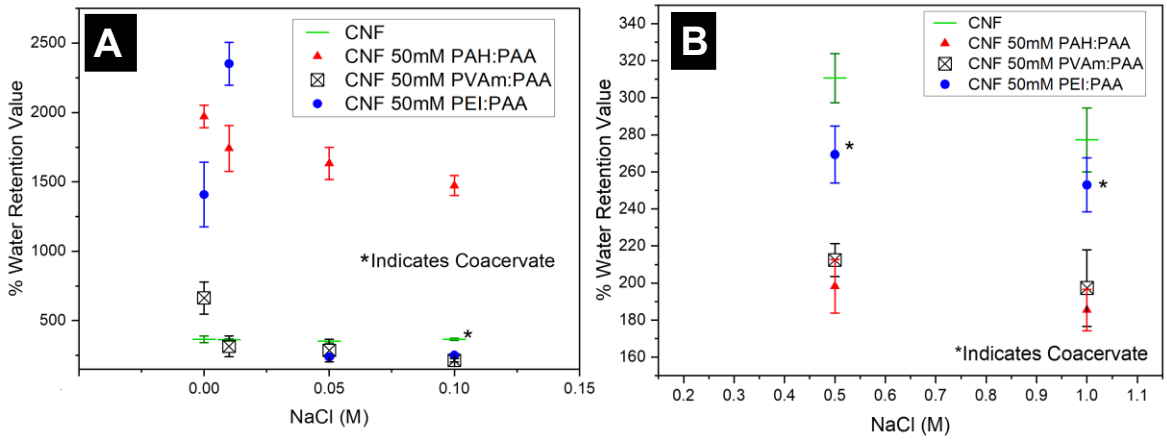

Figure 3-7. WRV of 0.5 wt.% CNF and 50 mM polycations (PEI, PVAm, and PAH) with PAA at maximum turbidity with increasing salt at low (0-0.1 M NaCl) salt regime (A) and high-salt (0.5-1 M NaCl) regime (B). The salt concentrations at which coacervate-like phase were detected for PEI/PAA is noted by *.

For all three polymer systems at 0 M NaCl in the low-salt regime, the WRV is significantly higher than the control and a large standard deviation in values is observed (Figure 3-7 A). As seen in the image in Figure 3-8 A, after centrifugation, for 0 M NaCl samples, water remains at the top of the fibrils, or the fibrils do not fully form into a mat but instead remain in a wet pulp-state (Figure 3-8 B). Here the PECs, which were prepared at maximum complexation (1:1 ratios), can be hypothesized to behave as fines that prevent water from going through the fibers and lead to densification of the forming fiber pad, thereby retaining significant amounts of water. Similar behavior was seen by Hubbe et al. in a system with polyampholytes, where the highest WRVs corresponded with the highest turbidity at a neutral pH for a high charge density polyampholyte and fiber system [182]. They saw membrane plugging, which confirmed that the polyampholyte molecules formed associative structures large enough to block the fiber pad or membrane pore [182].

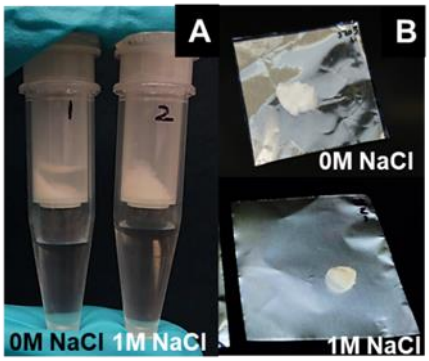

Figure 3-8. Photographs of WRV samples of 0.5 wt.% CNF PAH/PAA at 0M and 1 M NaCl after centrifugation (A) and after centrifugation and before oven-drying (B).

As the salt concentration increases from 0 M to 0.1 M NaCl in the low-salt regime, all PEC and CNF mixtures show a decrease in the water retention values and both the PEI and PVAm PEC and CNF systems have a WRV that is lower than the CNF control by 0.1 M NaCl. This decrease in WRV is likely due to a combination of a de-densification of the PECs with increased screening of electrostatic interactions of the polymers and decreased sticking of the PEC particles to the cellulose fibers from screened interactions between the adsorbed polycation and the PECs. In this complex system, it is not possible to deconvolute these factors, and both are likely contributing. In addition, the PEI/PAA complexes became more liquid-like at 0.01 M and 0.1 M NaCl (Figure 3-9), compared to the precipitates present at 0 M NaCl. This phase change behavior from very small precipitates that act as fines to liquid-like droplets may lead to the sharp drop in WRV seen for the PEI/PAA complexes.

In the region defined as the high-salt regime, the electrostatic interactions between the polycation and polyanions have been further screened and reduced. This allows for the hydrophobic, polymer structure and other molecular features to play a greater role in

interactions with CNFs (Figure 3-7B). It is seen that with 0.5 and 1 M NaCl, all CNF PEC samples are below the CNF 1 M NaCl control and the most water is retained in the samples with the most hydrophobic polycation (Figure 3-3), decreasing in the order of the polycation hydrophobicity (PEI>>PVAm>PAH). Additionally, as seen in Figure 3-8 A and B, when 1 M NaCl is added, water drained through and formed an intact fiber mat. It may be that, at these high-salt concentrations where attractions between the polyelectrolytes are weak in the complex, the polyelectrolyte backbones that are more hydrophilic lead to more water bound to the polyelectrolytes and a higher WRV. However, there are several other factors that could lead to the differences in WRV between the three polymers including changes in how they adsorb onto the CNFs at these high-salt concentrations [223–225], the differences in polymer stiffness [134], and its effect on swelling of the fiber network and the differences between charges from a primary, secondary and tertiary amine [226]. The clear trend that emerges here is that the screening of the electrostatic interactions is particularly important to obtaining low WRV with PECs.

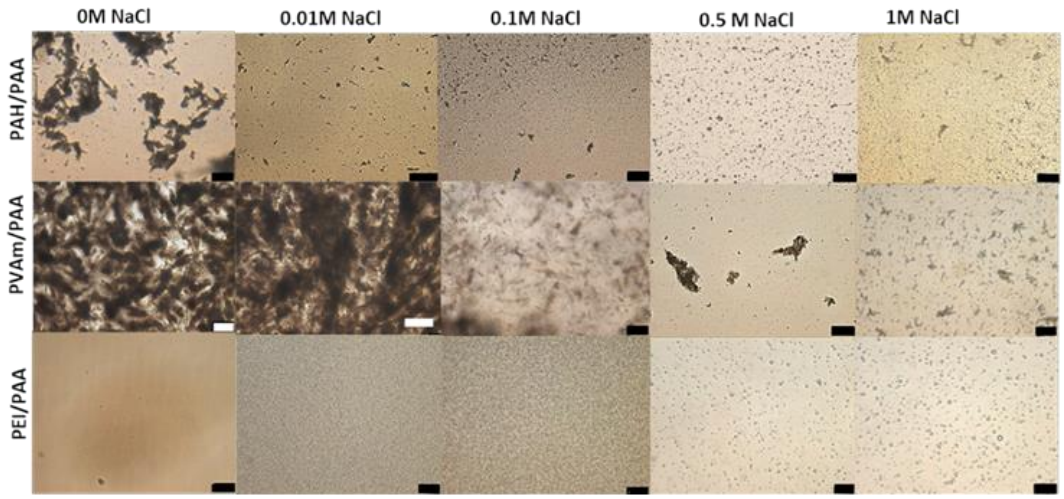

Figure 3-9. Micrographs of 50 mM PECs in solution at maximum turbidity with increasing salt at low (0-0.1 M NaCl) salt regime and high-salt (0.5-1 M NaCl) regimes. Scale bars are 50 µm.

To further understand the connection between electrostatic interactions and the WRV behavior in the low and high-salt regimes, images were taken of the 0.5 wt.% CNF + 50 mM PEC slurries at 0 and 1 M NaCl at the 1:1 ratio (Figure 3-10) in a six-sample flow cell in an optical scanner. This allowed us to visualize their flocculation behavior prior to centrifugation and formation of a fiber mat. From the image, it is clear that the fiber network structure at high-salt (1 M NaCl) is more open in terms of the area between the fibers compared to the conditions with no added salt (0 M NaCl) for all three polyelectrolyte systems. The flocculation and coagulation behavior of fibers with polyelectrolytes [9,140,227] and the network structures they form are tied to improved drainage [33]. Additionally, increased bonding and coagulation has been linked to decreased WRV [178]. In the low-salt regime, at 0 M NaCl for all three PEC combinations, more dense fibril networks can be seen, as marked by brighter and more dense aggregates of CNF and PECs. The brighter PVAm/PAA and PAH/PAA samples show greater scattering of light than the

PEI/PAA at 0 M salt, which is consistent with the very small particle sizes and small number of precipitate particles seen in the PEI/PAA microscope images in Figure 3-9.

In the high-salt regime, at the 1 M NaCl, the aggregation behavior changes such that the highly dense areas are reduced and free space between these is higher. This indicates that there are fewer PEC particles at the high-salt concentrations, leading to more polyelectrolytes in solution, which do not block drainage, can lead to swelling of the network, and may reduce the formation of dense fiber pads. The change in the network to have more free space between CNF bundles also supports the decrease in WRV observed (Figure 3-7), where more water has the potential to drain during centrifugation. The images in Figure 3-10 support the hypothesis that both the screening of the surface charges on the fibers as well as resulting changes in flocculation behavior to the network may correspond to the lower WRVs seen with PECs at high-salt concentrations.

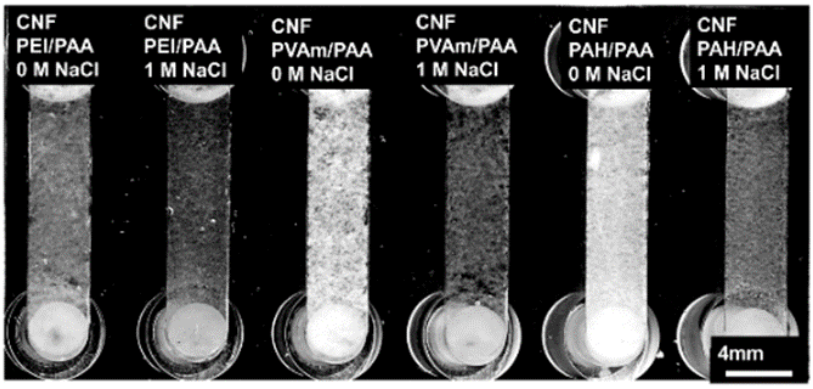

Figure 3-10. Images of 0.5 wt.% CNF and 50 mM polycations (PEI, PVAm, and PAH) with PAA at maximum turbidity ratios at low (0 M NaCl) and high-salt (1 M NaCl) showing variation in flocculation. Samples are in flow cell microscope slides and taken at the same time in a scanner.

3.2.6 Water retention values of cellulose nanofibers with polyelectrolyte complexes "away-from-charge-match"

To further understand the influence of electrostatic interactions in PECs on WRVs, CNF + 50 mM PEC slurries were made at ratios away from the charge-match ratio to reduce the number of intrinsic ion pair interactions between PECs and with the fibrils. This is another strategy to decrease the number of interactions between the polyelectrolytes in the complex but maintain some complexation. Here we examine the PAH: PAA, PVAm: PAA, and PEI: PAA systems at approximately 4:1 polycation: polyanion (f= 0.8), where the polycation is in excess compared to the polyanion at 1:1. As is seen in Figure 3-2, the turbidity values of PAH: PAA, PVAm: PAA, and PEI: PAA at the high polycation: polyanion 4:1 are similar and much lower than that at maximum turbidity for PAH: PAA and PEI: PAA. Reduced turbidity of PECs away-from-charge-match conditions is expected and has been previously observed and is linked to reduced concentrations of PECs and changes in phase behavior [122,219]. Additionally, the electrophoretic mobilities of 0.05wt% CNF with 5mM PAH/PAA, PVAm /PAA, PEI/PAA at these ratios are listed in results section 3.2.2 and indicate that the overall samples are positively charged and away-from-charge-match conditions.

The results comparing the WRVs of CNF with PECs formed at 1:1 and 4:1 charge ratios of PAH:PAA, PVAm:PAA, and PEI:PAA in low and high NaCl concentration regimes are shown in Figure 3-11 A-C (Figure A. 2 in the appendix shows 4:1 ratio WRVs results on one plot). For all three systems at 4:1 ratio and 0 M NaCl, the WRVs are significantly lower than those at 1:1 ratio. For example, the WRV at 0 M NaCl for PAH/PAA at 1:1 is approximately 2000%, while at 4:1 it is approximately 400%. However,

the effects at 0 M NaCl for the PVAm/PAA are not as strong as for PEI/PAA and PAH/PAA as the charge ratio is changed from 1:1 to 4:1. The lower WRV at 0 M NaCl for all systems at 4:1 ratio is likely due to a combination of decreased formation of PEC particles due to fewer intrinsic ion pairs and greater swelling of the network from increased free polyelectrolytes in the system. This may improve the ability of water to flow through a less dense fiber pad.

As the salt concentration is increased, the PAH/PAA and PVAm/PAA coacervate samples follow the same trend at 4:1 charge ratio as they did at 1:1 ratio. Interestingly, at the highest salt concentrations, the WRVs are less than the CNF-only control but are slightly higher for the 4:1 than the 1:1 charge ratio rather than identical, as would be expected for the regime where electrostatic interactions are minimized. The 4:1 ratio samples have more relative mass of polycation than 1:1 so this may be due to specific features of the polycation, such as solubility in water or degree of swelling, but further study is needed to fully understand this phenomenon.

The PEI/PAA polyelectrolyte combination micrographs show significantly different behavior than the PAH/PAA and PVAm/PAA complexes (Figure 3-12), especially at high-salt concentrations. At 0 M and 0.01 M NaCl, moving away-from-charge-match decreases the water retention significantly (Figure 3-11 C), similar to the results seen for the other polyelectrolyte systems. The PEI/PAA complexes at 4:1 charge ratios never show WRVs lower than the CNF-only controls and they essentially have equal WRVs as the controls at all salt concentrations. PEI is the most hydrophobic polycation and has the most flexible backbone, so it is not surprising that it behaves differently than PAH and PVAm. It is possible that at high-salt concentrations, where the charges are

screened, PEI solubility is sufficiently reduced to lead to PEI precipitates, a phenomenon that will be stronger for the 4:1 compared to the 1:1 charge ratios due to the greater amount of polycation. The reduced drainage from these precipitates may be sufficient to lead to WRV similar to the controls but further work is needed to conclusively determine the role of PEI molecular features in the drainage at 4:1 charge ratio.

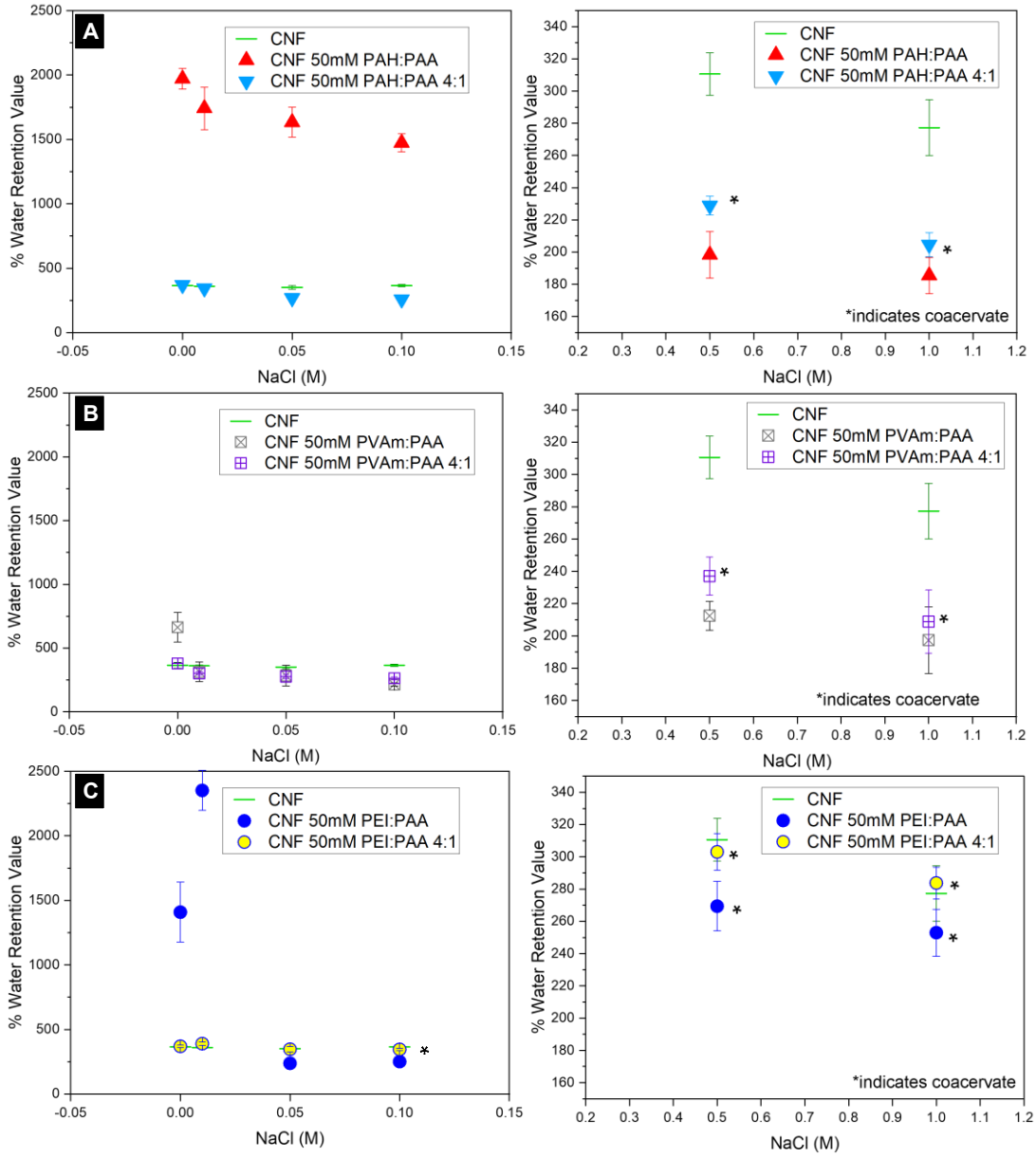

Figure 3-11. WRV of 0.5 wt.% CNF+ 50 mM PECs made at charge-match and at 4:1 charge ratio in low (0-0.1 M NaCl in left column) and high-salt regimes (0.5 and 1 M NaCl in right column) for PAH/PAA at 1:1 ratio (orange triangle) and at 4:1 ratio (blue triangle) (A) for PVAm/PAA at 1:1 ratio (light gray square) and 4:1 ratio. (purple square) (B) for PEI/PAA at 1:1 ratio (blue circle) and 4:1 ratio (yellow circle). Asterisk (*) indicates coacervate-like phase.

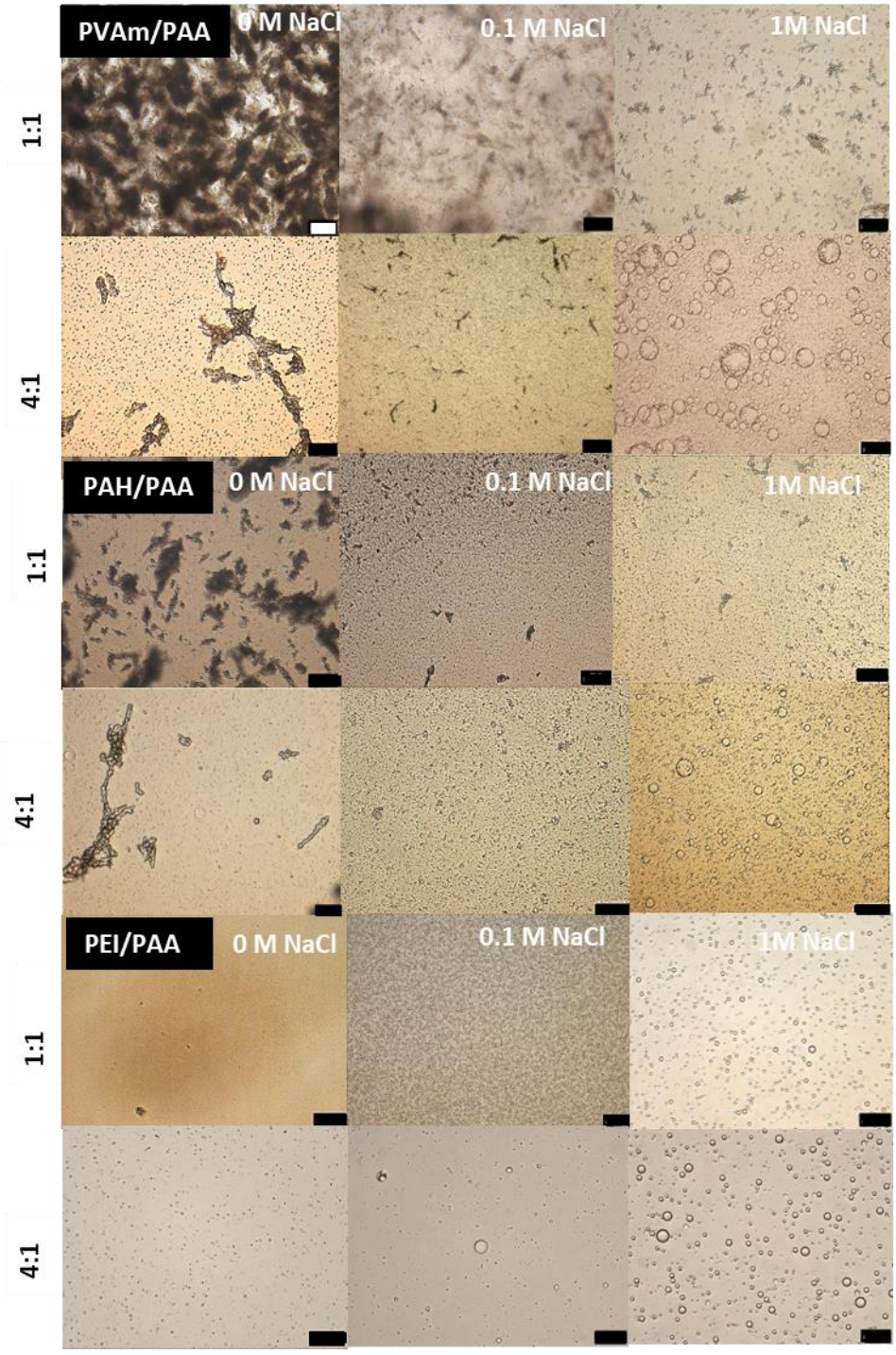

Figure 3-12. Micrographs of 50 mM PECs in solution at 1:1 (charge-match) and 4:1 with NaCl at low-salt regime (0 and 0.1 M NaCl) and high-salt (1 M NaCl) regimes. Scale bars are 50 µm.

3.2.7 Water retention values with PDMAEMA/PAA

Given that all three polyamines in the previous sections formed precipitates at zero and low NaCl concentrations, a different but known coacervate-forming polycation (PDMAEMA) was complexed with PAA and tested for WRV. This served as an initial comparison and direction of future work Because this polycation is notably different than the others in many ways and deconvoluting the factors that influence the WRV is outside the scope of this work. This is serves to add breadth for future selection of polycations in formulation for papermaking.

As with the other systems, turbidity was tested, and it was found that a ratio of 0.5 gave maximum complexation. Electrophoretic mobility data for CNF with PDMAEMA is given in the Appendix (Figure A. 3). As with the other systems, the surface of the fibers was completely saturated and excess PDMAEMA was present in the solution at 25 mM polycation concentration. Consequently, samples were with 0.5 wt.% CNF and 50 mM total PDMAEMA/PAA was used at increasing salt concentrations. The WRV results of CNF with 25 mM PDMAEMA controls at 0 M NaCl was 391± 27.8% (compared to CNF-only at 0 M NaCl at 365.8 ± 23.4%). This is similar and expected to the other controls that suggested that CNF with the polycation alone does not appreciably improve WRVs.

The WRVs for 50 mM PDMAEMA/PAA are shown in Figure 3-13 below. As can be seen in the low-salt concertation regime, the WRVs are significantly improved (decreased) compared to the control. At the high-salt concentration regime, the WRVs, while improved compared to the control, are higher than in the low-salt concentration

regime. Again, this is likely due to a weakening of the electrostatic interactions with increasing salt concentration, which in this case leads to a solution phase and no liquid/liquid phase separation at high-salt concentrations, reducing the effectiveness of the PDMAEMA/PAA in improving WRV. This was supported by the micrographs of the PECs in Figure 3-14, which show that coacervate-like PECs are formed at 0 M NaCl, larger coacervates are formed at 0.5 M NaCl coacervates, and by 1 M NaCl the chains are sufficiently electrostatically screened such that mostly solution phase is preferred and only a few small coacervates can be seen.

It is clear that, unlike the other PECs tested, PDMAEMA/PAA did not lead to a blockage of water during the formation of the fiber pad at 0 M NaCl. This may be because the coacervate phase is favored, even in the low-salt concentration regime and may not form as dense fibril networks as in the other cases. Because these systems are multi-component and a number of different factors can contribute, more investigation would be needed to determine if this can be attributed to the coacervate phase specifically. For example, the longer reported MW would likely favor a bridging, rather than a charge-patch mechanism between the fibrils, which may influence flocculation behavior.

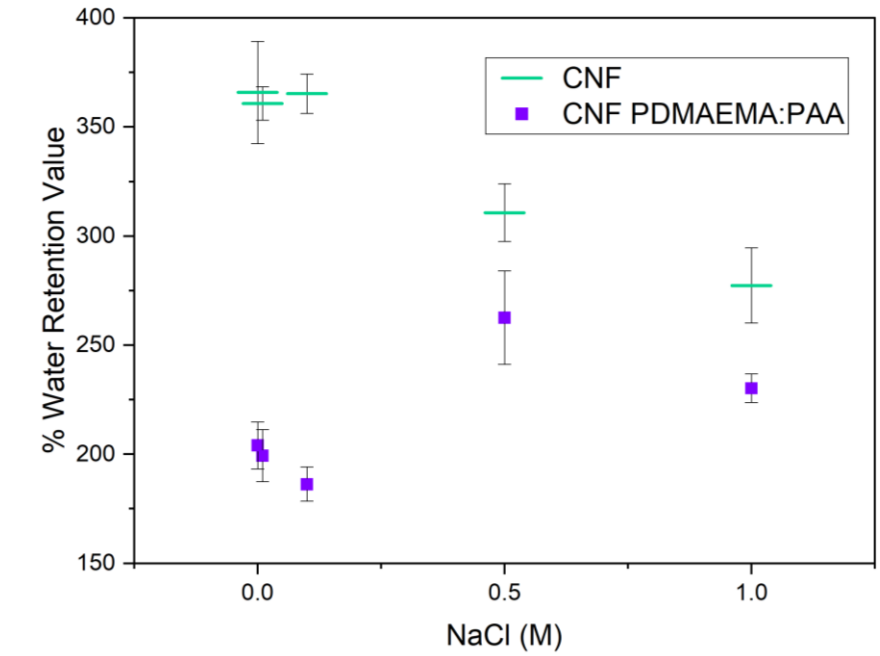

Figure 3-13. WRV of PDMAEMA/PAA coacervate-forming PEC.

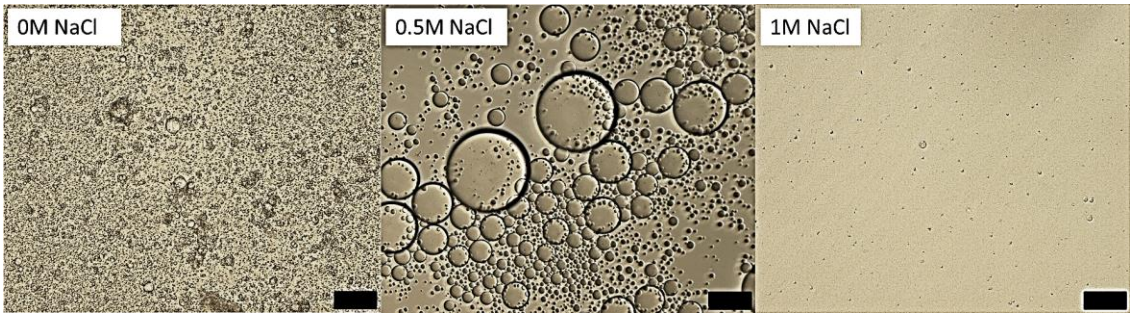

Figure 3-14. Micrographs of 50 mM PDMAEMA/PAA in solution at 1:1 (max turbidity) at low-salt regime (0 M NaCl) and high-salt (0.5 and 1 M NaCl) regimes. Scale bars are 50 µm.

3.3 Conclusions

The appropriate formulation of cellulose with polyelectrolytes is technologically important to improve the sustainability of the paper-making process and the energy it takes to dry paper, particularly with CNFs that are known to be difficult to drain and tend to

retain water. In this study we showed that WRVs of CNF fiber pads with PEC, that exhibit either precipitate or coacervate-like phase behavior, can be tuned by experimentally altering the electrostatic interactions within PECs and PECs with CNFs by increasing ionic strength of the suspension or by reducing the number of intrinsic ion pairs through changing charge-match ratio. The dosing strategy allowed for excess PECs in suspension, so that the response of the PECs with CNFs was investigated and their combined influence on the dewatering was measured by WRVs.

Electrostatic interactions were experimentally changed by either adding salt or changing the charge-ratio between the polycation and polyanion in the PECs, or both. At charge-match conditions and 0 M NaCl concentrations, WRVs of CNFs with PECs of three different polyamines with PAA were significantly above those of control samples and the formation of fiber pads after centrifugation is hindered, preventing water from draining. In general, this behavior was seen at low-salt concentrations (<0.1 M NaCl), but depending on the polycation, the transition from high to low WRV can occur at different added NaCl concentrations. At high-salt concentrations (0.5 and 1 M NaCl), the WRVs were improved and below control values and the values followed a polycation hydrophobicity ranking (PEI>PVAm>PAH) as inferred by measured polycation turbidity at pH values where they are uncharged. At the high-salt concentrations, electrostatic interactions are diminished, and other molecular features, like hydrophobicity based on turbidity, can dominate. Furthermore, reducing the number of intrinsic ion pairs within a PEC by selecting a charge-match ratio of 4:1, did not exhibit the large WRVs at low-salt concentrations that were seen at the charge-match condition.

It can be hypothesized that densification of the fiber pad from the presence of PECs and reduction of fine-like behavior from free PECs is reduced due to increased free polyelectrolytes in the system from NaCl or from off charge-match conditions. This may lead to a swelling of the PECs and creating a more open network structure to allow drainage. These findings show that there are multiple parameters (ionic strength, PEC charge-match ratio, and polycation hydrophobicity) that can be used to formulate and tune dewatering through WRVs.

Another coacervate-forming PDMAEMA/PAA system was tested to serve as an initial comparison to PECs that prefer coacervation rather than precipitation in low-salt regimes. While the presence of PECs has previously been seen to hinder drainage and plugging of membranes of cellulose fibers, exact mechanisms or the conditions that control this behavior have not been well understood. By properly formulating and appropriately balancing electrostatic interactions of a given PEC system with salt or polycation: polyanion ratio, the drainage of a CNF fiber pad, as characterized through WRVs, can be improved.

CHAPTER 4. PREPARATION AND PHYSICAL TESTING OF FIBER HANDSHEETS PREPARED FROM CELLULOSE NANOFIBERS AND POLYELECTROLTYE COMPLEX FORMULATIONS

The goal of this study was to lay the foundation of a method to understand water removal from handsheets made from CNFs with PECs such as those discussed in Chapters 2 and 3. By making and testing paper samples of a softwood bleached kraft with standard test methods, the smaller-scale findings discussed in Chapters 2 and 3 can be better correlated to paper manufacturing. Because a main goal of this thesis was to understand experimental parameters and selection of PECs to improve percent solids of the fiber web before it reaches the dryer section, the percent solids of handsheets after pressing were tested. The handsheets were also tested for tensile strength and opacity. These are consumer-facing properties that ensure a strong and visually appropriate product, and they can give insight into structure-property-and function of including CNFs and PECs in paper.

4.1 Materials and Methods

4.1.1 Materials

Stock pulp was prepared from unrefined bleached softwood fibers. This was used without further modification. Unrefined bleached softwood was chosen because softwood fibers are typically longer and have a greater surface area than hardwoods [7]. While the surface charges of these fibers were not characterized, the bleaching process [228] and

presence of hemicelluloses are known to increase the surface charge of the fibers [229]. Together, these two aspects represent fibers that are likely to have lower percent solids in the press section compared to shorter fibers with less fibrillation. The use of unrefined fibers ensures that there is less fibrillation on the surface of the fibers. While it is expected that fines are present in the standard pulp, using unrefined pulp suggests that the effects of the fibrils in the study should be largely from the addition of CNFs rather than the standard pulp itself.

The same CNF used in Chapters 2 and 3 were used for this study. For simplicity and to ensure enough material was available, the CNF was used as received as the 3 wt.% stock slurry solution without dialysis or further modification. Two polyelectrolyte systems were used, the polyallylamine hydrochloride (PAH) and polyacrylic acid (PAA) sodium salt complexes (Chapter 3) that formed precipitates at 0 M salt and thus had high water retention and should have low percent solids and poly[2-(dimethylamino)ethyl methacrylate (PDMAEMA) and PAA (Chapter 3), which formed coacervates even at 0 M salt and thus had lower water retention and should have a higher percent solids. By comparing the two, the aim is to see if the water retention value conclusions and the phase of the complexes at low-salt are applicable to handsheets. Solutions were prepared in the same way as described in Chapters 2 and 3 and at a pH value of 6.5.

4.1.2 Preparation of handsheets

Handsheets were prepared using a modified procedure of TAPPI standard for forming handsheets for physical tests of pulp (T 205 sp-12). Briefly, approximately 25 grams of dry pulp was soaked overnight in 1L of distilled water. It was disintegrated at

approximately 27,000 rpm for 15 minutes. This stock was then diluted so that the overall volume of the stock was 8 L (0.3 % consistency). The consistency (concentration) was measured following the standard TAPPI 240 and as described in the equation below:

$$\%\ consistency = \frac{w - f}{g} \tag{5}$$

where w is the weight of the oven-dried pad and filter paper, f is the weight of the oven-dried filter paper, and g is the weight of the original pulp.

The weight of stock needed to achieve samples of 0.3 wt.% consistency corresponding with the required dry sheet weight of approximately 1.2 grams was calculated and used during sheet making. When adding CNFs or CNFs with PECs to the pulps, only the consistency of the softwood pulp fibers was measured. After CNFs or CNFs with PECs were added to the stock solution, the calculated weight for the 0.3% consistency of the softwood pulp was kept at the same to target the same dry sheet weight. This ensures that the basis weights of all samples are consistent.

After preparing the stock, sheet making, and couching steps from the TAPPI standard were followed. For the sheet making step, the appropriate weight of the stock was weighed out in 6 beakers and consequently 6 handsheets were formed and couched consecutively. Then another 5 beakers were measured out and handsheets were made. Once all 11 handsheets were formed, they were then all put on the handsheet press at one time. This includes pressing each handsheet on a polished plate and on two blotter sheets for one 5-minute cycle in the press and another 2-minute cycle on a new single dry blotter sheet.

The pressing step deviated from the TAPPI standard in that samples were pressed with the weight of the press and no additional pressure was applied.

4.1.2.1 Preparing the pulp stock solutions with CNFs and PECs

Pulp was prepared using solutions of the standard pulp by itself, pulp with 1 wt.% CNF, 5 wt.% CNF, and 10 wt.% CNF for the percent solids tests. To test the effectiveness of the addition of polyelectrolytes, PECs were tested with 5 wt.% CNF and the standard pulp. The pulp, pulp with 5 wt.% CNF, and pulp with 5 wt.% CNF and polyelectrolyte samples were additionally tested for opacity and tensile strength. Samples of pulp with 10 wt.% CNF were also tested for opacity.

For the pulp stock with CNF, the stock was prepared as normal with the dried pulp as described above and following T 205 sp-12. The percent consistency of the standard pulp was measured and the weight of the stock was used to be able to achieve an appropriate final average dry weight of the handsheets between 1.14 and 1.26 grams. Once the % consistency was measured for the standard pulp, a CNF slurry was added to the stock solution while stirring so that the overall addition is approximately the dry weight% CNF based on the overall handsheet. For example, if 24 g of oven dry pulp is need in the overall stock, a 10 wt.% CNF addition means 2.4 dry grams of CNF was added with the original 24 grams of pulp.

CNF solutions were prepared separately before they were added to the stock solution. For the 10% CNF sample, 80 grams of 3 wt.% CNF was measured into a plastic beaker and then added directly to the pulp stock. An additional 50 grams of water was poured into the same beaker to ensure any residual CNF was captured and then also added

to the stock. For 1 and 5% CNF samples, these were first diluted and mixed with water and then added to the stock solution. For each case, the final weight of additional CNF, water, and polyelectrolytes (if added) to the pulp stock solution was 130 g (~130 mL assuming a 1 g/mL density). Therefore, the total volume of the sample stocks used to make handsheets were 8.13 L.

For CNF and polyelectrolyte solutions, water was added to 3 wt.% CNF such that the total final concentration would be 1 wt.% in 120 mL of solution. This was mixed on a stir-plate on a setting that was high enough such that a vortex formed, and the slurry was well mixed. Then appropriate calculated volume of 0.5 M polycation solution was added using a syringe while the slurry was mixing. This was left stirring for at least 15 minutes. A minimum of 15 minutes was chosen to ensure completely mixing. As was seen from the electrophoretic mobility time-lapse data in Chapter 2 (Figure 2-11), the electrophoretic mobility was measured up to 32 minutes, but the electrophoretic mobility in all cases showed that the charges plateaued by around 15 minutes. This was for a case in which there was no additional agitation so it is expected that with stirring 15 minutes after the polycation add is sufficient such that changes to surface charge of the CNF with adsorption of the PECs should be stabilized. Polycation was added first then polyanion to the solution while mixing, as this was determined to give the best WRVs when testing different orders of addition in Chapter 2. After the polyanion, PAA, was added, the mixture was allowed to stir for at least another 15 minutes.

Polyelectrolytes were added to the CNF corresponding to a 25 mM total PEC concentration based on monomer weight to a total 1 wt.% CNF solution of 120 mL, which is above the saturation concentration of the CNFs (Figure 3-4) and was the dosing strategy

used in Chapter 3 to understand the influence of the phase of the PECs on the WRVs of CNF slurries. Enough 0.5 M polycation was added so it scaled to the appropriate volume from 0.05 wt.% CNF and 1.25 mM polycation (2.5 mM total PEC) to the 1 wt.% slurry solution made here.

After adding the PECs to the pulp and CNF mix, the stock solution was allowed to stir at 1000 rpm for at least 15 minutes before preparing the hand sheets. After this the stock was allowed to continue to stir while the handsheets preparation proceeded.

4.1.2.2 Preparing physical handsheets

A total of eleven handsheets of one sample type were prepared at one time. The first one was excluded and the following 5 were selected for percent solids testing and the other 5 were prepared following the TAPPI standard for tensile testing. The same screen was used in the handsheet former each time for consistency between sample types.

4.1.3 Physical testing of handsheets

4.1.3.1 Percent solids testing of handsheets

Percent solids of handsheets were tested immediately after pressing the sheets. As soon as the sheets were pressed, the blotter paper was removed and the sheets were weighed with the metal plates from the couching and pressing process. The weight of the metal plates were measured separately after being oven dried. The sheets with plates were then placed in an oven set to 105°C for 30 minutes until they were completely dry. The dried sheets were weighed with the plates or stand alone. Percent solids were calculated as follows:

$$\% \, solids = \frac{hd}{hw - p} \times \, 100 \tag{6}$$

where h*w* is the wet weight of handsheet and metal plate after the pressing, *p* is the weight of the oven-dried metal plate, and *hd* is the weight of handsheet oven-dried.

4.1.3.2 Tensile testing

Tensile testing was conducted using TAPPI standard for tensile properties of paper and paperboard (using constant rate of elongation apparatus) (TAPPI/ANSI T 494 om-13) [230]. Briefly, it describes the procedure for determining of four tensile testing metrics (breaking properties) of paper and paperboard: tensile strength, stretch, tensile energy absorption, and tensile stiffness. It requires the use of a constant-rate-of-elongation equipment and is applicable to all types of paper and paperboard. It describes the sample size, rate of separation of the jaws, and sample preparation to carry out the tensile tests.

After handsheets were prepared they were dried at room temperature and then stored and equilibrated at standard atmosphere chamber (50% RH and 23°C) following TAPPI/ANSI T 402 sp-13 [231]. The samples were stored for several days before they were tested. Samples were cut to shape using a die-press and at least 2 strips were cut per handsheet for a minimum of 10 strips. Care was taken to avoid areas in the samples that were thinner or inconsistent due to imperfections of the screen used during the handsheet formation. The width of the samples were 0.59 in (1.5 cm) and long enough that the specimen length tested is 4 in. The thickness of samples was measured. Using a platen gauge, one measurement was taken on each individual strip per sample type and then all

measurements of the sample type were averaged and used in the Young's Modulus calculation (stress/strain). The measurements were taken in the area that would be clamped by the grips to avoid handling of the test area. If a sample failed at grip, the sample results were excluded from the average calculations, as is specified to do so in the standard A total of 9 measurements were used to average.

The rate of separation was set to 0.5 in/min instead of the TAPPI standard 1 in/min. The load cell used was 1000 lbf. Samples were tested on a Instron 440R in a room where relative humidity was 50% and temperature was 23ºC.

4.1.3.3 Opacity

Measuring opacity is a standard technique to assess the visual appearance in terms of transmission of light through paper. This is called out as customer facing metric in TAPPI T-425 and TAPPI T-220 sp-10 standards for physical testing. The TAPPI T-425 has three different opacity tests but only the 89% reflectance backing (contrast ratio) test was measured here. This gives the ratio of the diffuse reflectance of the sample to that of a standard white back tile with a 89% reflectance to a sample backed by a black body of 0.5% or less reflectance ($C_{0.89}$= 100 x ($R_0/R_{0.89}$)). This is specific to this standard and for the pulp and paper industry and a contrast ratio of 100% represents perfectly opaque paper. A high opacity ensures a product that can be printed on without the print being visible on the other side due to the opacity of the paper.

A BNL-3 Opacimeter from Technidyne corporation was used for the measurements. First the specimen is backed by a standard white backing and then the instrument is set to read 100 with the sample. Then a black backing is placed behind the

sample and a measurement is taken to obtain the contrast ratio. The measurements were taken with the smooth side facing the detector but it is not expected that the side makes a significant difference. Six measurements were taken on different spots on each individual handsheets and 5 handsheets per sample type were taken. Therefore, a total of 30 measurements were taken per sample type and averaged. Because the average values of sample types were similar, the probability that the averages were different (null hypothesis that the averages are not different) was calculated using two-tail z-test. Because Z and t-tests give approximately similar values at a sample size of n=30, a z-test was used. It is not expected that a t-test will change the outcome of the results. A normal distribution was assumed.

4.2 Results and Discussion

4.2.1 Percent solids of handsheets

The results of the handsheets average and sample standard deviation of percent solids, dry weight, and their basis weights are seen in Table 4-1. To establish a concentration at which the presence of CNF appreciably decreased the % solids of the handsheet compared to the pulp control, the percent solids of handsheets of several concentrations of CNF addition were tested. It is known that increasing fines content and CNFs to pulps increases the WRVs and that the percent solids of handsheets decrease with the addition of CNFs [66] . Handsheets with 1 wt.% CNF did not decrease the percent solids (retain more water) than the pulp alone control samples. However, both the 5 and 10 wt.% CNF percent solids decreased compared to the control and 1 wt.% sample but not compared to each other. This suggests that with this method there is limit of detection of percent

solids where differences between samples of increasing CNF concentration cannot be detected. Samples with polyelectrolytes added (PAH alone, PAH/PAA, or PDMAEMA/PAA) in addition to 5 wt.% CNF, did not show improvements in percent solids relative to the pulp control or pulp + 5 wt.% CNF. Again, it is likely that the differences in terms of the water left within in the handsheets when there are sufficient concentrations of CNFs present are not detectable with this method. Given that the pulp and pulp with 1 wt.% CNF did have higher percent solids, it is possible to detect appreciable improvements. Suggestions for improving the method are discussed below.

Table 4-1. Average percent solids, dry weight, and basis weight of handsheet samples tested.

Sample	Sheet Percent solids	Dry weight of sheet	Basis weight (grams per meters squared)
Pulp	64.7 ± 5.2	1.21 ± 0.15 g	63.3 ± 1.81 gsm
Pulp + 1 wt.% CNF	65.6 ± 2.6	1.16 ± 0.06 g	58.5 ± 2.83 gsm
Pulp + 5 wt.% CNF	51.0 ± 3.6	1.21 ± 0.06 g	66.6 ± 3.10 gsm
Pulp + 10 wt.% CNF	54.0 ± 0.30	1.26 ± 0.02 g	63.6 ± 0.78 gsm
Pulp + 5 wt.% CNF+ PAH	51.2 ± 0.3	1.25 ± 0.15 g	67.9 ± 5.18 gsm
Pulp + 5 wt.% CNF+ PAH/PAA charge-match	49.4 ± 2.0	1.21 ± 0.08 g	68.1 ± 3.31 gsm
Pulp + 5 wt.% CNF+ PDMAEMA/PAA charge-match	51.3 ± 0.6	1.31 ± 0.06 g	69.9 ± 1.77 gsm

4.2.2 Suggestions for percent solids method

The test method can be improved and supported with additional testing. In this study, the handsheets were pressed with the weight of the press and the 50 psig as in the TAPPI standard was not applied. Therefore, maximum compression and likely the dryness of the sheets was not achieved. The pressure gradient achieved from the hydraulic press helps to remove water that is still saturated in inter-fiber or inter-fibril spacing [232]. Likely some inter-fiber water still remained in the samples tested here. Additionally, the TAPPI method calls for pressing two times with new blotter sheets in between. Pressing the samples with the first set of blotter paper and then measuring the wet handsheets before pressing again with a new set of blotter paper will show greater differences between the percent solids of the sample type, including between the 5 and 10 wt.% CNF samples. Because the second blotter paper soaks up additional water from the sheets, the test includes the capacity of the blotter paper to adsorb water. It was observed that after that for both the 10 wt.% CNF and 5 wt.% CNF with PDMAEMA/PAA, the first set of blotter paper was considerably more wet after the first press than other sample types.

Finally, the drainage time in the handsheet former was observed to be notably slower for the 10 wt.% CNF, but this was not recorded. The drainage time can be measured using a stop-watch while preparing handsheets [66]. This will allow for the evaluation of drainage and percent solids and their relationship with variations to formulation.

4.2.3 Tensile testing

The results of tensile testing results that are typically reported for the TAPPI standard are shown below and in the appendix in Table A. 1. Imperial units were used during the testing and are shown as such the results in the appendix.

. These include ultimate tensile strength (TAPPI tensile strength) and Young's Modulus. The tensile strength is the maximum force measured in the sample before it breaks per unit width of the sample. The Young's Modulus calculated is based on the engineering stress using the initial area of the specimen. An average thickness value per sample type was used for the calculations and were between 0.0068-0.0080 inches. The Young's Modulus is more generalizable and comparable to other material types.

The TAPPI standard reports a tensile stiffness which is the Young's Modulus times the thickness of the sample. This can be further normalized by dividing by the basis weight in grams per square meter (gsm) of the samples tested (Figure 4-1). The tensile strength can also be normalized with basis weight to calculate tensile index (Figure 4-2). These values were converted to metric units as shown in the figures. The basis weight of the samples ranged from 61-74 gsm.

The inclusion of 5 wt.% CNF to pulp increased the tensile strength, tensile index, and stiffness (Young's Modulus) of the handsheets. An increase in tensile strength with increasing CNF concentration to pulp in handsheets is expected [65]. Here, the tensile strength and index of the handsheets with CNF was nearly double the strength of the handsheets without CNF. Further adding PAH in excess did not appreciably improve the tensile properties but adding both PECs (PAH/PAA and PDMAEMA/PAA) further increased the tensile strength, stiffness, and index of the handsheets beyond the addition of PAH with CNF or CNF to pulp. This is expected given that PECs are known to be strength aids for pulps [121] and can be expected to improve formulations with CNF as well. PECs also act as retention aids and therefore may have allowed for more CNFs to be retained in handsheets, which further improved properties. Because both PECs resulted in similar

improvements, the strength improvements may not be influenced by the phase of the PECs, but more testing would be needed to confirm this.

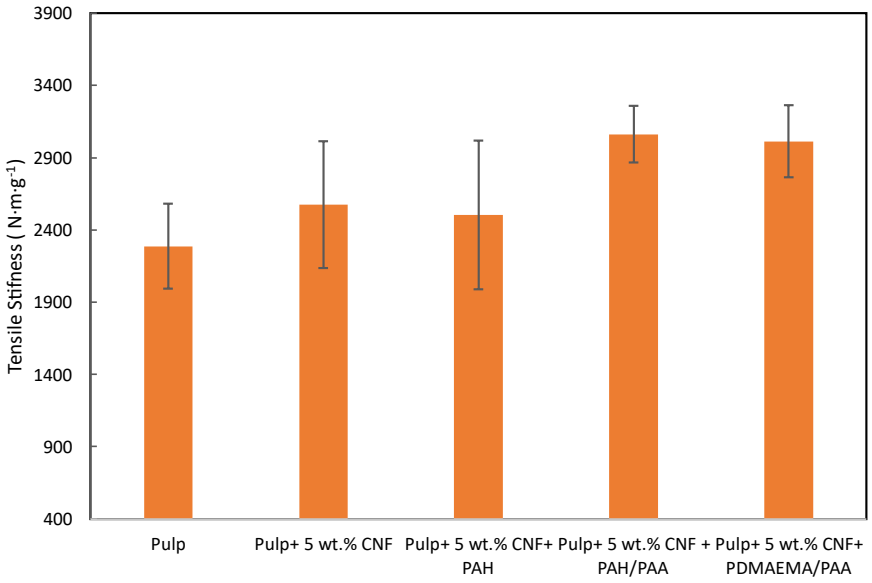

Figure 4-1. Tensile stiffness of handsheets tested.

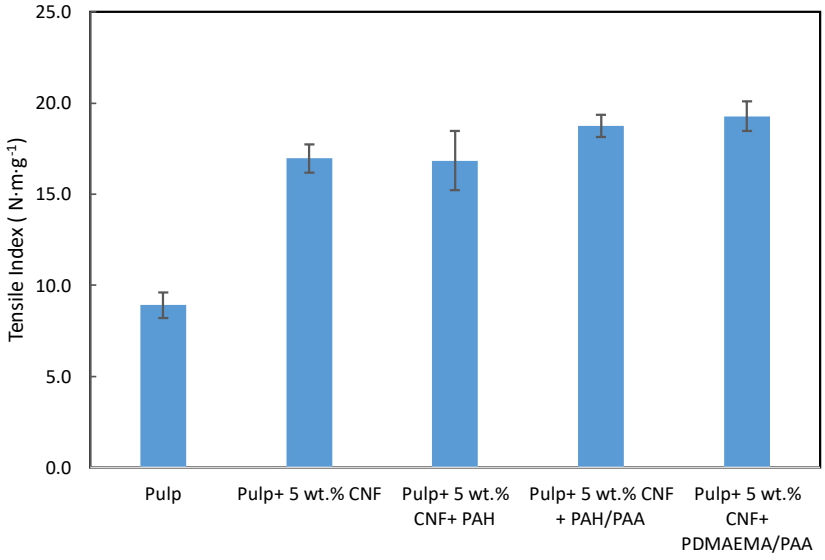

Figure 4-2. Tensile index of handsheets tested.

4.2.4 Opacity

The opacity of the handsheets were tested to characterize a physical and measurable property that is relevant to consumers. Opacity is an optical property of paper and is important in terms of the appearance of paper, in particular writing and printing grades [233]. High opacity is needed to be able to print or write on without the text being detectable on the other side. It can be altered by increasing the thickness of the sheet, including white mineral or pigment fillers, and more.

For consumers, opacity gives a characteristic of appearance. Paper samples are typically compared under identical conditions, such that small differences in measured opacity result in visually detectable and real differences in appearance to the consumer. Consumers are known to make judgements and purchasing decisions based on strength and visual appearance [234].

The average opacity values and their standard deviations for the handsheets tested are seen in

Table 4-2. The pulp control sample has the lowest opacity but adding CNFs with either 5 or 10 wt.% loadings increased opacity and resulted in the same average opacity. Adding PAH or PECs to handsheets with 5 wt.% CNF appeared to further increase opacity.

Table 4-2. Average opacity values of handsheets with CNF and PECS.

Sample	Average Opacity
Pulp	82.4 ± 0.7
Pulp+5% CNF	83.8 ± 1.0
Pulp+10% CNF	83.8 ± 0.5
Pulp+5% CNF+ PAH	84.9 ± 1.3
Pulp+5% CNF+ PAH/PAA	85.1 ± 0.9
Pulp+5% CNF+ PDMAEMA/PAA	85.2 ± 0.5

Because the average opacity values were similar, the averages were compared using a two-tail z-test. The null hypothesis assumed that the averages are the same. Table 4-3 shows the calculated p-values and corresponding probability comparing the means of different handsheet sample types. The presence of the 5 wt.% loading did significantly increase opacity compared to the pulp alone. Adding PAH also significantly increased opacity compared to the 5 wt.% and 10 wt.% loading samples. This implies that the presence of the polycation enhances opacity beyond that what increasing the CNF content could do alone. However, the opacity of handsheets with CNF and PECs (either PAH/PAA or PDMAEMA/PAA) were not significantly different from the samples with PAH alone or between each other. This suggests the presence of the polycation changed the opacity but

the presence the PECs did not change the opacity more than what was measured with just the inclusion of the polycation (PAH).

Table 4-3. P-values to compare of averages of the opacity values between handsheets of different values using a z-test showing whether the samples had statistically different opacity values (probability that the averages are not the same).

Averages opacity values compared	p-value	Probability that the averages are not the same
Pulp vs. Pulp + 5% CNF	3.67×10^{-10}	1.000
Pulp + 5% CNF+ PAH vs. Pulp + 5% CNF	3.20×10^{-4}	1.000
Pulp + 5% CNF+ PAH/PAA vs. Pulp + 5% CNF + PAH	3.97×10^{-1}	0.603
Pulp + 5% CNF+ PAH vs. Pulp + 10% CNF	2.87×10^{-5}	1.000
Pulp + 5% CNF+ PAH/PAA vs. Pulp + 5% CNF + PDMAEMA/PAA	6.95×10^{-1}	0.305

CNF films are known to be able to form highly transparent and clear films [64,235]. The opacity in these cases is low because transmission of light through the samples are high. Because opacity is physically influenced by increasing fiber to fiber contacts and decreasing air-fiber interfaces and therefore decrease opacity, this is expected. However, when CNFs are added to pulps, they can act as fillers and increase the opacity [66]. This may be because presence of CNF increase scattering through increased air-filler interfaces which leads to greater portion of internal scattering of light being reflected to increase

opacity. This is further enhanced by the presence of polycations or PECs. While some have seen an increase in opacity with CNF [66], reduction in opacity with increasing CNFs and polyacrylamide has also been observed [236].

Figure 4-3 shows images of the handsheets (pulp and pulp with 10 wt.% CNF) as examples. In the image, the samples were held up to the light. Because the same screen was used to make all the handsheets in this study, as seen in pulp control sample, there are spots of thinner coverage as a result of imperfections in the screen. These were consistently in the same areas and in the same pattern for all handsheets. The presence of CNF with the pulp are able to provide better coverage in those spots, while the weight of the samples is similar. Previously SEM images have shown CNFs act as a filler and provide coverage in voids of pulps [237].

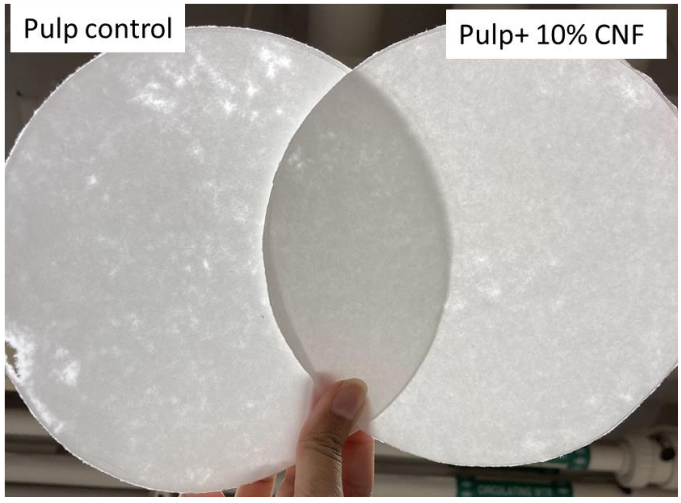

Figure 4-3. Photograph of pulp control and pulp with 10% CNF handsheets. The image was taken while the samples are held up to indoor white fluorescent light.

Opacity can vary with the basis weight of the sheet [233]. Because polycations can act as retention aids, it is possible that the inclusion of PAH or the PECs increased the retention of CNFs and therefore further increased the opacity. While the overall dry weight of the samples was maintained (Table 4-1), changes in retention of the fibrils and changes in flocculation patterns with the polyelectrolytes, may have attributed to increased scattering of light and therefore opacity. Adding CNFs with polyelectrolytes may be an alternative way to increase opacity without the addition of other fillers such as titanium dioxide (or using less filler content) while maintain a lighter-weight product.

The evaluation and optimization of percent solids, tensile strength properties, and opacity all contribute to sustainable design. Increasing percent solids reduces the energy needed during the drying and production of CNF and paper products. Optimizing tensile strength (durability [238]) and opacity can influence how consumers interact with products and their perception of quality [234,239,240], which has implications on their purchasing and recycling behavior, particularly for packaging. The next chapter discusses the role of manufacturing and consumer decision-making to improve circular economy with a case-study of CNF and packaging.

4.3 Conclusions

In this chapter handsheets with CNF and PECs were prepared and tested. The percent solids were tested after handsheet pressing, which is more representative of the paper web on a paper machine before it goes to the dryer section. Initial results showed differences in percent solids of handsheets without CNF and those with either 5 or 10 wt.% CNFs. More refinement of the technique will be needed to observe differences or

improvements with higher CNF content or with the presence of PECs. Suggestions and limitations were discussed in the chapter. Differences between PEC systems or CNFs alone in the handsheets were not detected.

Besides percent solids, tensile and opacity testing were conducted. Tensile strength increased with CNF content and further increased with the inclusion of polycation and PECs. Opacity testing showed statistically significant increase in opacity with the presence of polyelectrolytes compared to CNF and pulp or pulp alone. Overall, in each test, appreciable differences between the two PEC systems were not detected. Strength and visual appearance are parameters that influence how people perceive, purchase, use, and dispose of products and may have an impact on circular economy and sustainability, in addition to the sustainability impacts from improving percent solids.

CHAPTER 5. CONSUMER AND MANUFACTURING DECISION-MAKING IN SUSTAINABLE PRODUCT DEVELOPMENT: AN APPLICATION IN CELLULOSE NANOMATERIALS

Khan, N., Brettmann, B.K., Reeves, D.C., Consumer gatekeeping in sustainable materials streams: an application in cellulose nanomaterials packaging. Manuscript in preparation.

Products are made for consumers, but often early-stage research and developmental thinking does not include consumer purchasing and end-of-product-life (disposition) behaviors. Consumer behavior is often neglected in circular economy frameworks and absent in green chemistry design principles. All technology, especially those intended to be used by people impact people in some way [241]. This is problematic because consumer behavior has direct impacts on the decisions that go into making products with virgin or post-consumer materials. Ultimately, the fate and sustainability of the material is dictated by whether people choose to keep, recycle, or landfill.

A framework for a circular economy is presented here which includes the role of manufacturing functional products and of consumers as gatekeepers. In doing major areas R&D efforts and control points of virgin or recycled materials in products made for consumers are pointed out. Then how consumer gatekeeping is responsible for moving material through the circular economy and creating value of post-consumer material is discussed. The framework is tied together with a discussion of the application of cellulose

nanomaterials in packaging. Finally, policy implications stemming from to the application of this framework are discussed.

5.1 Background

5.1.1 Circular economy of cellulose nanofibers and packaging

CNFs are often touted as being better than fossil-fuel based polymers for the circular economy, but this is primarily with the framing that they are bioderived and biodegradable and better in single-use multi-layer packaging. Single-use multilayer packaging, regardless of biodegradable materials, still follows a linear economy, where the product is designed to be used once and it is acceptable if it is disposed into landfill. This is different than a circular economy, in which the material is designed to return to the manufacturer to be reused and extend its function beyond one single use. CNFs are already energetically costly to extract and to dry when making products. Therefore, to make CNFs truly sustainable and improve their circular economy, manufacturing decisions and formulations are reframed to include a key mover of material in a circular economy: consumers.

5.1.2 Current framing of sustainability

In general, from the perspective of product y designers, circular economy frameworks already exist to consider sustainability such as the principles of green chemistry and engineering [242,243]. The principles and the associated metrics take a mass-based systems approach and can be applied to various processes to minimize impact or waste in a chemical process [244]. However, none of these frameworks or metrics explicitly

consider the magnitude of the impact of consumers or their behavior on manufacturing decisions or waste. One metric, the F-factor, seeks to maximize the function of a material for its mass [242–244]. Function here is broadly defined as "performance". Another metric, the E-factor, calculates the amount of waste produced and accounts for yields from manufacturing processes but still lacks a circular economy and consumer-inclusive perspective [245].

5.1.3 Consumer behavior and gatekeeping

Consumers are a major gatekeeper in the circular economy. Human decision-making for adopting or using sustainable technology leads to a few decisions that are influenced by many drivers and factors. While consumer purchasing and disposition (landfill, keep, and recycle) [246] behaviors and motivators are largely variable, there is an aggregate or average behavior. This aggregate consumer purchasing behavior in this framework is treated as price [238] while the disposition behavior is based on material type. For circular economy to work, consumers must be willing to buy a product and they recycle for the material in the product to move through the circular economy. Furthermore, their disposition behavior dictates if it will return to manufacturing to recirculate back.

5.1.3.1 Consumer purchasing behavior

While consumers are increasingly becoming more aware of issues surrounding sustainability and want to do more to help the environment through their purchasing habits [247–251], for a typical consumer, the price is a major driver of sustainable purchasing decisions [238,251,252] but many other drivers are at play. Other product features such as quality and function or effectiveness (including that of the packaging) [238,247,249,252] are more

important to consumer purchasing decisions than recyclability [249,253], environmental impact [238] or sustainability [254].

Considering the consumer gate, as illustrated in Figure 5-1, once a manufacturer produces a product, the role of consumers as gatekeepers is to acquire (acquisition) the product through their purchasing behavior. Although there are many different models and motivators to explain consumer purchasing behavior, here an economic approach was chosen to the treat consumer purchasing habits [255]. Because quantity of a product purchased decreases with increasing price of that product with all else equal, to make a product more sustainable and increase a material's ability to move through a circular economy, the prices of the products or packaging that contain those sustainable materials should match or be less than the price of a competing less sustainable product for the same quality and function of that product. Specifically for packaging, the quality or function of the package should not hinder or negatively alter a consumer's willingness to buy the product. Consumer responses to specific features in packaging and how they influence purchasing behavior has been previously studied [254,256], so is not a focus of the work here.

For a CNM-containing packaging to be successful, consumers must first be willing to purchase it. Concurrently, manufacturers must be able to make packaging at price such that they can meet consumer demands in terms of quantity and price supplied. At the same time, manufacturers must meet profit margins to be self-sustainable while attempting to provide more sustainable products. Here setting up a model for the circular economy of cellulose-based packaging will enable industries at a national level to take consumer choices into consideration when assessing whether they can meet all these demands,

especially given the availability and cost of post-consumer materials which is influenced by consumers at local and national levels.

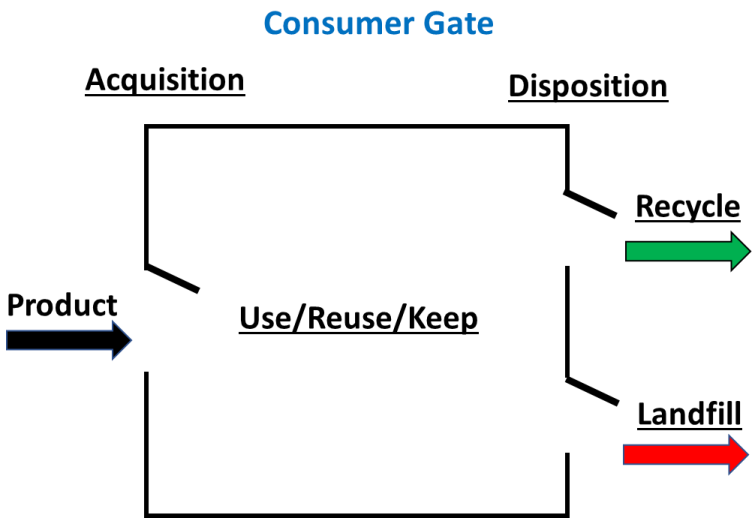

Figure 5-1. Schematic representing consumer gatekeeping behavior which controls the flow of material through a circular economy. Consumers first acquire products based on product attributes including price and dispose of products through landfill, keep, and recycling behaviors based on other attributes including physical material properties.

5.1.3.2 Consumer disposition behavior

After consumers purchase and use a product, they continue to influence the circularity depending on what they do with it at the end of its useful life, choosing one of three disposition routes: retain, recycle, or waste (landfill). Note that incineration is not considered here because burned material cannot be recovered or reused. A variety of determinants [246,257] including physical and non-physical attributes of the products and packaging influence consumer disposition behavior. Non-physical aspects include social norms [258], socio-economic factors [259], gender [252,258], [259], and accessibility of recycling facilities [252,260(p20)]. Physical attributes include perception of quality based on the material [252,258,259], and durability and strength [258,261].

Here, the assessment is limited to the physical attribute material type because recycling rates at local, national, and global levels suggest that the overall aggregate disposition behavior of consumers is correlated to the material type [256]. The preference towards recycling of paper and cardboard compared to other material types, particularly plastic, is evidenced by the recycling rates. Figure 5-2 shows that over the last 60 years the tonnage of both paper and plastic waste sent to municipal waste streams across the U.S. increased. In this timeframe more than double the amount of paper waste has been generated compared to plastic waste but the rate of recycling of paper-products by consumers (~67% in 2018) is significantly greater than plastic (~10%). In 2009, the tonnage of paper going to landfill fell below that of plastic [262]. Meanwhile, plastic going to landfill is still increasing. This gives insight into the way consumers recycle or landfill products that they dispose of at the end of the usefulness of the product. While they purchase and dispose of paper-based products more than plastics, they also recycle them more.

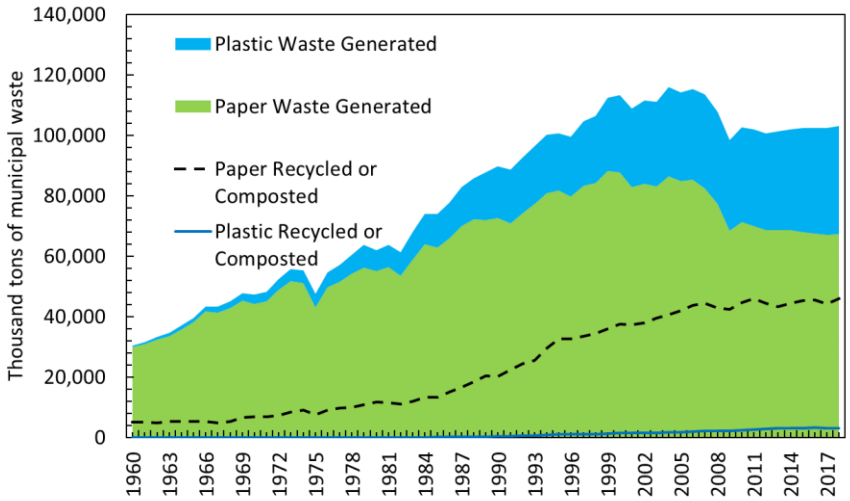

Figure 5-2. Historically more paper waste has been generated than plastic waste but people recycle paper at greater rates than plastic given the tonnage of paper in landfill. Data plotted from available EPA report [262].

The recycling rate metric, while useful for indicating overall preference for recycling over all of the municipal end-of-life wasting options, does not incorporate keep and reuse behavior. It only reflects the tonnage recycled out of all the waste that is sent to municipal waste systems, not the amount of product manufactured. Consider that in 2018, an average of 76 million metric tons of paper and cardboard [263,264] was manufactured and produced in the United States. This means that more than 80% (~63 million metric tons) of the paper and cardboard produced is disposed of by consumers (landfill, recycled, composted, or incinerated). Given that 41 million metric tons of paper and cardboard were recycled, approximately 55% paper and cardboard product was recycled. This value is referred to as recycling disposition rate here to highlight the idea that consumers can choose to dispose of materials in various ways. While there are many metrics to represent circular economy behavior [265,266], the recycling disposition rate metric incorporates the fact that people keep, recycle, or landfill products. When tracking this metric over time, it can also

account for the fact that consumer preferences for purchasing products changes over time or types of products [267]. It can also account for changes in the number of products of a given type that are made.

5.1.4 Manufacturing decision-making

Describing the manufacturing gate in packaging integrates the relationship between three main quantities:

1) Material recovery efficiency (yield): How much cellulose fiber is recovered/retained during upstream processing steps (i.e., extraction, blending, material transfer, etc.). All processes are lumped into one unit called "cellulose processing recovery efficiency"
2) Percent content: the proportion of the product by dry mass that is composed of a given material type. Here the percent post-consumer fiber content is examined.
3) Marginal cost: the aggregate cost per ton to acquire, incorporate, and manufacture virgin materials into additional unit of a product or service. This accounts for being able to produce a product for consumers at the customary price-point.

In each of these are opportunities for sustainable improvement, particularly improvements that can be made during product development and formulation. Depending on the marginal costs of virgin or recycled materials, the most sustainable improvement may not necessarily be to increase yield or recycled content.

The first step of manufacturing a product is to source material, which means recovering the necessary material from either virgin biomass or cellulosic waste product.

Here green chemistry and engineering principles can be considered. The primary quantities that feed into metrics are the yields, for example the yield of cellulose fiber from the recovery process, and they are defined either based on theoretical maximum recovery based on the chemistry or based on how much mass of the final desired product is obtained relative to the raw material is added to an extraction process [242,244]. From the perspective of waste reduction, a process is designed such that it leads to maximum yields from the raw material, though that can oversimplify the problem, particularly if high solvent usage is needed to get high extraction yields. In this model, an overall yield in all upstream processes is included as the cellulose process recovery efficiency, as an input parameter. It does not examine models for optimizing sustainability of extraction processes.

Once virgin material is sourced and fibers recovered, significant R&D efforts go into formulation to turn this material into a functional product considering the structure, function, and property of the product needed for the consumer. As has been discussed in Chapters 2-4, appropriate formulation considers the concentration a material can be incorporated by mass to achieve required properties like strength. Because this has extensive implications on formulation, for this chapter it is assumed that with appropriate R&D efforts, a wide range of % content of a material in a product is scientifically achievable without mass loss, unless explicitly stated.

Finally, economic factors are paramount to achieve price points for consumers' willingness to buy products and for a manufacturer to make profit. Not only do the extracted materials need to be scientifically appropriate, but they must also be able to deliver the function for a price that consumers are willing to pay and meet profit margins. The high energetic cost associated with manufacturing and drying CNFs, not only impacts

sustainability, but it also adds to the marginal cost to produce the product. The more expensive to manufacture, the higher the price facing consumers. When price increases, all else equal, consumers acquire less and less material can move through the consumer gate into a circular economy.

5.2 Development of a consumer-centric circular economy framework

Given that consumer and manufacturing gatekeeping behavior are critical to moving material into a circular economy, a generic framework that ties consumers to manufacturing, is illustrated in Figure 5-3 B. The framework starts when the consumer demands a given quantity of a product and manufacturing must produce enough supply to meet the demand.

In a linear economy framework, virgin material is designed and manufactured into a product that delivers a function to consumers once and, after the product is used by consumers, it is turned into waste and then landfilled (Figure 5-3 A). Here, a consumer-centric circular economy framework is introduced (Figure 5-3 B) that explicitly ties consumers to manufacturers. During the first loop through a circular economy, the product supplied is manufactured entirely of virgin material. The virgin material is sourced and extracted with some cellulose recovery by mass and then incorporated in some percentage by mass into a product. Once manufacturing makes the product, the product supplies value and function to consumers. Consumers gatekeep by purchasing the product to extract its function and then can return value to manufacturing through their disposition behavior. Once a recycled product is back at manufacturing, manufacturing can extract material and reincorporate into new product. The waste produced at the manufacturing gate includes

recycled and new virgin manufacturing waste and the useful product continues into a new cycle.

In an ideal circular economy, both the consumer and manufacturing waste are minimized or do not exist, and the original material put into the system continues to provide function to the consumer after it is remanufactured into new product. At the consumer gate, this can be through a combination of keep and recycling disposition behaviors [268], where the consumer can continue to use a manufactured product that provides function without losing its properties and they return the material to be remanufactured This ideal only relates to the mass of a material and assumes that it does not degrade with remanufacturing. It does not include other inputs in the system, such as energy expenditure during the reprocessing of post-consumer manufacturing steps.

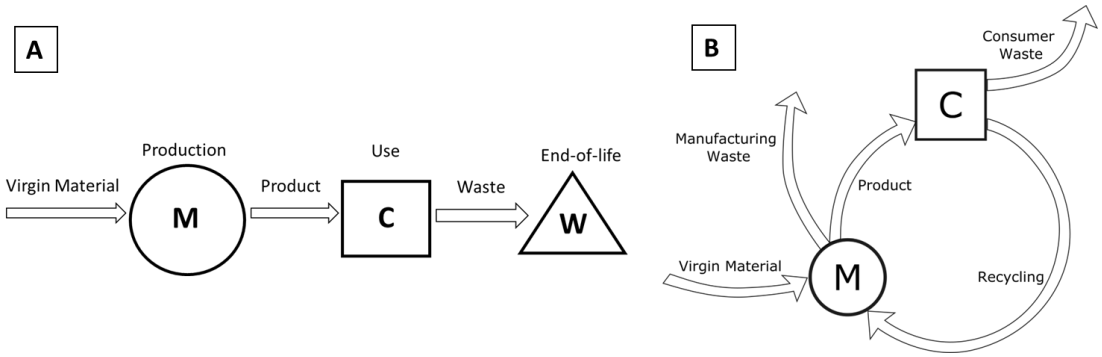

Figure 5-3. Representation of a linear economy framework in which virgin material is turned into a product by manufacturing, which is used by consumers and then turned into waste and landfilled at the end of the product's life (A). Circular economy framework that includes both manufacturing and consumer gatekeeping in which manufacturing turns virgin material into a product, which at equilibrium is purchased by consumers. Consumers then move the material to either consumer waste or recycle and send the material to manufacturing to recover its value (B).

Figure 5-4 introduces a more nuanced framework for the circular economy that includes both manufacturing and consumer gatekeeping, the details of which will be

described in the following sections. This framework is designed to be flexible to. Further developments can include specific manufacturing steps and decision-making for the recovery and incorporation steps. It can also be modified to include more sophisticated treatments of consumer gatekeeping. It also groups all manufacturing into two steps, an upstream processing step that accounts for cellulose recovered from the incoming streams and a general processing/manufacturing decision step, which can be used to account for external factors such as pricing. This parsimonious approach showcases the power of a consumer focus while allowing flexibility to increase complexity of manufacturing decision-making through multiple separate processing steps later.

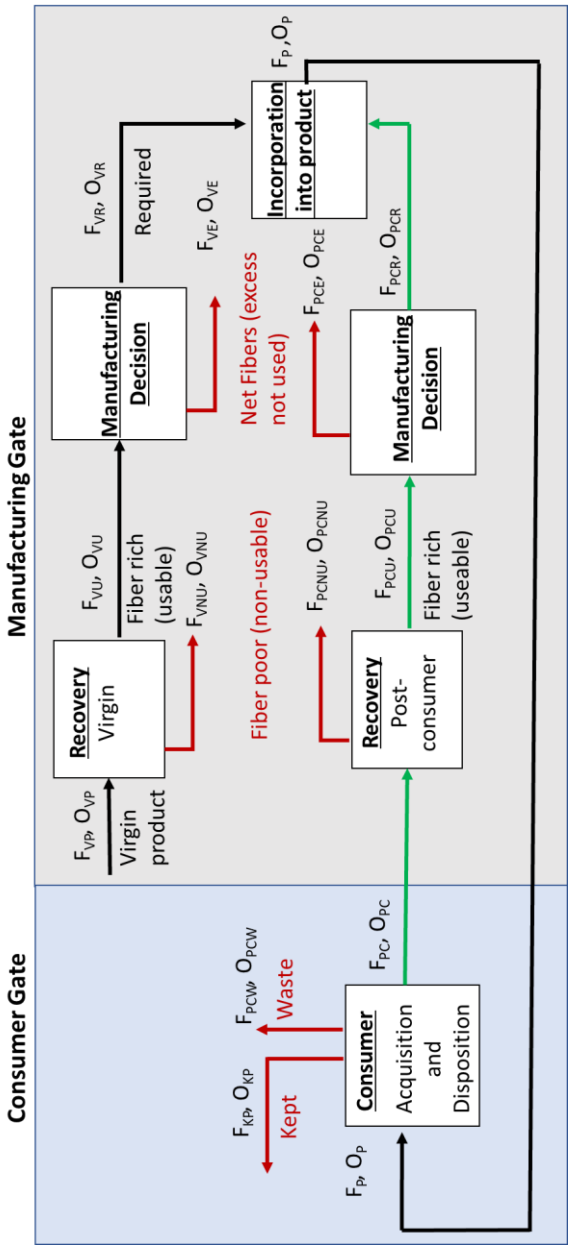

Figure 5-4. Circular economy framework represented as a system considering mass flows into various manufacturing processing (upstream processing, manufacturing decisions, and incorporation) and to and from consumer gate (acquisition and disposition). The black, green, and red arrows represent the flow of virgin material, post-consumer material, and waste-streams, respectively. In each stream both cellulosic fiber (F) and other non-cellulosic components (O) are represented.

5.3 Formalizing a mathematical treatment for a consumer centric circular economy

To support the framework depicted in Figure 5-3 B and Figure 5-4, a mathematical treatment is formalized below by specifying the recycling disposition rate, cellulose processing recovery efficiency (yield of cellulose), and incorporation rate (% material in product). The values are related to the monetary cost of producing a product that incorporates both virgin and recycled materials given assumed marginal costs for virgin and recycled materials and a required product needed to meet consumer demand. The results of varying these parameters are described in Section 5.4, which highlight non-intuitive finding that it is only worthwhile in some cases to improve recovery efficiency or desired post-consumer percent content into a product

5.3.1 Manufacturing meets consumer gate

In this economic-based treatment it is assumed that manufacturers design products with the consumer purchasing behavior in mind. Therefore, the circular economy starts where the consumer and manufacturer meet at the total manufactured product produced, TM_p. The consumer demands a total manufactured product, TM_D and in the economic equilibrium the manufacturer supplies it. This value for paper and cardboard is known at a national level for the United States.

$$TM_P = TM_D \tag{7}$$

As shown in Figure 5-4, entering the consumer gate, the overall product includes useable fibers from both virgin and post-consumer cellulose fibers (F_P) and some other non-cellulosic material (O_P). These two components are present in some ratio A, where A=

O_P/F_P and it is assumed that this ratio does not change in any stream going into or out of the consumer gate (i.e., consumers are not changing the make-up of the product by adding or taking away other chemical components).

5.3.2 Consumer gate

At the consumer gate, once the consumer purchases the product, they then either keep, TPC_{KP}, recycle, TPC_P, or landfill, TPC_W, some tonnage of the product. A metric is defined, the recycling disposition rate (δ_{PC}), for product P that is the ratio of the tonnage of post-consumer material recycled to the tonnage of total manufactured product produced:

$$\delta_{PC} = \frac{TPC_P}{TM_P} = \frac{F_{PC}+O_{PC}}{F_P+O_P}. \quad (8)$$

Similarly, the recycle rate is given by the tons of product recycled by consumers over the total amount sent to municipal waste streams (recycled or landfilled):

$$R_P = \frac{TPC_P}{TPC_W+TPC_P} = \frac{F_{PC}+O_{PC}}{F_{PCW}+O_{PCW}+F_{PC}+O_{PC}}. \quad (9)$$

When the recycle and recycling disposition rates are given for a particular year, the amount of product kept by consumers can be calculated. For simplification, in this treatment, calculations are performed only on the cellulose component and therefore O_P=O_{PC}= O_{PCW}= O_{KP}= 0 and A= 0. This means that other chemical components that are likely remaining in fibers, such as lignin or hemicellulose, are not considered here. To implement this for an actual process, the amount of cellulose flowing into and out of the upstream processes would need to be measured (including steps like extraction, blending,

material transfer, etc.) independent of the non-cellulose components. Because this can be a challenge, the model is described with all the non-cellulose component variables, but for the hypothetical model here, only the balance on cellulose is performed. Describing the model in terms of both cellulose and non-cellulose component will also enable future work to consider separation efficiencies in extracting cellulose from the different sources in the manufacturing gate.

5.3.3 Manufacturing gate- recovery and decision-making from post-consumer sources

Once product is recycled by consumers and received by manufacturers, the post-consumer products can be used in subsequent manufacturing processes after upstream processing steps to obtain useable post-consumer fibers.

In the upstream processing step, post-consumer fibers, TPC_F, are recovered with an efficiency or yield, η_{PC}, as given by:

$$\eta_{PC} = \frac{F_{PCU}+O_{PCU}}{F_{PC}+O_{PC}}. \quad (10)$$

Where $F_{PCU} + O_{PCU}$ represent the total amount of useable material that is extracted and includes the cellulosic and non-cellulosic components that go into a fiber-rich stream. The non-useable materials ($F_{PCNU} + O_{PCNU}$) go into a fiber-poor and non-useable waste stream. The ratio between O_{PCNU}/F_{PCNU} and O_{PCU}/F_{PCU} can be given by B and C, respectively. Again, for these calculates, only consider the cellulose components were considered, but if separation efficiencies, etc. are also of interest, then the full model with ratios B and C may be used. These ratios are unique based on the manufacturing process and how much of each component (cellulosic or other) are in the fiber poor or rich streams.

Manufacturing decisions for incorporation into products do not change these ratios after the upstream processes.

Considering the material going through both the consumer disposition and post-consumer recovery streams, the useable amount of post-consumer fibers, $TPC_F = F_{PCU} + O_{PCU}$, to make new product is given by:

$$TM_P \times \delta_P \times \eta_{PC} = TPC_F. \quad (11)$$

Once the total amount of useable fibers is achieved, manufacturing decisions must be made in terms of how much of that material is needed to go into the incorporation step to make new product. The amount of fiber required is set by the post-consumer recycled fiber content ratio, β. This is given by:

$$\beta = \frac{TPC_F}{TM_P} = \frac{F_{PCR}+O_{PCR}}{F_P+O_P}. \quad (12)$$

β is subject to the requirements of a product and the availability of post-consumer material through yields and recycling disposition behavior. The amount of extracted fibers available to make product with the content set by β may not be enough or in excess depending on the other parameters. Therefore, at the post-consumer manufacturing decision step, the net quantity of fibers that go into the product is based on the minimum between what is useable or available ($TPC_{F\_useable} = F_{PCU} + O_{PCU}$) and what is required for the product ($TPC_{F\_required} = F_{PCR} + O_{PCR}$).

When $TPC_{F\_required} > TPC_{F\_useable}$, then there is a shortage of post-consumer material. In this case the product with required post-consumer content cannot be achieved

and the material shortfall must be made up with virgin fiber or fibers from another waste stream to make the required quantity of product. On the other hand, when $TPC_{F\_required} < TPC_{F\_useable}$, there is excess post-consumer material that is not used and will either accumulate in the short run as a stock or will go to waste. The net quantity in terms of excess ($TPC_{F\_excess} = F_{PCE} + O_{PCE}$) is represented by:

$$TPC_{F\_available} - TPC_{F\_required} = TPC_{F\_net\ quantity}\ . \tag{13}$$

5.3.4 Manufacturing gate- recovery and incorporation of fibers from virgin sources

To make the total amount of product, TM_p, the individual components must be combined by the manufacturing incorporation step. The overall incorporation of virgin and post-consumer materials into product is given by:

$$TV_F + TPC_F = (F_{VR} + O_{VR}) + (F_{PCR} + O_{PCR}) = F_P + O_P = TM_P. \tag{14}$$

Where TV_F is the combined required virgin material ($F_{VR} + O_{VR}$) that can go into the product, because the new product made can be made from either virgin or post-consumer material or both in different proportions depending on the product and need. The proportion of virgin material needed in the incorporation step is given by:

$$\alpha = \frac{TV_F}{TM_P} = \frac{F_{VR}+O_{VR}}{F_P+O_P}. \tag{15}$$

In the first cycle of the circular economy, it is assumed that α= 1 and the product is 100% the virgin material by dry weight. For subsequent cycles, post-consumer fibers can also be incorporated into the product. When the post-consumer fibers are extracted and incorporated, the amount of post-consumer is given by the proportion β. Depending on the manufacturing decisions and requirements of the product based on post-consumer content, it is assumed that both virgin and post-consumer fractions can be incorporated into the product which is given by:

$$\alpha + \beta = 1. \tag{16}$$

For a given amount of virgin fibers, TV_F ($TV_F = F_{VR} + O_{VR}$), required to make product TM_p, it is assumed that the manufacturing decisions are optimized such that there is no excess useable material ($F_{VE} + O_{VE} = 0$), unlike in the case of post-consumer fiber. In this case, the useable fibers in the fiber rich stream after recovery is equal to the required fibers ($F_{VR} + O_{VR} = F_{VU} + O_{VU}$).

Furthermore, it is assumed that that the virgin product ($TV_P = F_{VP} + O_{PR}$) that is used to make virgin fibers is readily available to meet the required supply of TV_F to make the product as set by α. Therefore, the amount of source virgin product such as forest biomass ($TV_P = F_{VP} + O_{VP}$) is given by:

$$\frac{TM_P \times \alpha}{\eta_{VF}} = TV_P. \tag{17}$$

where η_{VF} is the efficiency (yield) with which virgin product is turned into useable virgin fibers in the fiber rich stream is given by:

$$\eta_{VF} = \frac{F_{VU}+O_{VU}}{F_{VP}+O_{VP}}. \quad (18)$$

For simplicity it is assumed that O_{VP}=O_{VU}= $O_{VR=}$ $O_{VNU=}$ 0 but the ratio between O_{VNU}/F_{VNU} , $O_{VU}/F_{VU,}$ and O_{VP}/F_{VP} can be given by values D, E, and F, respectively. As with the corresponding post-consumer streams, these D and E are unique based on the manufacturing process and how much of each component (cellulosic or other) remain in the fiber poor or rich streams. The ratio, F, is unique to the type of biomass used to extra virgin fibers. For example, if a particular species undergoes thermo-mechanical instead of Kraft pulping, the amount of lignin in the other (O) component will be different and D and E values will be different even if F is the same in both cases.

5.3.5 Value of the product to consumers

When products are sold at the consumer gate and are only composed of virgin material, the monetary value to produce the product is given by:

$$TV_F \times MC_V = \$_{VP}. \quad (19)$$

Where TV_F is the required virgin fibers needed to produce the product, including excess virgin fibers needed if there is a shortage in required post-consumer fibers. MC_V is the aggregate marginal cost (cost per ton) to acquire, incorporate, and manufacture virgin materials into product. The total value embedded product P, $\$_{VP}$, reflects the minimum per-unit price at which product P must be sold to recoup manufacturing costs. Note that profit adds to the overall price.

When products that are made partially from post-consumer fibers are sold, the value is given by:

$$(TPC_F \times MC_{PC}) + (TV_F \times MC_V) = \$_P. \quad (20)$$

where MC_{PC} is the aggregate cost to extract, acquire, incorporate and manufacture post-consumer materials in the new product, P. Here TPC_F is the minimum amount of post-consumer fibers that can go into the product depending on whether the post-consumer content required is less than what is useable and available. Now $\$_P$ reflects the minimum per-unit price at which product P must be sold to break even. Note the overall price would include fixed costs, profit, overhead, etc. It is assumed here that the flexibility in $\$_{VP}$ are from the portion of this value that can be changed with manufacturing choices and influences overall profit margins.

When $MC_{PC} \ll MC_V$ or $MC_{PC} \gg MC_V$, $\$_P$ decreases depending on the tons of either virgin or post-consumer is included in the product. To minimize the cost to manufacture the product, and therefore increase profit margins or decrease the price offered to consumers, the process or materials must be changed.

5.3.6 Waste

Waste is generated in both the consumer and manufacturing gates. At the consumer gate, waste is generated when products are not reused or recycled. For the manufacturing gate, waste is generated turning product into useable fibers. For each recovery step (virgin or post-consumer) after useable fibers are extracted with some efficiency, a manufacturing waste stream is generated which is fiber-poor stream which has some cellulose that was

not useable and other materials that did not remain in the fiber-rich useable streams. In this initial model, only the cellulose, not the total, waste quantities are analyzed because calculations are only performed over the cellulose. The model is setup to have the ability to perform calculations over the non-cellulose components. This will enable future work to consider the total waste, not just the cellulose waste.

5.4 Results and application of framework

5.4.1 Recycled versus virgin fibers in paper manufacturing

To apply the model that supports the framework, three empirical quantities applicable to the consumer and manufacturing steps: recycling disposition rate, recovery efficiency (yield), and incorporation rate (% material in product). There were related to the monetary cost of producing a product that incorporates both virgin and recycled materials, given assumed marginal costs for virgin and recycled materials and a required tonnage. To reiterate, the non-cellulosic material is not included in the streams.

To illustrate how the desired recycled content of a product, recycling disposition rate, and post-consumer fiber processing recovery efficiency influences the quantity and price of post-consumer fibers, six cases were evaluated (Table 5-1). A basis of 100 tons of paper demanded and supplied at equilibrium was assumed. Price was graphed in two ways:1) virgin pulp ($VF) pulp price per ton is greater than recycled pulp ($PCF) and 2) when recycled pulp price per ton is greater than virgin fiber. For these calculations, the marginal costs of $0.9/ton and $0.8/ton were applied, with the larger value corresponding to either virgin pulp or recycled pulp when the overall cost to produce was plotted in all cases. The marginal costs were arbitrarily scaled down by a factor of 1000 from 2017 pulp

prices of ~$900/ton for southern bleached softwood kraft pulp and ~$800/ton for post-consumer deinked pulp [53]. This was to reflect the trends in the final results rather than the actual costs. A virgin material cellulose processing recovery efficiency, defined as the ratio of virgin cellulose that exits the upstream process to the amount of cellulose that enters the upstream process, of 0.9 (90% yield) was assumed in the calculations.

Table 5-1. Six circular economy post-consumer fiber cases for various disposition, recycled content, and post-consumer efficiency values.

	δ_{PC} **(Consumer recycling disposition rate)**	β **(Post-consumer content)**	η_{PC} **(Post-consumer recovery efficiency)**
Case 1	0.5	0.1	0 to 1
Case 2	0.5	0.9	0 to 1
Case 3	0.9	0.9	0 to 1
Case 4	0.1	0 to 1	0.9
Case 5	0.5	0 to 1	0.9
Case 6	0.9	0 to 1	0.9

5.4.1.1 Influence of post-consumer efficiency at low and high post-consumer content (β)

Figure 5-5 illustrates two cases, both with a consumer recycling disposition rate of 50% (δ_{PC}=0.5) and with Case 1 (Figure 5-5 A and B): low post-consumer fiber content β=0.1 and Case 2 (Figure 5-5 C and D): high post-consumer fiber content, β=0.9. The net

quantity of post-consumer fibers as a function of post-consumer processing recovery efficiency are shown in Figure 5-5 A and C and the corresponding price (USD/ton) to manufacture the product as a function of post-consumer processing recovery efficiency is shown in Figure 5-5 B and D. Figure 5-5 B and D also show the cost assuming that virgin fiber has a higher cost than post-consumer fiber (orange triangles) and the cost assuming that post-consumer fiber has a higher cost than virgin fiber (gray asterisks).

In Case 1, when 90% of the product is virgin material and the recycling disposition rate is 50%, only a 20% post-consumer cellulose processing recovery efficiency (0.2= η_{PC}) is needed to supply enough post-consumer fiber (PCF) to make the product. Improving efficiency beyond that results in excess material that is not included in the product due to a low desired PC content (β=0.1). In this case, the salient barrier to improve circularity is not yield but PC content. In Case 1, Figure 5-5 B, when the marginal cost of virgin fiber is more expensive (orange triangles), increasing post-consumer cellulose processing recovery efficiency decreases the price of the product until all the desired PC material is incorporated. After that the price plateaus as only virgin fibers are included after that and increasing post-consumer cellulose processing recovery efficiency has no influence on the product. When virgin fiber is cheaper than post-consumer fiber, it is more cost-effective to not include any post-consumer fibers, therefore post-consumer cellulose processing recovery efficiency does not appreciably change the price of the product. Here manufacturer cannot reduce costs by improving post-consumer cellulose processing recovery efficiency, as the higher virgin fiber content is economically cheaper.

Alternatively, in Case 2 (Figure 5-5 C and D), when 90% post-consumer is required in the product and the recycling disposition rate is 50%, more post-consumer fibers are

required for the product than can be provided by the consumer. Thus, the recycling disposition rate is not high enough and improving the post-consumer cellulose processing recovery efficiency, even up to 100% recovery, will not be able to supply enough material to achieve the required recycled content in the product. However, when virgin fiber is more expensive than post-consumer fiber, the higher the post-consumer cellulose processing recovery efficiency and the greater the percent of recycled fibers, the cheaper the price becomes. Still, when virgin fiber is cheaper, it does not benefit the manufacturer to include post-consumer fibers. Only at a post-consumer cellulose processing recovery efficiency of 1 does the cost to produce a 90% post-consumer content product reach approximately the same cost as that to produce the product when post-consumer marginal cost is cheaper. There would also be little incentive for manufacturing to reduce the PC marginal costs below virgin material by improving process.

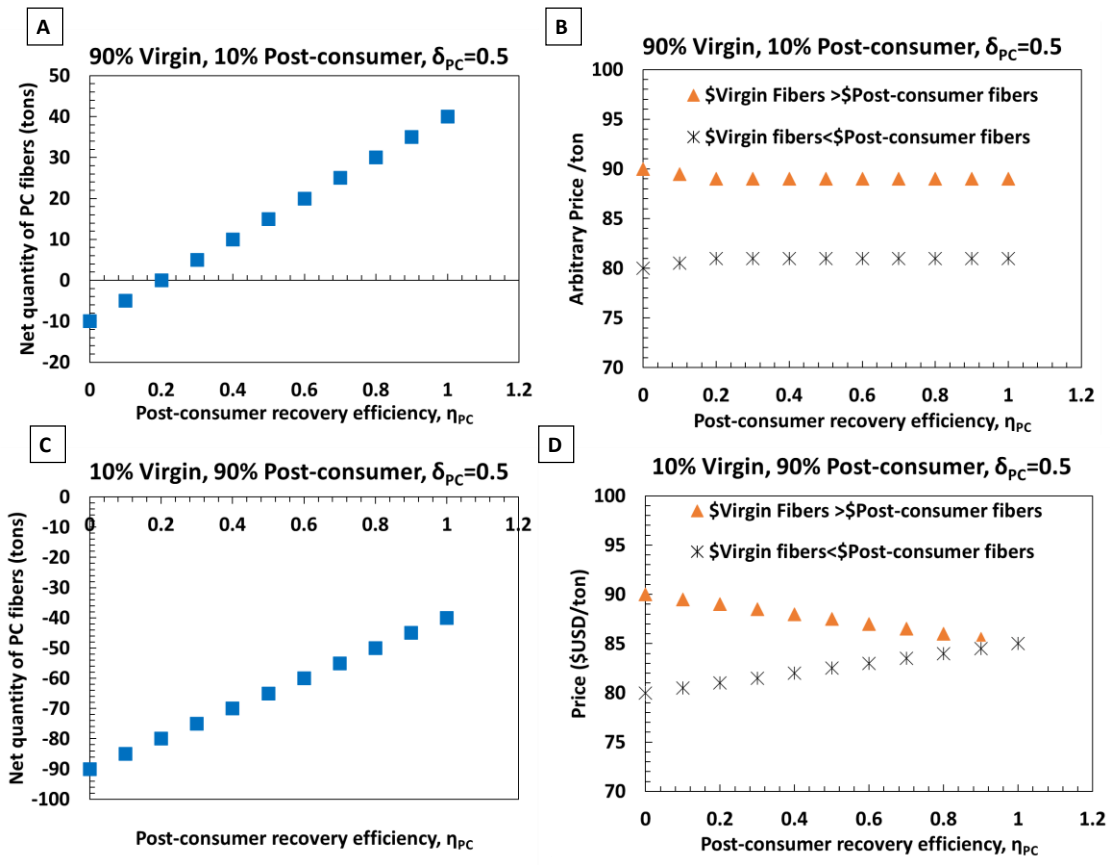

Figure 5-5. Graphs of net quantity of post-consumer fibers (Tons of excess PC) versus post-consumer recovery efficiency when δ_{PC}= 0.5 (recycling disposition rate) and β= 0.1 (PC fiber content) in Case 1 (A) and its corresponding price in Case 1 to produce product when either virgin or post-consumer fiber pulp is more or less expensive (B) and Tons of excess PC fiber versus post-consumer efficiency when δ_{PC}= 0.5 and β= 0.9 in Case 2 (C) and corresponding price in Case 2 when virgin or post-consumer fiber pulp is more or less expensive (D).

Because the δ=0.5 shows that in Case 1 and 2 increasing post-consumer recovery efficiency may not be enough to increase circularity, Case 3 examines a 90% post-consumer fiber product with a 90% recycling disposition rate. This is compared to Case 2: 90% post-consumer fiber product with 50% recycling disposition rate (Figure 5-6 A and B). While a 90% recycling disposition rate may be difficult to achieve, this illustrates that a higher recycling disposition rate allows manufacturing to make a more 90% post-consumer fiber product at yields less than 1. At a cellulose PC recovery efficiency of 0.6

or greater, the price to produce a product with 90% PC content is cheaper in the case when post-consumer fiber marginal cost is cheaper than virgin, compared to when virgin fiber is cheaper than post-consumer. This is incentive to reduce MC_{PC} and PC recovery efficiency at efficiencies greater than 0.6 but less than 0.6, there is no incentive to do either. This suggests that in some cases , it can be beneficial for a manufacturer to produce high recycled content paper products if both the cellulose processing recovery efficiency and the recycling disposition rates from consumers are sufficiently high. There are two key takeaways:

1) If the goal is to increase desired PC content when $MC_V < MC_{PC}$, then the public would need to pay, when manufacturing yields are low. Otherwise, firms may not have incentive to reduce profits.
2) With high recycling diversion rates, more material is available and therefore yields do not need to be as high. This sets up yields at which firms have incentive to have higher PC content material.

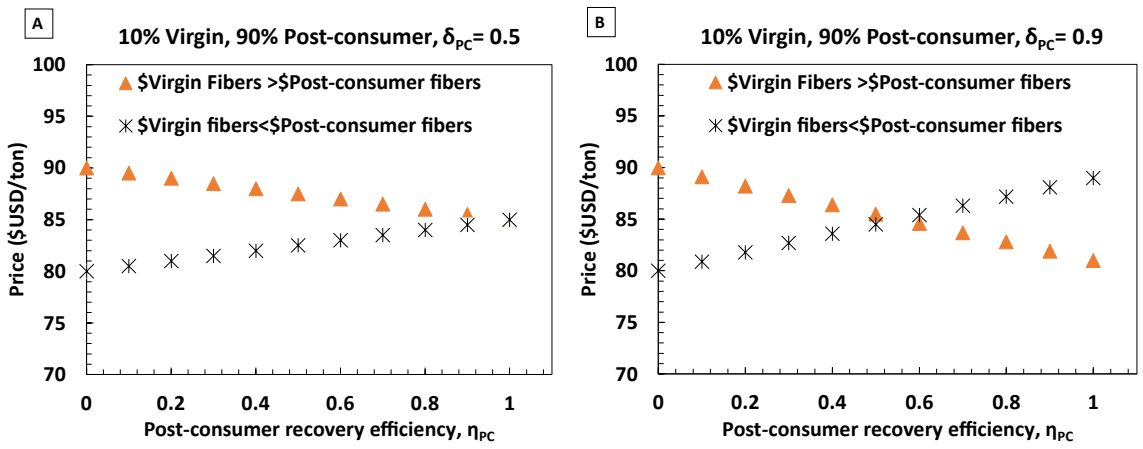

Figure 5-6. Graphs of price to produce product versus post-consumer recovery efficiency when either virgin or post-consumer fiber pulp is more or less expensive in Case 2 when recycling disposition rate is δ_{PC}= 0.5 and post-consumer content is β= 0.9 (A) and when δ_{PC}= 0.9 and β= 0.9 in Case 3 (B).

5.4.1.2 Influence of post-consumer content at high post-consumer cellulose processing recovery efficiency and recycling disposition rates

In the previous cases, how the cost of production of the product changes with cellulose processing recovery efficiency was described. Achieving high yields during cellulose processing from post-consumer waste is not always feasible but even when high yields are achievable, the feasibility of making high PC content products may be limited by the disposition behavior . In Cases 4-6, the analysis was reframed to assess how the decision to include post-consumer content in the product changes the price to produce when post-consumer cellulose processing recovery efficiency is high at 90% (η_{PC}= 0.9) and with three different consumer recycling disposition rates (δ_{PC}=0.1, 0.5 and 0.9) in Figure 5-7 A, B, and C, respectively.

First, increasing the recycling disposition rate increases the supply available to make products with increasing post-consumer fiber content. The point in the curves where

a plateau is reached represents where there is no longer enough of the original post-consumer content fibers and it must be substituted with another stream, in these cases with virgin fibers. Note that this means that the x-axis in Figure 5-7 shows the *desired* amount of post-consumer fibers, not the actual amount. At low disposition, there is very little change in the marginal cost as the desired fraction of post-consumer fiber in the product increases because there is insufficient supply of the fibers. Increasing the recycling disposition rate to 90% when the cellulose processing recovery efficiency is 90% allows the manufacturer to make a product with up to 80% post-consumer content (Figure 5-7 C), as seen by the plateau not being reached until the desired amount of post-consumer fibers is 80%.

Second, when the marginal cost of virgin fibers is less than post-consumer fibers, initially increasing efforts to incorporate post-consumer material increases costs, especially at low recycling disposition rates. When there is a given price-point that consumers are willing to purchase a product, if manufacturers add more expensive recycled content, they either have to reduce their profit margins or pass those costs on to consumers. If consumers are not willing to pay, then they will not buy the product with higher recycled content and circularity will improve. If neither option is feasible, then there is no motivation to increase recycled content. If there is sufficient added benefit to society to included recycled-content, then this is justification for policy intervention.

Additionally, there is cutoff at high recycling disposition rates (0.9) of post-consumer content above which the overall cost to produce the product with high recycled content is cheaper when the marginal costs of post-consumer fiber is below marginal costs of virgin ($\beta > 0.5$ to beta = 0.8 in Figure 5-7 C). Here it would benefit manufacturing to put

research efforts into reducing marginal costs of post-consumer fibers to increase profit margins or decrease price for the consumer, while increasing circularity by increasing post-consumer content. This regime lasts up until the point (80% post-consumer content), where this is no more recycled content available from the initial post-consumer product stream.

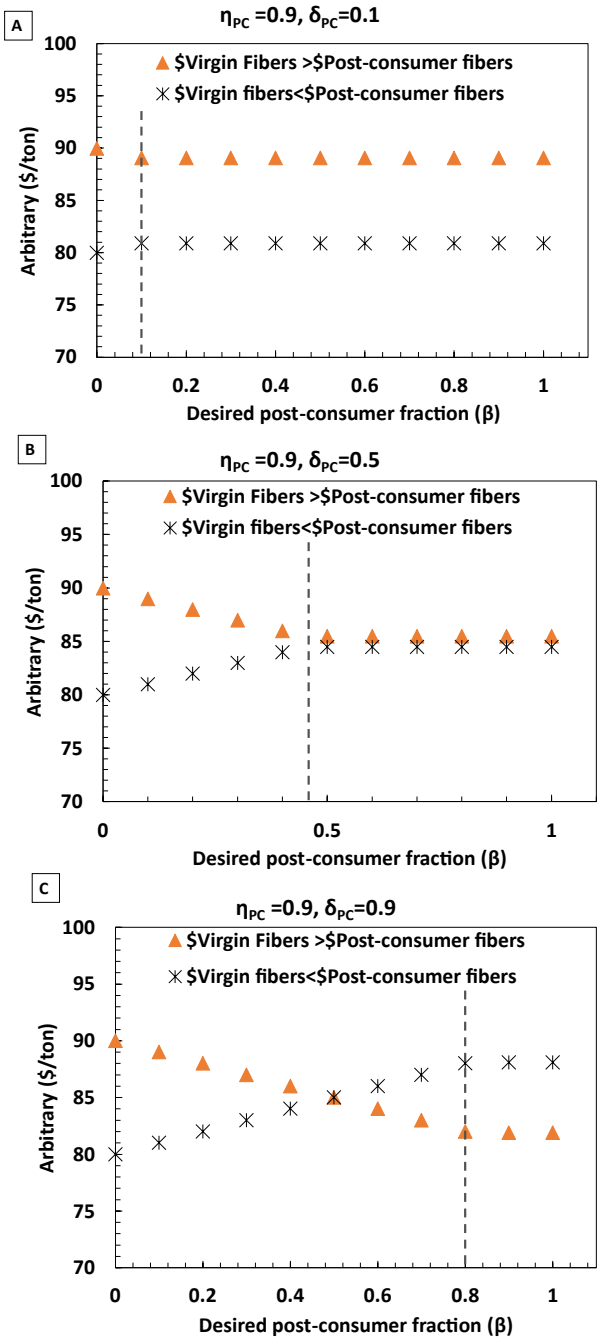

Figure 5-7. Graphs of price to produce product versus the desired post-consumer fiber content when recycling disposition rate is δ_{PC}= 0.1, 0.5, and 0.9 and recovery efficiency is η_{PC}= 0.9 in Case 4 (A), 5 (B), and 6 (C) when either virgin or post-consumer fiber pulp is more or less expensive. The dashed lines represent the point where there is no longer enough post-consumer material and the remaining amount is substituted by virgin fibers.

5.4.2 Application of cellulose nanofibers in the framework

There are several ways to approach the application of CNMs into this circular economy framework . They can be produced from both consumer and manufacturing waste streams that may not currently utilized as illustrated in Figure 5-8 . This is an active area of research and includes sources such as sludge [269], waste-water [68], cartons and variety of other waste paper streams [61]. Extracting CNMs from waste streams and putting them back into products as additives or stand-alone products increases circularity by reducing waste.

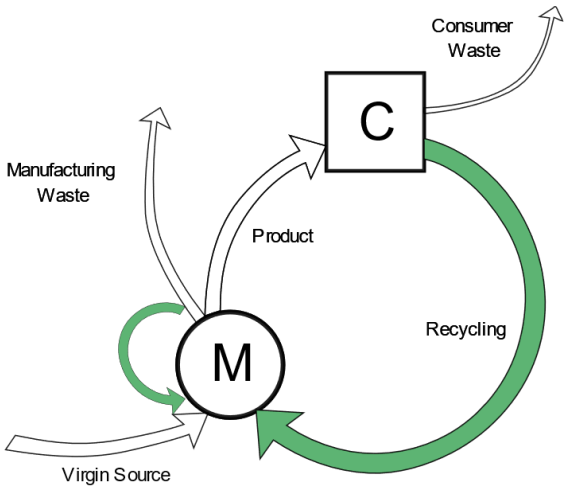

Figure 5-8. Circular economy-based framework highlighting which waste stream segments the use of CNFs can be sourced from and from which they can help improve the incorporation.

Figure 5-4 shows how small particles of cellulose may be present in the fiber-poor waste streams after the recovery steps for larger pulp fibers, particularly if separation is

based on size. In extracting CNMs from the fiber-poor waste streams and putting them into the useable fiber-rich stream, they will change the ratios of non-cellulosic and cellulosic components in the fiber poor and fiber rich streams (O_{NU}/F_{NU} and O_U/F_U) and increase overall yield in the useable fiber rich stream if they are used in the manufacturing of the same product.

If CNMs are extracted from a non-usable waste stream from a different manufacturing process (for example from beer residuals in the production of beer or agricultural waste) or from consumer waste, while they may not increase the yields of the source material for that process, they are reducing waste streams and recuperating value of what would otherwise be waste. As suggested in Figure 5-6, when supply of post-consumer material is high through increasing recycling disposition rates, the yields required to make a high post-consumer and cost-effective recycled product can be lower. Because yields of CNMs from non-virgin sources are currently highly variable and low in many cases at the lab scale [61], the PC recovery efficiency will need to be off-set by higher recycling disposition.

The available quantity and marginal cost of post-consumer products are also subject to the economic equilibrium supply and price as illustrated in Figure 5-9A. It can be expected that an increased supply of post-consumer product through increased recycling disposition, will decrease the equilibrium price of those products for firms. Additionally, both economies and diseconomies of scale will apply and affect the cost per unit to recycle post-consumer product, but this was not reflected in this model and can be considered for future works. As illustrated in Figure 5-9 B, initially the recycling costs associated with accessing new CNF supplies and having initial low yields will decrease over time as the

collection and recycling rate and recycling disposition rates increase [270,271]. An increased supply from consumers should decrease marginal costs, leading to lower overall values of the product to be sold to consumers, while maintaining quality of the product. Consequently, a loss in yield (recovery of cellulose from sources during processing) may be offset by quantity and price of available cellulose supply.

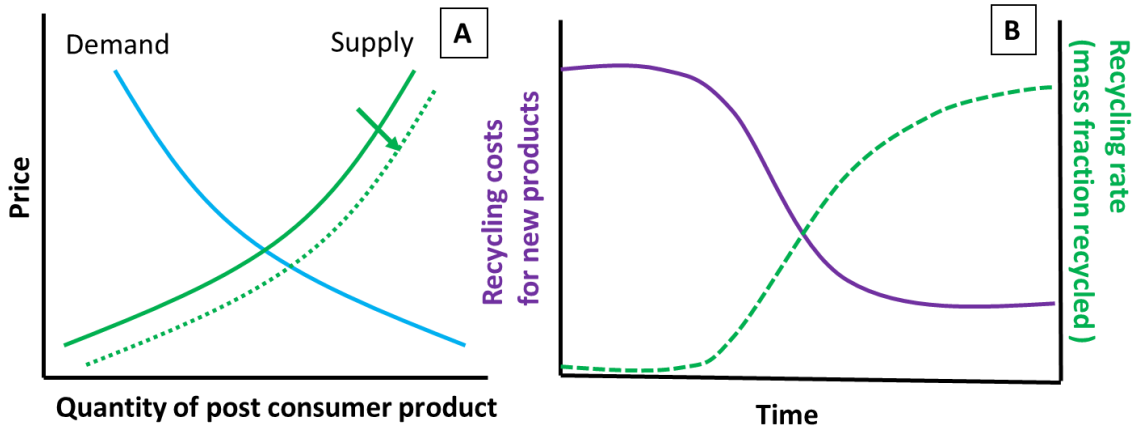

Figure 5-9. Illustration of a typical supply and demand curve representing a decrease in price point when quantity of post-consumer product supplied increases (A). For new technologies, economies of scale applies with recycling as initial recycling costs are high and recycling rates are low but change over time until plateauing (B).

5.4.3 Incorporation of polyelectrolyte complexes

So far, the treatment here assumes that all fibers put into a product are completely retained during the incorporation manufacturing step but the retention of fines is papermaking is a significant challenge. Because CNFs are small enough to be considered fines, the total CNF content added to pulp fibers may not be retained in the product. The appropriate addition of PECs can improve CNF retention (reduce CNF mass loss to

manufacturing waste during a mixing and incorporation step). The appropriate use of PECs allows for cellulose fibers, particularly fines, to continue through to the circular economy by decreasing manufacturing waste. They also alter the strength and physical properties which consumers may alter consumer perception of the packaging. These can be considered as part of the total weight of the product by solids and have their own marginal and manufacturing costs. Their recyclability should be considered in future works to incorporate these and other additives into the mathematical treatment.

5.5 Discussion

5.5.1 Cellulose nanomaterials in products

In general, the advantage of CNFs in packaging is that they can be added at smaller weight percentages by dry mass (0-10% CNF) than virgin fibers, while achieving the required strength and barrier properties and making the overall product more lightweight. They allow for the displacement of virgin pulp fibers with recycled pulp by improving properties and thereby increasing the tonnage of recycled fibers going into the product. Zambrano et al. showed that a cost reduction as high as $149/ton of fiber can be driven by the addition of CNFs in paper by reducing the weight of typical pulp fibers while achieving the same tensile strength. They also saw an increase in cost reduction with increasing CNF content and displacing pulp fibers with as low as 1 wt.% and up to 10 wt.% [53].

Given that after successive processing and recycling, particularly drying, fibers collapse, the level of fibrillation to create CNF from some recycled fibers may be difficult and instead a greater percentage of CNF with lower fibrillation in the product may be required [39,60]. Still, Delgado-Aguillar et al. showed that paper sheets made of virgin

chemical pulp fibers with non-chemically treated CNF (35% yield) maintained the same breaking length (a property tied to its strength) for 6 more recycling cycles than the unrefined virgin pulp by itself [59]. Their LCA analysis comparing the CNF added to the virgin pulp versus refining the pulp itself suggested that the overall impact to the environment or human health is not higher, though energy demand for recycling them is greater. The incorporation of CNCs in PLA films has also shown to increase number of times the composite can be recycled [272], facilitated recycling of epoxies [273], and can be recycled as solar cell components [274].

5.5.2 Cellulose nanomaterials in recycling streams

If CNMs make into the recycling stream, the challenge is whether manufacturing can efficiently sort, recycle, and extract the material to be able to transform it back into useable material for products. Making post-consumer CNMs must be feasible from a technical standpoint and should be cheaper than virgin CNMs for the desired post-consumer CNM content (β in the framework) at a given recycling disposition rate (δ_{PC}). To incentivize firms to use post-consumer CNMs and increase circularity, the marginal cost of recycling CNM should be cheaper than landfilling them or recovering them from virgin sources.

The ability for CNMs or CNM-containing products to be recycled is still in its infancy and being actively developed primarily at the lab scale [273,274]. Initial testing suggests that separation of CNM, particularly as multi-layer with other material types is feasible, efficient, and cheap [274]. Ang et al. found that CNF sheets made from virgin, industrial, and lab recycled pulps, are recyclable with a standard disintegrator and could be

remade into CNF sheets. The recycled CNF sheets maintained 80% of their original strength and significantly reduced drainage times [60]. The reduced drainage times and that the recycled CNF films do not have to be re-homogenized may translate to reduced marginal costs when using recycled CNF streams over virgin pulps to make CNF films. Still, scale up and practicality of recycling CNMs effectively in available manufacturing equipment, for either paper or plastic, needs to be addressed to understand true manufacturing efficiency. Currently if CNMs act as thin plastic films, this may be problematic in current industrial sorting and recycling equipment, but if in the cases where they are coatings or additives in an all cellulose-based product, potentially they can be recycled with typical paper or cardboard machinery thus contributing to an attainable post-consumer recovery efficiency (η_{PC}).

5.5.3 Consumer perceptions and response to cellulose nanomaterial-containing products

Since few CNM-containing products are on the market currently, an understanding of consumer response to products containing them is developing. If the marginal costs to produce the products exceed those of currently available paper or plastic alternatives without improving quality or product performance, consumers will likely not purchase CNM-containing products.

How consumers respond to physical attributes of CNM-containing products may influence consumer disposition behavior and therefore circularity. Since CNMs are likely to be produced as thin films [50,275] and used in a multi-layer or be blended into other materials [53], they may not be visible to consumers who thus may not respond differently to CNM-containing products compared to other products currently on the market that provide

the same function. It is possible that CNMs will look and feel like plastic given that CNC and CNF films have low opacity [64,274], have a low surface roughness (more smooth) [274], and are stronger and more durable than typical paper [54,65]. Because consumers rely on physical attributes such as material and structural cues to form judgements on sustainability [254] and disposition behavior [258], they may not treat CNMs in the same way as other paper products, which have higher recycling rates than plastic. Thus, recycling disposition rates of CNMs may be low.

Other determinants such as consumer knowledge of the ability of the products to be recycled, peer-behavior, and learned perceptions about the material will dictate their disposition to send the material back through the circular economy. Without knowledge of whether the product can go into regular recycle streams, consumers will not know what to do with CNM-containing materials even when they are designed to be recyclable. However, consumers have been willing to accept the inconvenience of recycling paper after education, even when labeling is not effective [258], which implies that educational interventions can improve recycling behavior [260]. Additionally, firms value proposition is different based on the recycling disposition rate regime.

5.6 Policy implications

In this study the focus was on the role of three parameters (recovery of cellulose from processing such as recovery, recycled content, and disposition) in the cost of manufacturing a product in cases where either virgin or recycled fibers are more expensive. All three parameters can influence the price of the product that manufacturers can make. By considering the overall cost to produce paper products with recycled fiber content, policy

interventions can be suggested in cases where incorporating recycled content is too expensive either to produce or for the consumer to buy and thus it does not benefit the manufacturer. If there is social or environmental benefit to be gained from the inclusion of more recycled content and improving the circular economy, but manufacturers do not have incentive to produce enough quantity of recycled products, then there may be justification for policy interventions such as subsidies can be considered to offset the cost to manufacturing to achieve optimal marginal benefit to society. Alternatively, if there are negative externalities and consequences to using virgin material over recycled content, then there is again justification for intervention to price in these externalities so that firms favor the inclusion of recycled content in products.

Negative externalities may exist in the form of pollution from waste to landfill and in the environment from disposition behavior, waste from low yields in the recovery processes, or over-producing useable material, which implies excess energy consumption. The framework presented here give an opportunity to consider negative externalities at individual steps in the circular economy depending on product, efficiency, and disposition cases. Cases exist where firms have no financial incentive to incorporate post-consumer material into products and consequently a policy case may be made to price in negative externalities. In terms of recycled content, the United States already has some policies and recommendations for recycled post-consumer content in a variety of paper products[276,277] but it is possible that these may not be feasible for manufacturers to achieve if appropriate yields and consumer disposition are not high enough to be able produce useable post-consumer fibers. Here additional policy recommendations may be to provide funding of R&D and manufacturing that can improve methods and techniques to extract more useable

material at better marginal costs with less waste. This highlights where firms are not willing to make these changes on their own because it would not be cost-effective to do so. A known issue with recycled material streams is lower yields, in part due to contamination from single stream recycling collection. Here policy interventions that fund recycling education, give incentives or increase clean collection of post-consumer products may be beneficial, which then result in downstream improvements in the amount of recycled content manufacturers can put back into new products through higher recovery efficiencies.

For each gate in the circular economy framework presented, more work and a deeper analysis is needed to understand additional impacts that influence the price to collect, recover, and incorporate recycled content, beyond a material balance approach and its relationship to pricing. This can include energy used, number of cycles the material can provide function, and waste in terms of negative externalities that can arise at the consumer and manufacturing gates and the discrete steps within them.

5.7 Conclusions

In this chapter the aim was to create a framework and present the idea that consumers are major contributors in the circular economy. Aframework was formalized to understand circularity based on three variables: consumer disposition behavior, recycled fiber content, and post-consumer cellulose process recovery efficiency. Each of these influence flow of material through the circular economy and can be used to understand areas for policy recommendations and improve outcomes for manufacturing, consumers, and sustainability. This approach can lend itself to more effective product design that incorporates people and reduces both economic and landfill waste.

. By discussing the purchasing and disposition behavior of consumers it was shown that the consumers participate in altering the supply and cost of recycled material through the rate at which they chose to recycle (recycling disposition rate). If the recycling disposition rate value falls too low, manufacturing (who also has virgin material available) may not be able to recuperate the revenue of producing product with recycled material.

Once consumers recycle a product, manufacturing can re-extract cellulose material from these recycled products. This recycled material must be recovered with a sufficiently high cellulose yield and can then be reincorporated into new product once again. Whether manufacturing chooses to do this is based on whether they have incentives to do so from a policy, economic and material standpoint. Even when manufacturers are required to produce paper products with recycled content, given that recycled products often lose strength and other material properties, it makes it difficult to use recycled fibers compared to virgin material. There must also be other incentives to use these including the economic value of a recycled content containing product. The cost of the recycled material and whether the new product can again meet price points determines whether it will be returned to the consumer to cycle again through the circular economy.

CHAPTER 6. CONCLUSIONS AND FUTURE WORK

In this chapter the contributions of the work from the previous chapters and how they contribute to the overall field of improving sustainability of the papermaking process by utilizing formulation with cellulose nanofibers and polyelectrolyte complexes are summarized. Based on the conclusions, future work in this area is also presented.

6.1 Conclusions and impact of current work

6.1.1 Order-of-addition and coacervates

Polyelectrolyte complexes (PECs) are often used in papermaking but the interactions between polyelectrolyte complex coacervates with cellulose nanofibers (CNFs) are not well understood. In Chapter 2, how the order-of-addition as a mixing strategy of polyelectrolytes in a coacervating system influences their interactions with CNF was studied. Specifically, the impacts that electrostatic interactions have on the aggregation behavior of the coacervates to the fibers over time were examined, in terms of molecular interactions, morphology in suspension, and water retention values, a relevant dewatering parameter to the paper industry.

In this study, the morphological aggregate formation and time of association of coacervates with CNF were shown by forming low molecular weight and weak polyallylamine hydrochloride (PAH) polycation and polyacrylic acid salt (PAA) polyanion coacervates at 1M NaCl with CNFs in three different mixing sequences without the influence of external mixing. It was observed that by changing the order-of-addition of the polyanion and polycation to (CNFs), the interactions between PECs and CNFs can be

tuned, which in turn changes the extent of association of the coacervates to the CNFs and the rate at which they aggregate. Without any additional agitation, the electrostatic interactions drive the aggregation of the PECs with CNFs, which is faster and shows morphological differences of the aggregates on the CNF and with measured electrophoretic mobility at early time points. Importantly for the papermaking process, when adding the polycation to the CNFs first, the statistically significant lowest water retention values were found, compared to the other cases. Pre-formed coacervates with CNF did not have lower values than the CNF controls.

Coarse-grain molecular dynamic simulations further illuminate the fundamental mechanism of aggregation by taking into consideration the interaction between cellulose and the complexes at the molecular level. They were carried out in a similar manner as the experimental tests, where first CNFs were introduced to one polyelectrolyte with counterions and salt and an implicit solvent. After the simulation has equilibrated for some time, the second polyelectrolyte was added. Simulation snapshot showed that many smaller PEC coacervates for with PAH first, whereas when PAA is introduced first, few larger PEC coacervated form. The radial distribution function showed that the density of polycations spike near the surface of the CNFs, unlike the density of the polyanions which was low. Mean square displacement overtime showed that the polyelectrolytes move slower than fibers because they are part of an agglomerate in the PECs and the presence of the polycation near the fibers cause them to move slightly slower when polycation are added first.

The simulations corroborate the experimental observations by showing the importance of strong electrostatic interactions in aggregate formation. More broadly, this work improves the understanding of how order-of-addition, not just polyelectrolyte charge and structure, plays a significant role in polyelectrolyte complexation and interactions with particles from the molecular scale. This is impactful because properties such as adsorption, strength, flocculation size, or drainage have been shown to be improved in some cases with varying order-of-addition of polyelectrolytes or PECs, but mostly with large molecular weight polyelectrolytes that favor bridging mechanisms between particles and fibers [162,196]. Here, the simulations with experimental testing support the idea that the underlying mechanism that result in experimentally measurable differences from order-of-addition are a result of the electrostatic interactions at a molecular level.

6.1.2 Water retention values of cellulose nanofibers and polyelectrolyte complexes

PECs formed with different polycations and experimental conditions can exhibit solid-like (precipitate), liquid-like (coacervate), or solution phase behavior. In Chapter 3, the aim was to gain a more specific understanding of how the formulation strategies of using low molecular weight polyamines in a PEC system impact its phase behavior and corresponding dewatering of the CNF-PEC networks as measured by the WRV test developed in Chapter 2. In this work, three readily available polycations (PAH, PVAm, and PEI) were complexed with the polyanion polyacrylic acid (PAA) and the electrostatic interactions were experimentally varied by increasing the ionic strength of the solution and reducing the number of intrinsic ion-pairs of the PECs by changing the charge ratio of the polyelectrolytes. By dosing PECs in excess but keeping the system near neutral for charge-

match conditions (1:1) or highly charged for “away-from-charge-match” (4:1), the influence of PEC behavior on the WRVs of the CNF-PEC could be tested. The results showed that:

1. WRVs of CNF-PEC systems can be tuned by experimentally altering electrostatic interactions with increased salt concentration or changing the charge-match ratio. At 0M NaCl all systems had large WRVs at 1:1 charge-match ratio in a low-salt regime possibly due to densification of the network and improved (lower) WRVs in a high-salt regime due to changes in flocculation behavior.
2. A specific physical mechanism explaining why large WRVs are observed at 0M or low NaCl for the PEC complexes tested here was not identified but it is clear this behavior is related to electrostatic interactions in the systems because the WRVs decreased with increasing salt concentration or with the large deviation from charge-match conditions in the low-salt regime.
3. Polycation selection influences WRVs of CNF-PEC networks. Particularly at high-salt regimes, non-electrostatic interactions may play a role. The measured turbidity of the uncharged polycations was high at the lowest concentrations for PEI, suggesting that it is the most hydrophobic of the ones tested here. PEI/PAA complexes in the CNF system were coacervate-forming, particularly at a higher salt regime, and had the least improvement in WRVs, suggesting that the more hydrophobic polycation had decreased interactions with hydrophilic CNF when electrostatic interactions are reduced.
4. WRVs where a coacervate phase were observed were not necessarily better than those where solid-like precipitating phases were seen at the same high-salt

concentrations. More work is needed to deconvolute the impact of a coacervating phase on WRVs, particularly at low-salt concentrations. This may shed light on the physical mechanism leading to high WRVs at low-salt concentrations for some PEC systems.

Overall, this work gives insights into appropriately selecting polycations and experimental conditions when using PECs as drainage or retention aids in papermaking. Because CNF were used in this study, this will be further applicable to the formation of nanopapers, which are known to be difficult to dewater and have long drainage times due to the high surface area [41]. By understanding how polycation selection and PEC phase behavior influences WRVs of CNF-PEC networks, with reduced but not significantly diminished electrostatic interactions, there is potential to improve dewatering during fiber mat formation. While PECs are intended to improve dewatering, there are cases where these hinder drainage and dewatering [30], but more work is needed to attribute this to a specific physical mechanism. It has been hypothesized that free PECs may act as fines or the shape or size of the complexes may result in plugging of the fiber mats [30]. By systematically showing the influence of polycation selection and experimentally altering electrostatic interactions, this paper gives insight that the changes in WRV behavior with different polyelectrolytes is likely electrostatic in nature and that the dewatering of CNF-PECs can be improved.

6.1.3 Applicability and impact on percent solids of paper handsheet making

Because the appropriate formulation strategies with cellulose fibers and PECs have the potential to improve percent solids of paper products to decrease energy usage during

drying, in Chapter 4, the formulation strategies from Chapters 2 and 3 were used to scale up and make paper handsheets with CNFs and PECs. The purpose of this chapter was to lay the groundwork for a method to measuring percent solids changes when precipitate (PAH/PAA) or coacervate (PDMAEMA/PAA) forming PECs are included with CNF to a standard softwood fiber pulp. Tensile and opacity testing were also tested to both gain insights on how the two different PEC systems affect physical properties which will be important to consider when thinking about sustainable product design in terms of how these will influence consumer disposition behavior for future studies. Opacity of packaging is known to influence purchasing behavior [234].

Overall, a method for measuring percent solids was found to a show decrease in percent solids with the inclusion of 5 wt.% CNF compared to solely pulp, but further development is needed to see improvements when PECs are added because they did not show appreciable improvement or differences between the two systems. Tensile properties of handsheets improved with the inclusion of CNFs and further improved with the inclusion of either PEC systems. The opacity values of the handsheets were statistically significantly higher when CNFs and when polyelectrolytes (either just PAH polycation or either PEC systems) were added to the pulp.

In this study, the overall weight percent of PEC added to the total weight of dry pulp was 2.4% which is slightly higher than PEC addition to pulps. In typical paper product applications these anywhere from 0.01 to 3% [151,278,279] , although 3% is less common. Here, the PEC loading is realistic of those used in typical pulps. Further understanding how increasing concentration of PECs added to pulp and CNF slurries will likely help with formulation to improved percent solids. This study is broadly applicable relevant to the

current industry trends of creating CNF-containing paper products [41] which will likely be formulated with PEC drainage, retention, and flocculation aids. Additionally, limitations and recommendations for improving methods used here are discussed in Section 4.2.2.

6.1.4 Creating a circular economy framework that includes consumers and manufacturing for improved sustainability

Given that sustainability is a broad challenge, in this chapter a circular economy framework was created and a model was formalized to incorporate both consumer and manufacturing gates, and their waste streams. It introduces the idea that consumers are major contributors in the circular economy story of paper products, specifically packaging. By extension, how consumers will impact the circularity of developing cellulose nanofiber packaging was also discussed. While other circular economy frameworks may include consumer recycle and landfill behaviors [268], the framework here highlights the direct impact and the magnitude of consumer recycling disposition behavior on the manufacturing decision-making to include post-consumer material in subsequent manufactured products. Consumer purchasing behavior was considered from an economic approach in terms of the equilibrium price consumers are willing to pay to purchase products, whereas aggregate disposition behavior was considered as reflected through recycling rates based on material. Because each are of these are one of several known attributes that influence consumer purchasing or disposition behaviors, this framework can be modified and built upon for future work.

A simple mathematical model was developed to illustrate how the decision-making in consumer purchasing through their recycling disposition rate (δ_{PC}) influences the amount

of material that is available to manufacturing to turn into a product. Furthermore, how post-consumer recovery efficiency (yield) (η_{PC}) and desired post-consumer content (β) in the product influences the price to make a product during times when either virgin or recycled fibers marginal costs are cheaper, was investigated with low and high recycling consumer disposition rates. The results suggest there are regimes, for given recovery efficiencies or desired post-consumer contents, where firms will not have monetary incentive to include post-consumer material when virgin fibers are cheaper than post-consumer fibers or there is not enough material available for them to do so. Changes in research priorities and policy interventions can be considered depending on price-to-manufacture a product for given recycling disposition, yield, and post-consumer content within those regimes.

This framework was specifically used to illustrate recycled versus virgin fibers for standard pulps but can be extended to understand the inclusion of CNF or non-cellulosic components in the development of CNF packaging or other products. This lays the groundwork for consumer-centric thinking in product development specifically with the understanding of consumer disposition behavior, in developing products that will lead to improved circularity.

6.2 Recommendations for future work

6.2.1 Water retention values and drainage of cellulose nanofibers and polyelectrolyte complexes

The interactions between CNFs and PECs as they relate to dewatering from CNF slurries in this thesis were primarily tested through WRVs. However, WRVs are an imperfect way to evaluate dewatering, as they do not indicate how much water releases

over time during the formation of a CNF paper pad. Alternatively, drainage studies give an indication of the time it takes to release water, which is also relevant to the formation section of the paper machine and the time it takes to make a product on a machine influences the cost of production [66].

There are standard techniques for measuring dewatering and drainage of typical pulp fibers, but there are no standard techniques or equipment for drainage of CNF. Several researchers have created setups for measuring CNFs [27,66]. We have developed two drainage apparatus setups (Figure 6-1 and Figure 6-2) with initial data and propose a third (Appendix .Figure A. 5) based on the principles of a Britt Jar.

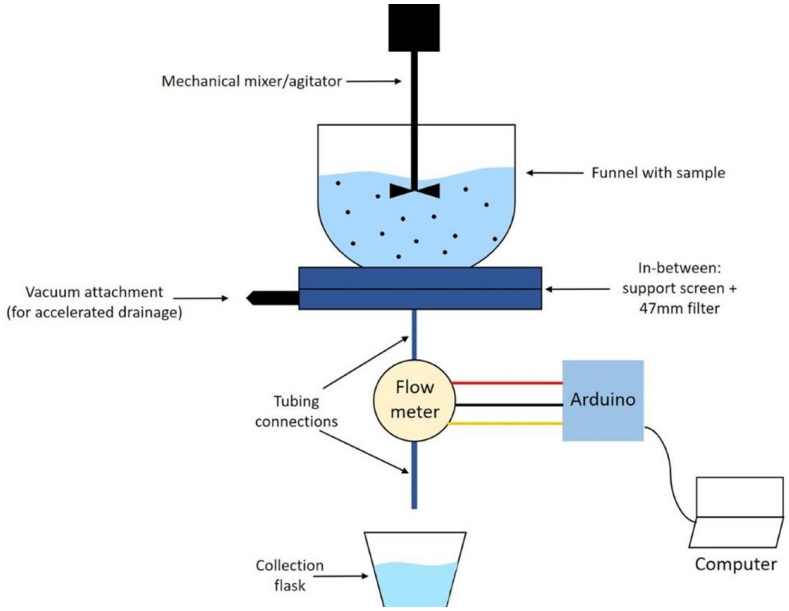

Figure 6-1. Schematic of drainage setup tested with funnel with vacuum attachment with flow meter and attached Arduino for data collection to a computer to measure drainage flow rate of CNF slurries.

A customizable prototype Britt Jar apparatus (Figure 6-1) to measure the drainage of CNF slurries was built and initial testing of slurries was performed to understand the

applicability of the design. The design was selected to be customizable for both vacuum and gravity filtration while a fiber pad forms during drainage process, can be used with and without agitation, and various filter types can be used. Sample suspensions of up to 300 mL can be tested. We included a flow meter to measure the water that drained out and added an electronic component to allow for automatic data collection. The initial data was collected automatically and manually for a 0.1 wt.% CNF slurry through the same filter type as used in the WRV studies in Chapters 2 and 3 which has a 0.2 µm pore size. It was found that this flow meter was not sensitive enough for the non-continuous drainage flow observed during the test and there were challenges with accurate detection of the fluid volume going through the sensor. An alternative design suggested is to place sensors along the length of a collection flask and continuously record this data (Figure A. 5 in Appendix).

A modified setup was attempted Figure 6-2 in which a 20 mL tube was attached to the bottom as a collector and time it takes for water to drain to a particular volume was recorded by with a camera. This was to remove the need for an automated flowmeter. After the drainage was stopped, the fiber pad and the filter were collected and weighted wet. After oven drying, they were weighed again to calculate percent solids. The weight of the filter was also collected prior to using it in the setup for drainage. Percent solids were calculated, and initial results are shown Figure A. 4 and Table A. 2 in the appendix. Although we provide some preliminary data, insufficient data were collected to draw conclusions on the performance of this apparatus for drainage measurement and future work should be performed to evaluate all designs to find the optimal for testing drainage through CNFs.

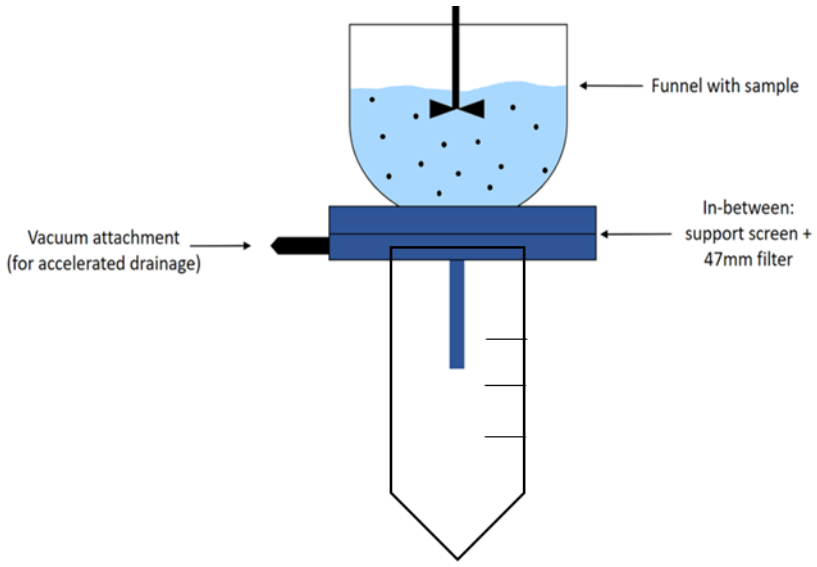

Figure 6-2. Schematic of drainage setup tested with funnel with vacuum attachment and 20mL centrifuge tube to measure volume of water drained over time of CNF and PEC slurries.

6.2.2 Testing cellulose nanofibers and polyelectrolyte complex retention in pulp handsheets

In Chapter 4, a method for testing handsheets was discussed. Another technically relevant aspect of forming handsheets with CNFs is characterizing the fibers and understanding the retention behavior of the CNFs and the PECs added.

While the dialyzed versions of CNFs used here were characterized in 2.1.1, the CNFs in handsheets described in Chapter 4 were used as received. The pulp was also disintegrated and used as received. Recharacterizing the non-dialyzed CNF and the pulp will be useful for understanding formulating with the appropriate polycation concentration because PEC dosing strategy are based on the overall charge of the fibers and in the system.

Controlling the amount of CNF that stay in the handsheets is a known issue and given the 200 mesh sizes typically used in the handsheet former, the potential for CNF to drain through is likely. In the results here, the 1 wt.% CNF percent solids were significantly lower than the 5 and 10 wt.% CNF handsheets, which had similar values. To study this behavior in more detail, CNFs can be tagged with a fluorescent label Rhodamine B isothiocyanate (RBITC) [237] or, alternatively, to understand both the retention of CNF and PECs, the PECs can additionally be fluorescently labeled with a different label. Either the polycation can be labeled with fluorescein isothiocyanate (FITC) [19], as was done in 2.1.2.2 or the PAA can be labeled and complexed with various polycations as has been shown with PDMAEMA previously [127]. With two different labels, which respond to different emission wavelengths, when they are used for the CNFs and PECs, their presence and interaction with each other and in a handsheet can be probed. Hobish et al. showed that the incorporation of RBITC did not change commonly tested handsheet properties and the zeta-potential of the fines after labeling was not changed [237]. With two different microscopic techniques (confocal laser scanning microscopy and two-photon microscopy), they were able to image primary and secondary fines. The primary being larger fiber segments that participate in the overall network like pulp fibers. Smaller secondary fines become concentrated in specific spots and are better able to migrate within the network and eventually fill in interstices spots between fibers. These are more likely attributed to reduced drainage. A better understanding of the mechanism that may be causing high WRVs of CNF and PECs in the suspensions in Chapter 3 and if a different behavior occurs when CNF and PECs are present in handsheets with larger pulp fibers would be valuable and could be probed through this fluorescent labeling. A supporting method to improve

understanding of the mechanisms would be to collect CNFs from the drained water and perform SEM and TEM and subsequent image analysis to calculate fiber sizes. This would provide information on which fiber sizes are most likely to drain for each formulation of interest and support mechanistic hypotheses.

6.2.3 Circular economy framework and life cycle assessments

In Chapter 5, we presented a new framework for circular economy that includes consumer behavior. We took a simple economic approach to explain consumer purchasing behavior although various models of decision making and technology adoption exist [255] and models to explain consumer reuse and disposition behavior [246,280,281]. These would influence circularity and offer other motivators and specific variables to be included in understanding consumer disposition in the initial stages of designing products. This includes how consumers would physically interact with and perceive new materials.

The framework presented here was designed with the flexibility to include non-cellulosic components with cellulose fibers in fiber poor and rich streams. Because most products are multi-component in which the components interact with each other to influence the retention and their incorporation in a final product, the model can be further utilized and developed to understand multicomponent systems. By adding another component, it can also be used to independently analyse additives, such as cellulose nanofibers, which might also be of interest to track through a circular economy and whose costs should be independently considered.

Furthermore, the framework did not include a discussion of collection and sorting of recycled products from consumers. These activities may manifest as a recycling

efficiency and be applied to recycling disposition rate in the model and impact the flow of material. We discussed disposition in terms of the number of recycled products that went to municipal waste systems and then returned to manufacturers. This means that there are several collection and sorting steps that happen that add to the cost and economics of recycling. An increasing number of private businesses and manufacturers exist that both make specialized products and ask their customers to ship used products back or their business is to specifically recycle specialized materials. This implies there are several and discrete paths between consumer and manufacturing beyond just municipal collection and other paths to manufacturing may be more sustainable.

In this thesis we discussed sustainability in terms of a circular economy framework. Circular economy in terms of mass flow is limited and call for additional ways of evaluating sustainability and policies. Other strategies include evaluating attributional life cycle analyses (LCAs) [282,283] or consequential LCAs [284]. Unlike circular economy treatments, LCA can better account for a variety of social and economic factors and can include impacts of products over time and are more standardized to be able to make better policy recommendations [283]. However, the same line of thinking in which various assessments of energy usage, CO_2 or other greenhouse gas emissions, and toxicity generated at each step of the circular economy as presented in the system in Figure 5-4 and through manufacturers and consumers gates can be evaluated. Consider that both recycled or virgin create their own waste streams, have energy and chemical demands to extract useable fibers, and have water and energy demands to incorporate them into fibers, without further analysis and there is no way to say one is better than the other in terms of costs, negative externalities, and how that affects consumers or the environment. Therefore,

LCAs that incorporate circularity or circular economy framework that consider consumer disposition should be considered that evaluate energy to produce, water consumption and recycling processes for CNMs. This is particularly important for the future CNM-containing products and packaging and which stream may require specific policy actions for development of this technology.

6.2.4 Development of consumer-centric metrics for circularity

We further recommend the formalization of a metric to represent circularity including consumer behavior. A single metric that includes the three variables that were discussed (consumer disposition behavior, recycled fiber content, and recycled fiber process recovery efficiency) can help understand how the individual components together influence overall circularity of a product. Various metrics have been proposed to evaluate circular economy with different strengths and limitations including at the product level [265,268,285]. A metric to measure circularity based on aggregating manufacturing costs from each successive manufacturing step until a product reaches the consumer has been proposed [285]. This type of treatment to can be applied to CNMs to evaluate circularity from recycled versus virgin streams and with different material blends and products.

6.2.5 Development of consumer-centric metrics for sustainable disposition behavior and product design

In Chapter 5, we discussed how consumers' purchasing and disposition behavior is influenced by a variety of factors including physical characteristics of packaging and other products. In Chapter 4, handsheets with CNF and PECs were made and tensile strength and opacity were measured. The idea was introduced that physical properties of paper such as

opacity and tensile strength are important for how humans perceive and interact with products. Because it is known physical attributes of packaging contribute to purchasing and disposition behavior, creating a metric that can incorporate human perceptions and measurable and changeable physical attributes to illicit a particular disposition response may be helpful in creating more sustainable products.

A well-documented and widely used metric that incorporates both scientific measurement techniques and human perception is the value ΔE in color science for formulating products of particular colors [286]. This and similar metrics combine studied and measured human perception of color of a standard observer and measurable spectrophotometric response of objects to various light sources. These behaviours can be mathematically combined using different models that then map color values in a multiple dimensional color space. From the color space one value (ΔE) is calculated based on its position in the space [287]. This metric is responsive to human perception of color and is used to formulate products to determine if a color is perceived as intended by people. While potentially challenging, a similar methodology can be applied to understand how perceptions of strength, opacity, or other physical and material metrics influence consumers perceptions and illicit particular disposition responses.

APPENDIX A. SUPPLEMENTARY INFORMATION

A.1 Water retention values of 0.5 wt.% CNFs with 50 mM total PEC concentration at maximum turbidity (charge-match) ratio with 0 to 1 M NaCl.

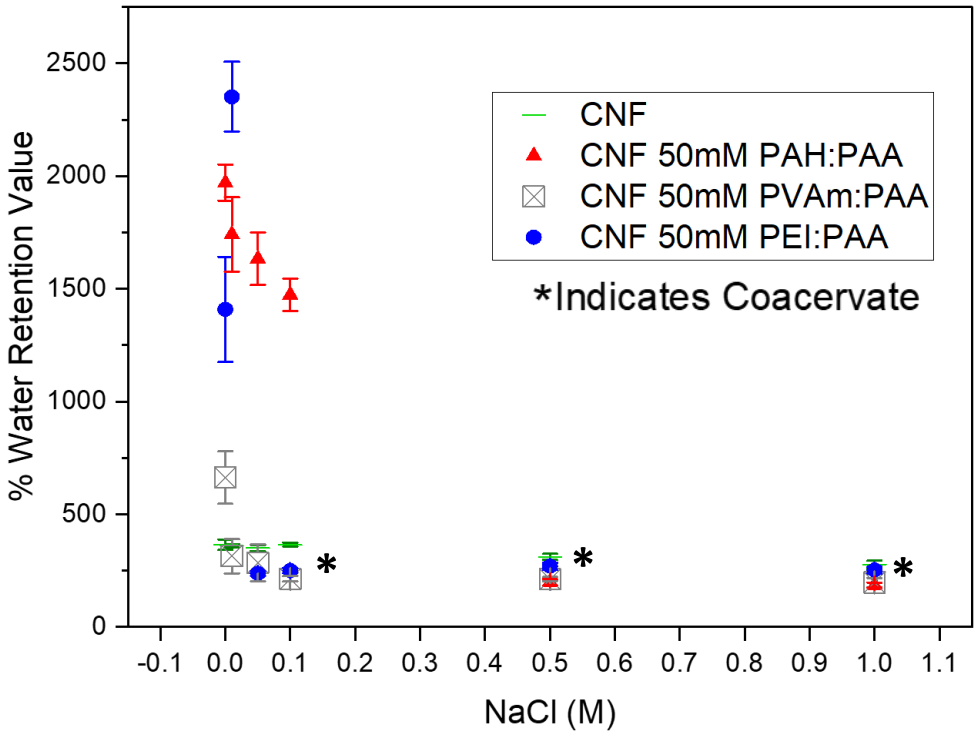

Figure A. 1. WRV of 0.5 wt.% CNF and 50 mM polycations (PEI, PVAm, and PAH) with PAA at maximum PEC turbidities for 0 to 1 M NaCl. The salt concentrations at which coacervate-like phase were detected for PEI/PAA is noted by * .

A.2 Water retention values of 0.5 wt.% CNFs with 50 mM total PEC concentration at "away-from-charge-match" (4:1) polycation: polyanion from 0 to 1 M NaCl.

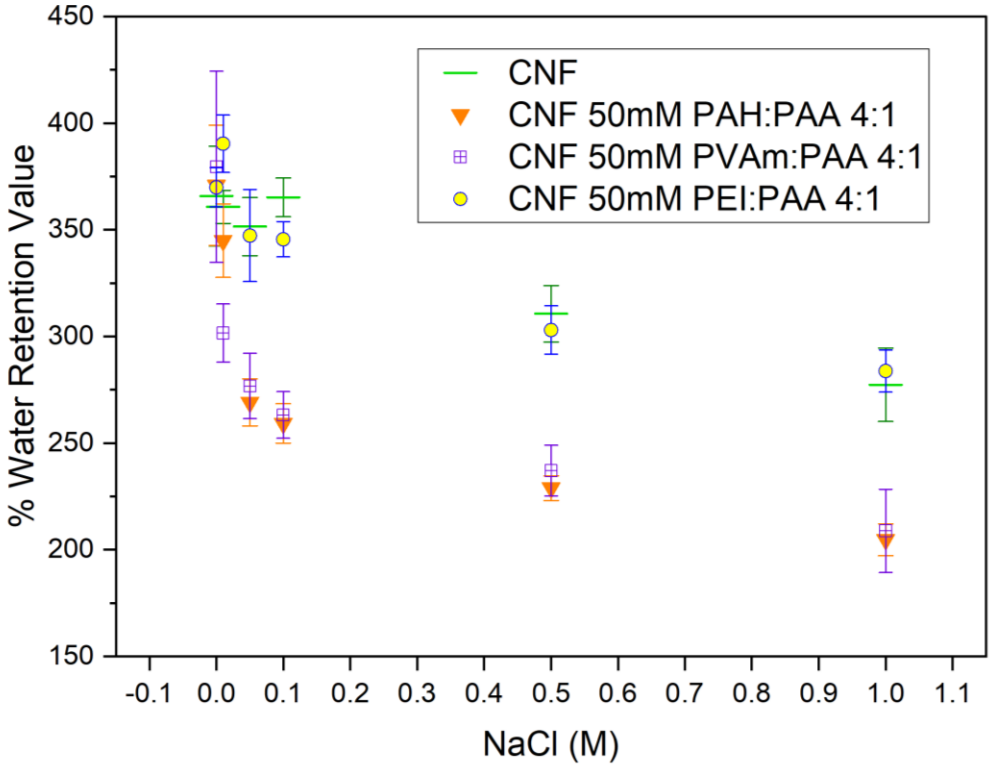

Figure A. 2. WRV of 0.5 wt.% CNF+ 50 mM PECs prepared at 4:1 polycation: polyanion charge ratio with CNF (green), CNF PAH/PAA at 0.77 mixing molar ratio (red triangle), CNF PVAm/PAA at 0.8 mixing molar ratio (purple square), and CNF PEI/PAA at 0.8 mixing molar ratio (yellow circle) with increasing NaCl concentrations.

A.3 Electrophoretic mobility of 0.05 wt.% CNF with up to 2.5 mM total PDMAEMA monomer unit concentration.

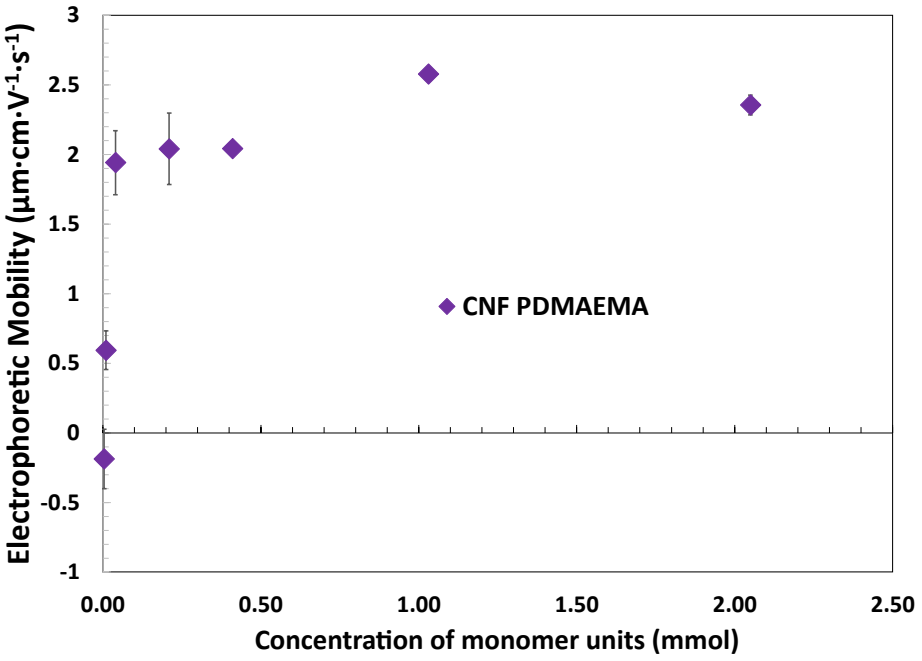

Figure A. 3. Electrophoretic mobility of 0.05 wt.% CNF with 1 mM NaCl and increasing concentration of PDMAEMA.

A.4 Handsheet tensile testing data in imperial units without normalization of basis weight.

Table A. 1. Handsheet mechanical testing results showing ultimate tensile strength, Young's Modulus, and tensile stiffness measurements.

Sample	Tensile strength (lbf/in)	Young's Modulus (psi)	Tensile Stiffness (lbf/in)
Pulp	3.23 ± 0.33	1.06E+05 ± 1.47E+04	828.4 ± 115.0
Pulp+ 5 wt.% CNF	6.45 ± 0.48	1.38E+05 ± 2.53E+04	995.2 ± 182.6
Pulp+ 5 wt.% CNF+ PAH	6.60 ± 0.79	1.44E+05 ± 2.98E+04	978.0 ± 202.9
Pulp+ 5 wt.% CNF + PAH/PAA	7.31 ± 0.43	1.59E+05 ± 1.19E+04	1193.0 ± 89.0
Pulp+ 5 wt.% CNF+ PDMAEMA/PAA	7.67 ± 0.43	1.58E+05 ± 1.11E+04	1198.0 ± 85.0

A.5 Preliminary drainage volume drained versus time data for CNF versus CNF with a precipitate PEC (PAH PAA) and a coacervate PEC system (PDMAEMA PAA).

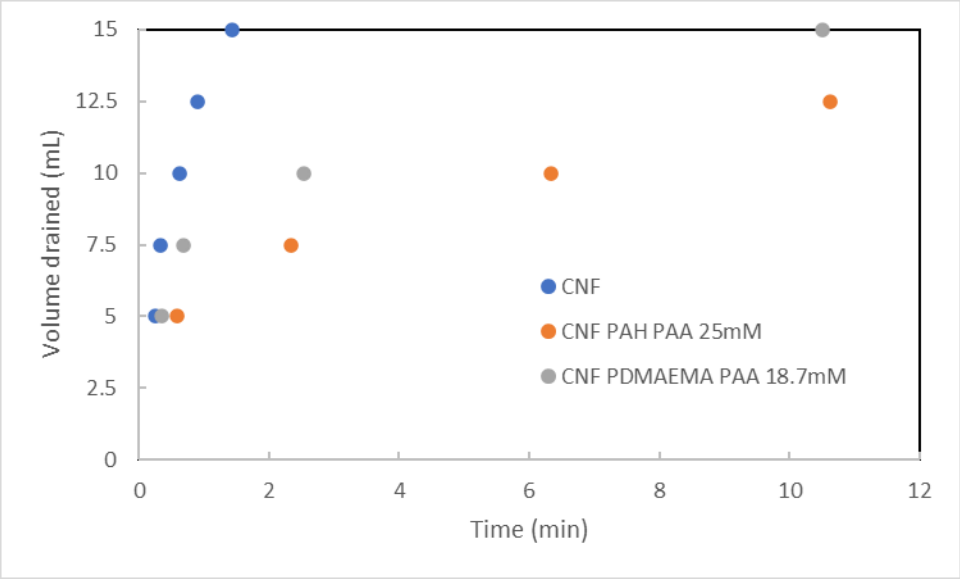

Figure A. 4. Initial drainage testing results of CNF and precipitate-forming PEC system (PAH PAA) and coacervate-forming system (PDMAEMA PAA). These are only demonstrative results of the potential use of the drainage setup and should not be used to make conclusions.

A.6 Preliminary percent solids of CNF versus CNF with a precipitate PEC (PAH PAA) and a coacervate PEC system (PDMAEMA PAA) formed in a drainage apparatus.

Table A. 2. Percent solids results of fiber pads made during initial drainage testing. These are only demonstrative results and should not be used to make conclusions.

Sample	**% Solids**	**Repeats**
CNF	21.8%	1
CNF PAH PAA	9.1%	1
CNF PDMAEMA PAA	26%	1

A.7 Schematic of a potential drainage apparatus that measures the water drained as a CNF fiber pad is forming

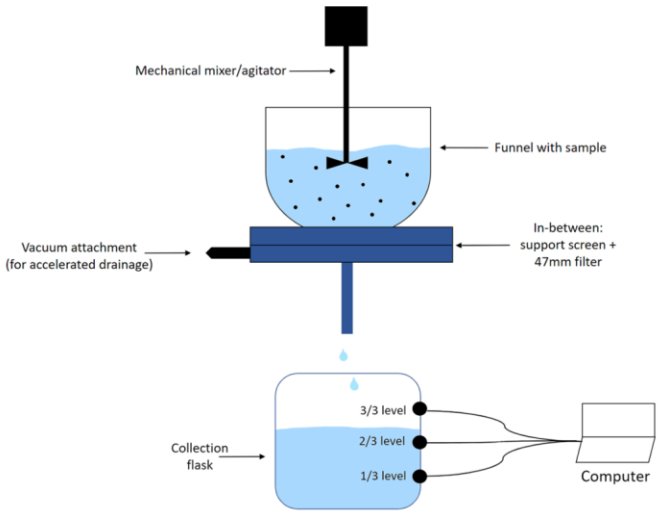

Figure A. 5. Schematic of a potential alternative automated drainage apparatus setup.

REFERENCES

1. Ian Tiseo. Statista; 2021. https://www.statista.com/topics/5268/us-pulp-and-paper-industry/#topicHeader__wrapper

2. M. Shahbandeh. Total consumption of paper and board in the United States from 2006 to 2019 (in 1,000 tons)*. Published online June 15, 2022. https://www.statista.com/statistics/252710/total-us-consumption-of-paper-and-board-since-2001/

3. Brun V, Hansen F, Turpin D, Bennett K. *Drier Web before Dryer Section*. Agenda 2020 Technology Alliance; 2016.

4. Laurijssen J, Faaij A, Worrell E. Benchmarking energy use in the paper industry: a benchmarking study on process unit level. *Energy Efficiency*. 2013;6(1):49-63. doi:10.1007/s12053-012-9163-9

5. Karlsson M. DRYING OF PAPER – AN OVERVIEW, THE STATE OF PAPER DRYING KNOWLEDGE. Published online 2001:30.

6. Phipps J. Applications of FiberLean microfibrillated cellulose in and out of the paper industry. Published 2019. https://fiberlean.com/applications-of-fiberlean-microfibrillated-cellulose-paper-industry/

7. Roberts JC. *The Chemistry of Paper*. Royal Society of Chemistry; 1996. doi:https://doi.org/10.1039/9781847552068

8. Hubbe MA, Gill RA. Fillers for Papermaking: A Review of their Properties, Usage Practices, and their Mechanistic Role. *BioResources*. 2016;11(1):2886-2963. doi:10.15376/biores.11.1.2886-2963

9. Korhonen M, Laine J. Flocculation and retention of fillers with nanocelluloses. *Nordic Pulp & Paper Research Journal*. 2014;29(1):119-128. doi:10.3183/npprj-2014-29-01-p119-128

10. Hubbe MA, Metts JR, Hermosilla D, et al. Wastewater Treatment and Reclamation: A Review of Pulp and Paper Industry Practices and Opportunities. *BioRes*. 2016;11(3):7953-8091. doi:10.15376/biores.11.3.Hubbe

11. Young RA, Kundrot R, Tillman DA. Pulp and Paper. In: Meyers RA, ed. *Encyclopedia of Physical Science and Technology (Third Edition)*. Academic Press; 2003:249-265. doi:10.1016/B0-12-227410-5/00619-0

12. Moon RJ, Martini A, Nairn J, Simonsen J, Youngblood J. Cellulose nanomaterials review: structure, properties and nanocomposites. *Chem Soc Rev*. 2011;40(7):3941. doi:10.1039/c0cs00108b

13. Paajanen A, Sonavane Y, Ignasiak D, Ketoja JA, Maloney T, Paavilainen S. Atomistic molecular dynamics simulations on the interaction of TEMPO-oxidized cellulose nanofibrils in water. *Cellulose*. 2016;23(6):3449-3462. doi:10.1007/s10570-016-1076-x

14. Foster EJ, Moon RJ, Agarwal UP, et al. Current characterization methods for cellulose nanomaterials. *Chem Soc Rev*. 2018;47(8):2609-2679. doi:10.1039/C6CS00895J

15. Maloney TC. Thermoporosimetry of hard (silica) and soft (cellulosic) materials by isothermal step melting. *J Therm Anal Calorim*. 2015;121(1):7-17. doi:10.1007/s10973-015-4592-2

16. Stana-Kleinschek K, Ribitsch V. Electrokinetic properties of processed cellulose fibers. *Colloids and Surfaces A: Physicochemical and Engineering Aspects*. 1998;140(1-3):127-138. doi:10.1016/S0927-7757(97)00301-4

17. Paajanen A, Ceccherini S, Maloney T, Ketoja JA. Chirality and bound water in the hierarchical cellulose structure. *Cellulose*. 2019;26(10):5877-5892. doi:10.1007/s10570-019-02525-7

18. Hubbe MA, Wang F. WHERE TO ADD RETENTION AID: ISSUES OF TIME AND SHEAR. *TAPPI J*. Published online 2002:12.

19. Gimaker M, Wagberg L. Adsorption of polyallylamine to lignocellulosic fibres : effect of adsorption conditions on localisation of adsorbed polyelectrolyte and mechanical properties of resulting paper sheets. *Cellulose*. 2009;(16:87-101):87-101. doi:10.1007/s10570-008-9240-6

20. Ribitsch V, Abstract. Electrokinetic properties of processed cellulose fibers. *Colloids and Surfaces A: Physicochemical and Engineering Aspects*. 1998;140(1-3):127-138. doi:10.1016/S0927-7757(97)00301-4

21. Aarne N, Kontturi E, Laine J. Influence of adsorbed polyelectrolytes on pore size distribution of a water-swollen biomaterial. *Soft Matter*. 2012;8(17):4740. doi:10.1039/c2sm07268h

22. Cheng Q, Wang J, McNeel JF, Jacobson PM. Water retention value measurements of cellulosic materials using a centrifuge technique. *BioResources*. 2010;5(3):1945-1954. doi:10.15376/biores.5.3.1945-1954

23. Mayr M, Eckhart R, Winter H, Bauer W. A novel approach to determining the contribution of the fiber and fines fraction to the water retention value (WRV) of chemical and mechanical pulps. *Cellulose*. 2017;24(7):3029-3036. doi:10.1007/s10570-017-1298-6

24. Miao Y, Chen Y, Jia Q, Bai Z, Shi K. Water retention and physical properties of recycled fibers treated with NaOH/urea aqueous solution. *IOP Conf Ser: Mater Sci Eng*. 2018;392:032012. doi:10.1088/1757-899X/392/3/032012

25. Fischer W, Mayr M, Spirk S, et al. Pulp Fines—Characterization, Sheet Formation, and Comparison to Microfibrillated Cellulose. *Polymers*. 2017;9(12):366. doi:10.3390/polym9080366

26. Kang T, Paulapuro H. Characterization of Chemical Pulp Fines. *Tappi Journal*. 2006;5(2):25-28.

27. Amini E, Tajvidi M, Bousfield DW, Gardner DJ, Shaler SM. Dewatering Behavior of a Wood-Cellulose Nanofibril Particulate System. *Sci Rep*. 2019;9(1):14584. doi:10.1038/s41598-019-51177-x

28. Hubbe MA. Fines Management for Increased Paper Machine Productivity. Published online 2002:22.

29. Hubbe MA. Selecting Laboratory Tests to Predict Effectiveness of Retention and Drainage Aid Programmes. In: Paper Technology; 2003. https://repository.lib.ncsu.edu/bitstream/handle/1840.2/9/Hubbe44(8).pdf?sequence=1

30. Hubbe MA, Heitmann JA. Review of factors affecting the release of water from cellulosic fibers during paper manufacture. *BioResources*. 2007;2(3):500-533. doi:10.15376/biores.2.3.500-533

31. Botha R. *Factors Influencing the Drainage and Drying of Pulp*. University of Pretoria; 2015.

32. Chan AKT, Pelton RH, Zhu S, Baird MHI. The effects of polystyrene beads and nylon fibres on the permeability of compressed wood fibre pads. *Can J Chem Eng*. 1996;74(2):229-235. doi:10.1002/cjce.5450740208

33. Forsberg S, Ström G. The effect of contact time between cationic polymers and furnish on retention and drainage. *Journal of Pulp and Paper Science (JPPS)*. 1994;20:J71-J76.

34. Sjöstrand B, Barbier C, Ullsten H, Nilsson L. Dewatering of Softwood Kraft Pulp with Additives of Microfibrillated Cellulose and Dialcohol Cellulose. *BioResources*. 2019;14(3):6370-6383.

35. Ferreira PJ, Matos S, Figueiredo MM. Size Characterization of Fibres and Fines in Hardwood Kraft Pulps. *Part Part Syst Charact*. 1999;16(1):20-24. doi:10.1002/(SICI)1521-4117(199905)16:1<20::AID-PPSC20>3.0.CO;2-M

36. Osong SH, Norgren S, Engstrand P. Processing of wood-based microfibrillated cellulose and nanofibrillated cellulose, and applications relating to papermaking: a review. *Cellulose*. 2016;23(1):93-123. doi:10.1007/s10570-015-0798-5

37. Onyianta AJ, O'Rourke D, Sun D, Popescu CM, Dorris M. High aspect ratio cellulose nanofibrils from macroalgae Laminaria hyperborea cellulose extract via a zero-waste low energy process. *Cellulose*. 2020;27(14):7997-8010. doi:10.1007/s10570-020-03223-5

38. Brodin FW, Gregersen ØW, Syverud K. Cellulose nanofibrils: Challenges and possibilities as a paper additive or coating material- A review. *Nordic Pulp and Paper Research Journal*. 2014;29(1):156-166. doi:10.3183/NPPRJ-2014-29-01-p156-166

39. Delgado-Aguilar M, González Tovar I, Tarrés Q, Alcalá M, Pèlach MÀ, Mutjé P. Approaching a Low-Cost Production of Cellulose Nanofibers for Papermaking Applications. *BioResources*. 2015;10(3):5345-5355. doi:10.15376/biores.10.3.5345-5355

40. Djafari Petroudy SR, Chabot B, Loranger E, et al. Recent Advances in Cellulose Nanofibers Preparation through Energy-Efficient Approaches: A Review. *Energies*. 2021;14(20):6792. doi:10.3390/en14206792

41. Li T, Chen C, Brozena AH, et al. Developing fibrillated cellulose as a sustainable technological material. *Nature*. 2021;590(7844):47-56. doi:10.1038/s41586-020-03167-7

42. Reid MS, Villalobos M, Cranston ED. Benchmarking Cellulose Nanocrystals: From the Laboratory to Industrial Production. *Langmuir*. 2017;33(7):1583-1598. doi:10.1021/acs.langmuir.6b03765

43. Dufresne A. Nanocellulose: a new ageless bionanomaterial. *Materials Today*. 2013;16(6):220-227. doi:10.1016/j.mattod.2013.06.004

44. Moser C, Henriksson G, Lindström ME. Structural Aspects on the Manufacturing of Cellulose Nanofibers from Wood Pulp Fibers. Published online 2019:8.

45. Amini E, Hafez I, Tajvidi M, Bousfield DW. Cellulose and lignocellulose nanofibril suspensions and films: A comparison. *Carbohydrate Polymers*. 2020;250:117011. doi:10.1016/j.carbpol.2020.117011

46. Filson PB, Dawson-Andoh BE, Schwegler-Berry D. Enzymatic-mediated production of cellulose nanocrystals from recycled pulp. *Green Chem*. 2009;11(11):1808. doi:10.1039/b915746h

47. Kangas H, Pere J. High-consistency enzymatic fibrillation (HefCel) – a cost-efficient way to produce cellulose nanofibrils (CNF). *Advanced Materials*. Published online 2016:3.

48. Luo J, Semenikhin N, Chang H, Moon RJ, Kumar S. Post-sulfonation of cellulose nanofibrils with a one-step reaction to improve dispersibility. *Carbohydrate Polymers*. 2018;181:247-255. doi:10.1016/j.carbpol.2017.10.077

49. Banerjee M, Saraswatula S, Williams A, Brettmann B. Effect of Purification Methods on Commercially Available Cellulose Nanocrystal Properties and TEMPO Oxidation. *Processes*. 2020;8(6):698. doi:10.3390/pr8060698

50. Yang X, Jungstedt E, Reid MS, Berglund LA. Polymer Films from Cellulose Nanofibrils—Effects from Interfibrillar Interphase on Mechanical Behavior. *Macromolecules*. 2021;54(9):4443-4452. doi:10.1021/acs.macromol.1c00305

51. Chen Y, Wan J, Dong X, Ma Y. Fiber properties of eucalyptus kraft pulp with different carboxyl group contents. *Cellulose*. 2013;20(6):2839-2846. doi:10.1007/s10570-013-0055-8

52. Karlsson RMP, Larsson PT, Pettersson T, Wågberg L. Swelling of Cellulose-Based Fibrillar and Polymeric Networks Driven by Ion-Induced Osmotic Pressure. *Langmuir*. 2020;36(41):12261-12271. doi:10.1021/acs.langmuir.0c02051

53. Zambrano F, Starkey H, Wang Y, et al. Using Micro- and Nanofibrillated Cellulose as a Means to Reduce Weight of Paper Products: A Review. *BioResources*. 2020;15(2):4553-4590.

54. Guan QF, Yang HB, Han ZM, et al. Lightweight, tough, and sustainable cellulose nanofiber-derived bulk structural materials with low thermal expansion coefficient. *Science Advances*. 2020;6(18):eaaz1114. doi:10.1126/sciadv.aaz1114

55. U.S. Bureau of Labor Statistics. Data Quality and Data Comparisons in the Consumer Expenditure Surveys. Consumer Expenditure Surveys: Personal Consumption Expenditures. Published 2021. Accessed June 23, 2022. https://www.bls.gov/cex/cecomparison/pce_profile.htm

56. Barlaz MA. Forest products decomposition in municipal solid waste landfills. *Waste Management*. 2006;26(4):321-333. doi:10.1016/j.wasman.2005.11.002

57. Satam CC, Irvin CW, Coffey CJ, et al. Controlling Barrier and Mechanical Properties of Cellulose Nanocrystals by Blending with Chitin Nanofibers. *Biomacromolecules*. Published online November 20, 2019. doi:10.1021/acs.biomac.9b01268

58. Wang J, Gardner DJ, Stark NM, Bousfield DW, Tajvidi M, Cai Z. Moisture and Oxygen Barrier Properties of Cellulose Nanomaterial-Based Films. *ACS Sustainable Chem Eng*. 2018;6(1):49-70. doi:10.1021/acssuschemeng.7b03523

59. Delgado-Aguilar M, Tarrés Q, Pèlach MÀ, Mutjé P, Fullana-i-Palmer P. Are Cellulose Nanofibers a Solution for a More Circular Economy of Paper Products? *Environ Sci Technol*. 2015;49(20):12206-12213. doi:10.1021/acs.est.5b02676

60. Ang S, Ghosh D, Haritos V, Batchelor W. Recycling cellulose nanofibers from wood pulps provides drainage improvements for high strength sheets in papermaking. *Journal of Cleaner Production*. 2021;312:127731. doi:10.1016/j.jclepro.2021.127731

61. Kumar V, Pathak P, Bhardwaj NK. Waste paper: An underutilized but promising source for nanocellulose mining. *Waste Management*. 2020;102:281-303. doi:10.1016/j.wasman.2019.10.041

62. Chen YW, Lee HV. Revalorization of selected municipal solid wastes as new precursors of "green" nanocellulose via a novel one-pot isolation system: A source perspective. *International Journal of Biological Macromolecules*. 2018;107:78-92. doi:10.1016/j.ijbiomac.2017.08.143

63. Shatkin JA, H. Wegner T, Bilek EM (Ted), Cowie J. Market projections of cellulose nanomaterial-enabled products ? Part 1: Applications. *TJ*. 2014;13(5):9-16. doi:10.32964/TJ13.5.9

64. Qing Y, Sabo R, Wu Y, Zhu JY, Cai Z. Self-assembled optically transparent cellulose nanofibril films: effect of nanofibril morphology and drying procedure. *Cellulose*. 2015;22(2):1091-1102. doi:10.1007/s10570-015-0563-9

65. Guan M, An X, Liu H. Cellulose nanofiber (CNF) as a versatile filler for the preparation of bamboo pulp based tissue paper handsheets. *Cellulose*. 2019;26(4):2613-2624. doi:10.1007/s10570-018-2212-6

66. He M, Yang G, Cho BU, Lee YK, Won JM. Effects of addition method and fibrillation degree of cellulose nanofibrils on furnish drainability and paper properties. *Cellulose*. 2017;24(12):5657-5669. doi:10.1007/s10570-017-1495-3

67. Liao J, Pham KA, Breedveld V. Rheological characterization and modeling of cellulose nanocrystal and TEMPO-oxidized cellulose nanofibril suspensions. *Cellulose*. 2020;27(7):3741-3757. doi:10.1007/s10570-020-03048-2

68. Paulina Mocchiutti, Maria V. Galvan, Maria C. Inalbon, Miguel A. Zanuttini. Improvement of paper properties of recycled unbleached softwood kraft pulps by poly(allylamine hydrochloride). *BioResources*. 2011;6(1):570-583.

69. Dautzenberg H. *Polyelectrolytes: Formation, Characterization and Application*. Hanser Publishers; 1994.

70. Koetz J, Kosmella S. *Polyelectrolytes and Nanoparticles*. Springer; 2007.

71. Winkler RG, Cherstvy AG. Strong and Weak Polyelectrolyte Adsorption onto Oppositely Charged Curved Surfaces. In: Müller M, ed. *Polyelectrolyte Complexes in the Dispersed and Solid State I: Principles and Theory*. Advances in Polymer Science. Springer; 2014:1-56. doi:10.1007/12_2012_183

72. Khan N, Brettmann B. Intermolecular Interactions in Polyelectrolyte and Surfactant Complexes in Solution. *Polymers*. 2018;11(1):51. doi:10.3390/polym11010051

73. López-Pérez PM, da Silva RMP, Pashkuleva I, Parra F, Reis RL, San Roman J. Hydrophobic−Electrostatic Balance Driving the LCST Offset Aggregation−Redissolution Behavior of *N* -Alkylacrylamide-Based Ionic Terpolymers. *Langmuir*. 2010;26(8):5934-5941. doi:10.1021/la903904t

74. Sugai S, Ebert G. Conformations of hydrophobic polyelectrolytes. *Advances in Colloid and Interface Science*. 1985;24(C):247-282. doi:10.1016/0001-8686(85)80034-8

75. Southall NT, Dill KA, Haymet ADJ. A View of the Hydrophobic Effect. *J Phys Chem B*. 2002;106(3):521-533. doi:10.1021/jp015514e

76. Harris FE, Rice SA. A chain model for polyelectrolytes. I. *Journal of Physical Chemistry*. 1954;58(9):725-732. doi:10.1021/j150519a010

77. Nagarajan R. Thermodynamics association of nonionic polymer-micelle. *Colloids and Surfaces*. 1985;13:1-17. doi:10.1016/0166-6622(85)80002-0

78. Dill KA, Bromberg S. *Molecular Driving Forces*. 2nd ed. CRC Press; 2011.

79. Norwood DP, Minatti E, Reed WF. Surfactant/polymer assemblies. 1. Surfactant binding properties. *Macromolecules*. 1998;31(9):2957-2965. doi:10.1021/ma971318n

80. Dautzenberg H. Polyelectrolyte complex formation in highly aggregating systems. 1. Effect of salt: polyelectrolyte complex formation in the presence of NaCl. *Macromolecules*. 1997;9297(97):7810-7815. doi:10.1021/ma970803f

81. Wang H, Fan Y, Wang Y. Thermodynamic Association Behaviors of Sodium Dodecyl Sulfate (SDS) with Poly(4-vinylpyridine N-oxide) (PVPNO) at Different pH Values and Ionic Strengths. *Journal of Surfactants and Detergents*. 2017;20(3):647-657. doi:10.1007/s11743-017-1939-7

82. Aoki K, Hort J, Sakurai K. Interaction between surface active agents and proteins III. Precipitation Curve of the System Sodium Dodecyl Sulfate-Egg Albumin at Various pH ' s and the determination of the concentration of protein by the titration using surfactant. *Bulletin of the Chemical Society of Japan*. 1956;29(7):758-761. doi:10.1246/bcsj.29.758

83. Bahadur P, Dubin PL, Rao YK. Complex Formation between Sodium Dodecyl Sulfate and Poly(4-vinylpyridine N-oxide). *Langmuir*. 1995;11(26):1951-1955.

84. Anghel DF, Saito S, Iovescu A, Băran A, Stîngă G. Counterion effect of cationic surfactants upon the interaction with poly(methacrylic acid). *Journal of Surfactants and Detergents*. 2011;14(1):91-101. doi:10.1007/s11743-010-1202-y

85. Dos Santos S, Gustavsson C, Gudmundsson C, Linse P, Piculell L. When do water-insoluble polyion-surfactant ion complex salts "redissolve" by added excess surfactant? *Langmuir*. 2011;27(2):592-603. doi:10.1021/la104256g

86. Bain CD, Claesson PM, Langevin D, et al. Complexes of surfactants with oppositely charged polymers at surfaces and in bulk. *Advances in Colloid and Interface Science*. 2010;155(1-2):32-49. doi:10.1016/j.cis.2010.01.007

87. Goddard ED, Hannan RB. Cationic polymer/anionic surfactant interactions. *Journal of Colloid And Interface Science*. 1976;55(1):73-79. doi:10.1016/0021-9797(76)90010-2

88. Guzmán E, Llamas S, Maestro A, et al. Polymer-surfactant systems in bulk and at fluid interfaces. *Advances in Colloid and Interface Science*. 2016;233:38-64. doi:10.1016/j.cis.2015.11.001

89. Anthony O, Zana R. Fluorescence Investigation of the Binding of Pyrene to Hydrophobic Microdomains in Aqueous Solutions of Polysoaps. *Macromolecules*. 1994;27(14):3885-3891. doi:10.1021/ma00092a031

90. Koetz J, Kosmella S. *Polyelectrolytes and Nanoparticles*. Springer Laboratory; 2007.

91. Tsuchida E, Abe K. Interactions Between Macromolecules in Solution and Intermacromolecular Complexes. In: *Advances in Polymer Science*. Vol 45. Springer Berlin Heidelberg; 1982. doi:doi.org/10.1007/BFb0017549

92. Chu D ying, Thomas JK. Effect of Cationic Surfactants. *Journal of the American Chemical Society*. 1986;108(20):6270-6276. doi:10.1021/ja00280a026

93. Kogej K, Evmenenko G, Theunissen E, Berghmans H, Reynaers H. Investigation of Structures in Polyelectrolyte / Surfactant Complexes by X-ray Scattering. *Langmuir*. 2001;17(2):3175-3184. doi:10.1021/la001249x

94. Tseng HW, Chen PC, Tsui HW, Wang CH, Hu TY, Chen LJ. Effect of molecular weight of poly(acrylic acid) on the interaction of oppositely charged ionic surfactant–polyelectrolyte mixtures. *Journal of the Taiwan Institute of Chemical Engineers*. 2018;0:1-8. doi:10.1016/j.jtice.2018.02.030

95. Wang H, Wang Y, Yan H, Zhang J, Thomas RK. Binding of sodium dodecyl sulfate with linear and branched polyethyleneimines in aqueous solution at different pH values. *Langmuir*. 2006;22(4):1526-1533. doi:10.1021/la051988j

96. Lindman B, Antunes F, Aidarova S, Miguel M, Nylander T. Polyelectrolyte-surfactant association—from fundamentals to applications. *Colloid Journal*. 2014;76(5):585-594. doi:10.1134/S1061933X14050111

97. Goddard ED. Polymer/surfactant interaction: Interfacial aspects. *Journal of Colloid and Interface Science*. 2002;256(1):228-235. doi:10.1006/jcis.2001.8066

98. Wallin T, Linse P. Monte Carlo simulations of polyelectrolytes at charged micelles. 2. Effects of linear charge density. *The Journal of Physical Chemistry*. 1996;100(45):17873-17880. doi:10.1021/jp961041d

99. Baldwin RL. The new view of hydrophobic free energy. *FEBS Letters*. 2013;587(8):1062-1066. doi:10.1016/j.febslet.2013.01.006

100. Baldwin RL, Rose GD. How the hydrophobic factor drives protein folding. *Proceedings of the National Academy of Sciences*. 2016;113(44):12462-12466. doi:10.1073/pnas.1610541113

101. Ben-Naim A. The rise and fall of the hydrophobic effect in protein folding and protein-protein association, and molecular recognition. *Open Journal of Biophysics*. 2011;01(01):1-7. doi:10.4236/ojbiphy.2011.11001

102. Ben-Naim A. *Hydrophobic Interactions*. Plenum Press; 1980.

103. Kogej K. Thermodynamic analysis of the conformational transition in aqueous solutions of isotactic and atactic poly(methacrylic acid) and the hydrophobic effect. *Polymers*. 2016;8(5). doi:10.3390/polym8050168

104. Sugai S, Ebert G. Conformations of hydrophobic polyelectrolytes. *Advances in Colloid and Interface Science*. 1985;24(C):247-282. doi:10.1016/0001-8686(85)80034-8

105. Baldwin RL. Temperature dependence of the hydrophobic interaction in protein folding. *Proc Natl Acad Sci USA*. 1986;83(21):8069-8072. doi:10.1073/pnas.83.21.8069

106. Huang DM, Chandler D. The Hydrophobic Effect and the Influence of Solute−Solvent Attractions. *J Phys Chem B*. 2002;106(8):2047-2053. doi:10.1021/jp013289v

107. Nilsson S, Blokhus AM, Hellebust S, Glomm WR. Influence of Hydrophobic Cosolutes on the Associative/Segregative Phase Separation of Aqueous Cationic Surfactant−Polymer Systems. *Langmuir*. 2002;18(17):6504-6506. doi:10.1021/la025636d

108. Magny B, Iliopoulos I, Zana R, Audebert R. Mixed Micelles Formed by Cationic Surfactants and Anionic Hydrophobically Modified Polyelectrolytes. :8.

109. Liu ZH, Lv WJ, Zhao SL, et al. Effects of the hydrophilicity or hydrophobicity of the neutral block on the structural formation of a block polyelectrolyte/surfactant complex: A molecular dynamics simulation study. *Computational Condensed Matter*. 2015;2:16-24. doi:10.1016/j.cocom.2015.01.002

110. Jackson NE, Brettmann BK, Vishwanath V, Tirrell M, Pablo JJ De. Comparing Solvophobic and Multivalent Induced Collapse in Polyelectrolyte Brushes. *ACS Macro Letters*. 2017;6:155-160. doi:10.1021/acsmacrolett.6b00837

111. Lee N, Thirumalai D. Dynamics of Collapse of Flexible Polyelectrolytes in Poor Solvents. *Macromolecules*. 2001;34(10):3446-3457. doi:10.1021/ma001604q

112. Sadman K, Wang Q, Chen Y, Keshavarz B, Jiang Z, Shull KR. Influence of Hydrophobicity on Polyelectrolyte Complexation. *Macromolecules*. 2017;50(23):9417-9426. doi:10.1021/acs.macromol.7b02031

113. Ou Z, Muthukumar M. Entropy and enthalpy of polyelectrolyte complexation: Langevin dynamics simulations. *Journal of Chemical Physics*. 2006;124(15). doi:10.1063/1.2178803

114. Priftis D, Laugel N, Tirrell M. Thermodynamic characterization of polypeptide complex coacervation. *Langmuir*. 2012;28(45):15947-15957. doi:10.1021/la302729r

115. Comert F, Dubin PL. Liquid-liquid and liquid-solid phase separation in protein-polyelectrolyte systems. *Advances in Colloid and Interface Science*. 2017;239:213-217. doi:10.1016/j.cis.2016.08.005

116. Perry SL, Li Y, Priftis D, Leon L, Tirrell M. The effect of salt on the complex coacervation of vinyl polyelectrolytes. *Polymers*. 2014;6(6):1756-1772. doi:10.3390/polym6061756

117. Priftis D, Xia X, Margossian KO, et al. Ternary, tunable polyelectrolyte complex fluids driven by complex coacervation. *Macromolecules*. 2014;47(9):3076-3085. doi:10.1021/ma500245j

118. Anema SG, de Kruif CGK. Complex coacervates of lactotransferrin and β-lactoglobulin. *Journal of Colloid and Interface Science*. 2014;430:214-220. doi:10.1016/j.jcis.2014.05.036

119. Ali S, Prabhu VM. Relaxation Behavior by Time-Salt and Time-Temperature Superpositions of Polyelectrolyte Complexes from Coacervate to Precipitate †. *MDPI*. 2018;4(11). doi:10.3390/gels4010011

120. Chollakup R, Beck JB, Dirnberger K, Tirrell M, Eisenbach CD. Polyelectrolyte molecular weight and salt effects on the phase behavior and coacervation of aqueous solutions of poly(acrylic acid) sodium salt and poly(allylamine) hydrochloride. *Macromolecules*. 2013;46(6):2376-2390. doi:10.1021/ma202172q

121. Gärdlund L, Norgen M, Wagberg L, Marklund A. The use of polyelectrolyte complexes (PEC) as strength additives for different pulps used for production of fine paper. *Nordic Pulp and Paper Research Journal*. 2007;22(02):210-216. doi:10.3183/npprj-2007-22-02-p210-216

122. Chollakup R, Smitthipong W, Eisenbach CD, Tirrell M. Phase behavior and coacervation of aqueous poly(acrylic acid)-poly(allylamine) solutions. *Macromolecules*. 2010;43(5):2518-2528. doi:10.1021/ma902144k

123. Priftis D, Tirrell M. Phase behaviour and complex coacervation of aqueous polypeptide solutions. *Soft Matter*. 2012;8(36):9396-9405. doi:10.1039/c2sm25604e

124. Qin J, Priftis D, Farina R, et al. Interfacial tension of polyelectrolyte complex coacervate phases. *ACS Macro Letters*. 2014;3(6):565-568. doi:10.1021/mz500190w

125. Kizilay E, Kayitmazer AB, Dubin PL. Complexation and coacervation of polyelectrolytes with oppositely charged colloids. *Advances in Colloid and Interface Science*. 2011;167(1-2):24-37. doi:10.1016/j.cis.2011.06.006

126. Sing CE. Development of the modern theory of polymeric complex coacervation. *Advances in Colloid and Interface Science*. 2017;239:2-16. doi:10.1016/j.cis.2016.04.004

127. Spruijt E, Westphal AH, Borst JW, Cohen Stuart MA, Van Der Gucht J. Binodal compositions of polyelectrolyte complexes. *Macromolecules*. 2010;43(15):6476-6484. doi:10.1021/ma101031t

128. Fu J, Fares HM, Schlenoff JB. Ion-Pairing Strength in Polyelectrolyte Complexes. Published online 2017. doi:10.1021/acs.macromol.6b02445

129. Zhang Y, Yildirim E, Antila HS, Valenzuela LD, Sammalkorpi M, Lutkenhaus JL. The influence of ionic strength and mixing ratio on the colloidal stability of PDAC/PSS polyelectrolyte complexes. *Soft Matter*. 2015;11(37):7392-7401. doi:10.1039/c5sm01184a

130. Meng S, Ting J, Wu H, Tirrell M. *Solid-to-Liquid Phase Transition in Polyelectrolyte Complexes*. Chemistry; 2020. doi:10.26434/chemrxiv.12121086.v1

131. Liu X, Haddou M, Grillo I, Mana Z, Chapel JP, Schatz C. Early stage kinetics of polyelectrolyte complex coacervation monitored through stopped-flow light scattering. *Soft Matter*. 2016;12(44):9030-9038. doi:10.1039/C6SM01979J

132. Jha P, Desai P, Li J, Larson R. pH and Salt Effects on the Associative Phase Separation of Oppositely Charged Polyelectrolytes. *Polymers*. 2014;6(5):1414-1436. doi:10.3390/polym6051414

133. Huang J, Morin FJ, Laaser JE. Charge-Density-Dominated Phase Behavior and Viscoelasticity of Polyelectrolyte Complex Coacervates. *Macromolecules*. 2019;52(13):4957-4967. doi:10.1021/acs.macromol.9b00036

134. Curtis KA, Miller D, Millard P, Basu S, Horkay F, Chandran PL. Unusual Salt and pH Induced Changes in Polyethylenimine Solutions. De A, ed. *PLoS ONE*. 2016;11(9):e0158147. doi:10.1371/journal.pone.0158147

135. Chen Y, Yang M, Shaheen SA, Schlenoff JB. Influence of Nonstoichiometry on the Viscoelastic Properties of a Polyelectrolyte Complex. *Macromolecules*. 2021;54(17):7890-7899. doi:10.1021/acs.macromol.1c01154

136. Khan N, Zaragoza NZ, Travis CE, Goswami M, Brettmann BK. Polyelectrolyte Complex Coacervate Assembly with Cellulose Nanofibers. *ACS Omega*. 2020;5(28):17129-17140. doi:10.1021/acsomega.0c00977

137. Ghasemi M, Friedowitz S, Larson RG. Overcharging of polyelectrolyte complexes: an entropic phenomenon. *Soft Matter*. 2020;16(47):10640-10656. doi:10.1039/D0SM01466D

138. Perry S, Li Y, Priftis D, Leon L, Tirrell M. The Effect of Salt on the Complex Coacervation of Vinyl Polyelectrolytes. *Polymers*. 2014;6(6):1756-1772. doi:10.3390/polym6061756

139. Böhme U, Scheler U. Hydrodynamic Size and Charge of Polyelectrolyte Complexes. *J Phys Chem B*. 2007;111(29):8348-8350. doi:10.1021/jp070611e

140. Petzold G, Schwarz S. Polyelectrolyte Complexes in Flocculation Applications. *Adv Polym Sci*. 2014;256(1):25-66. doi:10.1007/12_2012_205

141. Müller M. *Polyelectrolyte Complexes in the Dispersed and Solid State II Application Aspects*. Springer Berlin Heidelberg; 2013.

142. Müller M. *Polyelectrolyte Complexes in the Dispersed and Solid State I: Principles and Theory*. (Muller M, ed.). Springer Berlin Heidelberg; 2013.

143. Nasser MS, Twaiq FA, Onaizi SA. Effect of polyelectrolytes on the degree of flocculation of papermaking suspensions. *Separation and Purification Technology*. 2013;103:43-52. doi:10.1016/j.seppur.2012.10.024

144. Koethe JL, Scott WE. Polyelectrolyte interactions with papermaking fibers : the mechanism of surface-charge decay. *Tappi Journal*. 1993;76(12):123-133.

145. Petzold G, Nebel A, Buchhammer HM, Lunkwitz K. Preparation and characterization of different polyelectrolyte complexes and their application as flocculants. *Colloid and Polymer Science*. 1998;276(2):125-130. doi:10.1007/s003960050219

146. Rojas OJ, Hubbe MA. The Dispersion Science of Papermaking. *Journal of Dispersion Science and Technology*. 2005;25(6):713-732. doi:10.1081/DIS-200035485

147. Hubbe M, Nanko H, McNeal M. Retention aid polymer interactions with cellulosic surfaces and suspensions: A review. *BioRes*. 2009;4(2):850-906. doi:10.15376/biores.4.2.850-906

148. Hubbe MA, Nanko H, McNeal MR. Retention aid polymer interactions with cellulosic surfaces and suspensions: A review. *BioResources*. 2009;4(2):850-906. doi:10.15376/biores.4.2.850-906

149. Hubbe MA, Wang F. Where to add retention aid: Issues of time and shear. *Tappi Journal*. 2002;8005(1):23-33.

150. Zagala AP. (75) Inventors: Michael R. St. John, Chicago, IL (US); :8.

151. Smith D. United States Patent 5338406. Published online 1994:1-6.

152. Blockx J, Verfaillie A, Eyley S, et al. Cationic Cellulose Nanocrystals for Flocculation of Microalgae: Effect of Degree of Substitution and Crystallinity. *ACS Appl Nano Mater*. 2019;2(6):3394-3403. doi:10.1021/acsanm.9b00315

153. Gao Y, Li Q, Shi Y, Cha R. Preparation and Application of Cationic Modified Cellulose Fibrils as a Papermaking Additive. *International Journal of Polymer Science*. 2016;2016:1-8. doi:10.1155/2016/6978434

154. Watts S, Maniura-Weber K, Siqueira G, Salentinig S. Virus pH-Dependent Interactions with Cationically Modified Cellulose and Their Application in Water Filtration. *Small*. 2021;17(30):2100307. doi:10.1002/smll.202100307

155. Shet RT, Yabani AM. Polyelectrolyte behavior of chemically modified cotton cellulose. *Journal of Applied Polymer Science*. 1982;27(2):631-636. doi:10.1002/app.1982.070270225

156. Hubbe MA, Moore SM, Lee SY. Effects of charge ratios and cationic polymer nature on polyelectrolyte complex deposition onto cellulose. *Industrial and Engineering Chemistry Research*. 2005;44(9):3068-3074. doi:10.1021/ie048902m

157. Hubbe MA. Dry-strength development by polyelectrolyte complex deposition onto non-bonding glass fibres. *Journal of Pulp and Paper Science*. 2005;31(4):159-166.

158. Gärdlund L, Wågberg L, Gernandt R. Polyelectrolyte complexes for surface modification of wood fibres. *Colloids and Surfaces A: Physicochemical and Engineering Aspects*. 2003;218(1-3):137-149. doi:10.1016/s0927-7757(02)00588-5

159. Ankerfors C, Lingstrom R, Wågberg L, Ödberg L. A comparison of polyelectrolyte complexes and multilayers: Their adsorption behaviour and use for enhancing tensile strength of paper. *Nordic Pulp and Paper Research Journal*. 2009;24(1):77-86. doi:https://doi.org/10.3183/npprj-2009-24-01-p077-086

160. Gärdlund L, Forsström J, Andreasson B, Wågberg L. Influence of polyelectrolyte complexes on the strength properties of papers from unbleached kraft pulps with different yields. *Nordic Pulp and Paper Research Journal*. 2005;20(1):36-42. doi:10.3183/npprj-2005-20-01-p036-042

161. Feng X, Pouw K, Leung V, Pelton R. Adhesion of colloidal polyelectrolyte complexes to wet cellulose. *Biomacromolecules*. 2007;8(7):2161-2166. doi:10.1021/bm070307r

162. Hubbe MA. Bonding between cellulosic fibers in the absence and presence of dry-strength agents - A review. *BioResources*. 2006;1(2):281-318.

163. Illergård J, Römling U, Wågberg L, Ek M. Biointeractive antibacterial fibres using polyelectrolyte multilayer modification. *Cellulose*. 2012;19(5):1731-1741. doi:10.1007/s10570-012-9742-0

164. Jantas R, Połowiński S. Modifying polyester fabric surface with polyelectrolyte nanolayers using the layer-by-layer deposition technique. *Fibres and Textiles in Eastern Europe*. 2007;15:97-99.

165. Bhardwaj NK, Kumar S, Bajpai PK. Effect of zeta potential on retention and drainage of secondary fibres. 2005;260(March):245-250. doi:10.1016/j.colsurfa.2005.03.011

166. Szilagyi I, Trefalt G, Tiraferri A, Maroni P, Borkovec M. Polyelectrolyte adsorption, interparticle forces, and colloidal aggregation. *Soft Matter*. 2014;10(15):2479. doi:10.1039/c3sm52132j

167. Chodanowski P, Stoll S. Polyelectrolyte Adsorption on Charged Particles in the Debye−Hückel Approximation. A Monte Carlo Approach. *Macromolecules*. 2001;34(7):2320-2328. doi:10.1021/ma000482z

168. Decher G, Hong JD, Schmitt J. Buildup of ultrathin multilayer films by a self-assembly process: III. Consecutively alternating adsorption of anionic and cationic polyelectrolytes on charged surfaces. *Thin Solid Films*. 1992;210-211:831-835. doi:10.1016/0040-6090(92)90417-A

169. Gucht J van der, Spruijt E, Lemmers M, Cohen Stuart MA. Polyelectrolyte complexes: Bulk phases and colloidal systems. *Journal of Colloid and Interface Science*. 2011;361(2):407-422. doi:10.1016/j.jcis.2011.05.080

170. Saarinen T, Österberg M, Laine J. Adsorption of polyelectrolyte multilayers and complexes on silica and cellulose surfaces studied by QCM-D. *Colloids and Surfaces A: Physicochemical and Engineering Aspects*. 2008;330(2-3):134-142. doi:10.1016/j.colsurfa.2008.07.039

171. Hubbe M, Jackson T, Zhang M. Fiber Surface Saturation as a Strategy to Optimize Dual-Polymer Dry Strength Treatment. *Tappi Journal*. 2003;2.

172. Reihs T, Müller M, Lunkwitz K. Deposition of polylelectrolyte complex nano-particles at silica surfaces characterized by ATR-FTIR and SEM. *Colloids and Surfaces A: Physicochemical and Engineering Aspects*. 2003;212(1):79-95. doi:10.1016/S0927-7757(02)00293-5

173. Ankerfors C, Wågberg L. Polyelectrolyte Complexes for Tailoring of Wood Fibre Surfaces. In: Müller M, ed. *Polyelectrolyte Complexes in the Dispersed and Solid State II: Application Aspects*. Advances in Polymer Science. Springer; 2014:1-24. doi:10.1007/12_2012_206

174. Buchhammer HM, Kramer G, Lunkwitz K. Interaction of colloidal dispersions of non-stoichiometric polyelectrolyte complexes and silica particles. *Colloids and Surfaces A: Physicochemical and Engineering Aspects*. 1995;95(2-3):299-304. doi:10.1016/0927-7757(94)03036-Y

175. Buchhammer HM, Petzold G, Lunkwitz K. Salt Effect on Formation and Properties of Interpolyelectrolyte Complexes and Their Interactions with Silica Particles. *Langmuir*. 1999;15(12):4306-4310. doi:10.1021/la980992a

176. Hubbe MA. Selecting laboratory tests to predict effectiveness of retention and drainage aid programmes. *Paper Technology*. 2003;44(8):20-24.

177. Gu F, Wang W, Cai Z, Xue F, Jin Y, Zhu JY. Water retention value for characterizing fibrillation degree of cellulosic fibers at micro and nanometer scales. *Cellulose*. 2018;25(5):2861-2871. doi:10.1007/s10570-018-1765-8

178. Weise U, Maloney T, Paulapuro H. Quantification of water in different states of interaction with wood pulp fibres. *Cellulose*. 1996;3(1):189-202. doi:10.1007/BF02228801

179. Olejnik K, Skalski B, Stanislawska A, Wysocka-Robak A. Swelling properties and generation of cellulose fines originating from bleached kraft pulp refined under different operating conditions. *Cellulose*. 2017;24(9):3955-3967. doi:10.1007/s10570-017-1404-9

180. Carlsson G, Kolseth P, Lindstrom T. Polyelectrolyte swelling behavior of chlorite delignified spruce wood fibers. *Wood Sci Technol*. 1983;17(1):69-73. doi:10.1007/BF00351833

181. Strom G, Kunnas A. The effect of cationic polymers on the water retention value of various pulps. *Nordic Pulp & Paper Research Journal*. 1991;6(1):12-19. doi:10.3183/npprj-1991-06-01-p012-019

182. Hubbe M, Rojas O, Sulic N, Sezaki T. Unique Behaviour of Polyampholytes as Drystrength Additives. *Appita Journal*. 2007;60. Accessed February 6, 2022. https://www.semanticscholar.org/paper/Unique-Behaviour-of-Polyampholytes-as-Drystrength-Hubbe-Rojas/fa463cd1dcdb1bf6bb0352d1faddc33546c54b6f

183. Tomer G, Patel H, Podczeck F, Newton JM. Measuring the water retention capacities (MRC) of different microcrystalline cellulose grades. *European Journal of Pharmaceutical Sciences*. 2001;12(3):321-325. doi:10.1016/S0928-0987(00)00188-3

184. Moore EE. Charge relationships of dual polymer retention aids. *TAPPI J*. 1976;59(6).

185. The University of Maine Process Development Center- Cellulose Nanofibril Safety Data Sheet. Published online 2017:1-12.

186. Foster EJ, Moon RJ, Agarwal UP, et al. Current characterization methods for cellulose nanomaterials. *Chemical Society Reviews*. 2018;47(8):2609-2679. doi:10.1039/c6cs00895j

187. Saito T, Kimura S, Nishiyama Y, Isogai A. Cellulose nanofibers prepared by TEMPO-mediated oxidation of native cellulose. *Biomacromolecules*. 2007;8(8):2485-2491. doi:10.1021/bm0703970

188. Tardy BL, Yokota S, Ago M, et al. Nanocellulose–surfactant interactions. *Current Opinion in Colloid and Interface Science*. 2017;29:57-67. doi:10.1016/j.cocis.2017.02.004

189. Österbeg M, Claesson PM. Interactions between cellulose surfaces: effect of solution pH. *Journal of Adhesion Science and Technology*. 2002;14(5):603-618. doi:10.1163/156856100742771

190. Mazhari Mousavi SM, Afra E, Tajvidi M, Bousfield DW, Dehghani-Firouzabadi M. Application of cellulose nanofibril (CNF) as coating on paperboard at moderate solids content and high coating speed using blade coater. *Progress in Organic Coatings*. 2018;122:207-218. doi:10.1016/j.porgcoat.2018.05.024

191. Chauve G, Heux L, Arouini R, Mazeau K. Cellulose poly(ethylene-co-vinyl acetate) nanocomposites studied by molecular modelling and mechanical spectroscopy. *Biomacromolecules*. 2005;6(4):2025-2031. doi:10.1021/bm0501205

192. Lombardo S, Chen P, Larsson PA, Thielemans W, Wohlert J, Svagan AJ. Toward Improved Understanding of the Interactions between Poorly Soluble Drugs and Cellulose Nanofibers. *Langmuir*. 2018;34(19):5464-5473. doi:10.1021/acs.langmuir.8b00531

193. Paajanen A, Sonavane Y, Ignasiak D, Ketoja JA, Maloney T, Paavilainen S. Atomistic molecular dynamics simulations on the interaction of TEMPO-oxidized cellulose nanofibrils in water. *Cellulose*. 2016;23(6):3449-3462. doi:10.1007/s10570-016-1076-x

194. Zhao Z, Crespi VH, Kubicki JD, Cosgrove DJ, Zhong L. Molecular dynamics simulation study of xyloglucan adsorption on cellulose surfaces: Effects of surface hydrophobicity and side-chain variation. *Cellulose*. 2014;21(2):1025-1039. doi:10.1007/s10570-013-0041-1

195. Junka K, Filpponen I, Lindström T, Laine J. Titrimetric methods for the determination of surface and total charge of functionalized nanofibrillated/microfibrillated cellulose (NFC/MFC). *Cellulose*. 2013;20(6):2887-2895. doi:10.1007/s10570-013-0043-z

196. Petzold G, Schwarz S. Polyelectrolyte Complexes in Flocculation Applications. In: Müller M, ed. *Polyelectrolyte Complexes in the Dispersed and Solid State II*. Vol 256. Advances in Polymer Science. Springer Berlin Heidelberg; 2013:25-65. doi:10.1007/12_2012_205

197. Katja H, Mika S. Flocculation in paper and pulp mill sludge process Flocculation in Paper and Pulp Mill Sludge Process. 2015;11(SEPTEMBER 2007):96-103.

198. Haper BJ, Clendaniel Alicea, Sinche Federico, et al. Impacts of chemical modification on the toxicity of diverse nanocellulose materials to developing zebrafish. *Cellulose*. 2015;20(2):163-178. doi:10.1007/s10570-016-0947-5

199. *Water Retention Value*. Vol SCAN-C 62:; 2000.

200. Plimpton S. Fast parallel algorithms for short-range molecular dynamics. *Journal of Computational Physics*. 1995;117(1):1-19. doi:10.1006/jcph.1995.1039

201. Kremer K, Grest GS. Dynamics of entangled linear polymer melts: A molecular-dynamics simulation. *The Journal of Chemical Physics*. 1990;92(8):5057-5086. doi:10.1063/1.458541

202. Goswami M, Borreguero JM, Pincus PA, Sumpter BG. Surfactant-Mediated Polyelectrolyte Self-Assembly in a Polyelectrolyte-Surfactant Complex. *Macromolecules*. 2015;48(24):9050-9059. doi:10.1021/acs.macromol.5b02145

203. Borreguero JM, Pincus PA, Sumpter BG, Goswami M. Unraveling the Agglomeration Mechanism in Charged Block Copolymer and Surfactant

Complexes. *Macromolecules*. 2017;50(3):1193-1205. doi:10.1021/acs.macromol.6b02319

204. Borreguero JM, Pincus PA, Sumpter BG, Goswami M. Dynamics of Charged Species in Ionic-Neutral Block Copolymer and Surfactant Complexes. *The Journal of Physical Chemistry B*. 2017;121(28):6958-6968. doi:10.1021/acs.jpcb.7b05047

205. Pütz M, Kremer K, Grest GS. What is the entanglement length in a polymer melt? *Europhysics Letters (EPL)*. 2000;49(6):735-741. doi:10.1209/epl/i2000-00212-8

206. Zhao M, Zacharia NS. Protein encapsulation via polyelectrolyte complex coacervation: Protection against protein denaturation. *Journal of Chemical Physics*. 2018;149(16). doi:10.1063/1.5040346

207. Gärdlund L, Wågberg L, Norgren M. New insights into the structure of polyelectrolyte complexes. *Journal of Colloid and Interface Science*. 2007;312(2):237-246. doi:10.1016/j.jcis.2007.03.075

208. Hubbe MA, Rojas OJ, Lucia LA, Jung TM. Consequences of the nanoporosity of cellulosic fibers on their streaming potential and their interactions with cationic polyelectrolytes. *Cellulose*. 2007;14:655-671. doi:10.1007/s10570-006-9098-4

209. Saitoh K ichi, Ohno H, Matsuo S. Structure and Mechanical Behavior of Cellulose Nanofiber and Micro-Fibrils by Molecular Dynamics Simulation. *SNL*. 2013;03(03):58-67. doi:10.4236/snl.2013.33011

210. Serra A, González I, Oliver-Ortega H, Tarrès Q, Delgado-Aguilar M, Mutjé P. Reducing the Amount of Catalyst in TEMPO-Oxidized Cellulose Nanofibers: Effect on Properties and Cost. *Polymers* . 2017;9(11). doi:10.3390/polym9110557

211. Carlsson G, Kolseth P, Lindström T. Polyelectrolyte swelling behavior of chlorite delignified spruce wood fibers. *Wood Science and Technology*. 1983;17(1):69-73. doi:10.1007/BF00351833

212. Miao Y, Chen Y, Jia Q, Bai Z, Shi K. Water retention and physical properties of recycled fibers treated with NaOH/urea aqueous solution. *IOP Conference Series: Materials Science and Engineering*. 2018;392(3). doi:10.1088/1757-899X/392/3/032012

213. Pelton R. Polyvinylamine: A Tool for Engineering Interfaces. *Langmuir*. 2014;30(51):15373-15382. doi:10.1021/la5017214

214. Hughes AR, Pierre TS, Thornton RJ, Wingo RD, Tarwater OR. Poly(vinylamine hydrochloride) from Acrylic Acid. *Marcomolecular Synthesis*. 2.

215. Zelinskiy SN, Danilovtseva EN, Kandasamy G, et al. Poly(vinyl amine) as a matrix for a new class of polymers. *e-Polymers*. 2018;18(4):347-357. doi:10.1515/epoly-2018-0024

216. Nihar Ranjan Hundu. *Synthesis, Characterization and Chemical Modification of a Novel Cationic Polyelectrolyte Poly(Methylene Amine)*. Johannes Gutenberg-Universität; 2007.

217. Strand A, Vähäsalo L, Ketola A, Salminen K, Retulainen E, Sundberg A. In-situ analysis of polyelectrolyte complexes by flow cytometry. *Cellulose*. 2018;25(7):3781-3795. doi:10.1007/s10570-018-1832-1

218. Xiao L, Salmi J, Laine J, Stenius P. The Effects of Polyelectrolyte Complexes on Dewatering of Cellulose Suspension. *Nordic Pulp & Paper Research Journal*. Published online 2009:31.

219. Priftis D, Xia X, Margossian KO, et al. Ternary, Tunable Polyelectrolyte Complex Fluids Driven by Complex Coacervation. *Macromolecules*. 2014;47(9):3076-3085. doi:10.1021/ma500245j

220. Erbil C, Sezai Saraç A. Description of the turbidity measurements near the phase transition temperature of poly(N-isopropyl acrylamide) copolymers: the effect of pH, concentration, hydrophilic and hydrophobic content on the turbidity. *European Polymer Journal*. 2002;38(7):1305-1310. doi:10.1016/S0014-3057(02)00010-1

221. Saitoh T, Yoshida Y, Matsudo T, et al. Concentration of Hydrophobic Organic Compounds by Polymer-Mediated Extraction. *Anal Chem*. 1999;71(20):4506-4512. doi:10.1021/ac990478p

222. Li L, Srivastava S, Meng S, Ting J, Tirrell M. *Effects of Non-Electrostatic Intermolecular Interactions on the Phase Behavior of PH-Sensitive Polyelectrolyte Complexes*. Chemistry; 2020. doi:10.26434/chemrxiv.12213509.v2

223. Gimåker M, Wågberg L. Adsorption of polyallylamine to lignocellulosic fibres: effect of adsorption conditions on localisation of adsorbed polyelectrolyte and mechanical properties of resulting paper sheets. *Cellulose*. 2009;16(1):87-101. doi:10.1007/s10570-008-9240-6

224. Wågberg L. Polyelectrolyte adsorption onto cellulose fibres – A review. *Nordic Pulp & Paper Research Journal*. 2000;15(5):586-597. doi:10.3183/npprj-2000-15-05-p586-597

225. Wågberg L, Decher G, Norgren M, Lindström T, Ankerfors M, Axnäs K. The Build-Up of Polyelectrolyte Multilayers of Microfibrillated Cellulose and Cationic Polyelectrolytes. *Langmuir*. 2008;24(3):784-795. doi:10.1021/la702481v

226. Tang M, Szoka F. The influence of polymer structure on the interactions of cationic polymers with DNA and morphology of the resulting complexes. *Gene Ther*. 1997;4(8):823-832. doi:10.1038/sj.gt.3300454

227. Cadotte M, Tellier ME, Blanco A, Fuente E, van de Ven TGM, Paris J. Flocculation, Retention and Drainage in Papermaking: A Comparative Study of Polymeric Additives. *Can J Chem Eng*. 2008;85(2):240-248. doi:10.1002/cjce.5450850213

228. Cadena EM, Garcia J, Vidal T, Torres AL. Determination of zeta potential and cationic demand in ECF and TCF bleached pulp from eucalyptus and flax. Influence of measuring conditions. *Cellulose*. 2009;16(3):491-500. doi:10.1007/s10570-009-9275-3

229. Lyytikäinen K, Saukkonen E, Kajanto I, Käyhkö J. The effect of hemicellulose extraction on fiber charge properties and retention behavior of kraft pulp fibers. *BioRes*. 2010;6(1):219-231. doi:10.15376/biores.6.1.219-231

230. T494om13 Tensile properties of paper and paperboard (using constant rate of elongation apparatus).

231. T402sp13 Standard conditioning and testing atmospheres for paper, board, pulp handsheets, and related products. :5.

232. Ahrens F, Alaimo N, Nanko H, Patterson T. *Initial Development of an Improved Water Retention Value Test and Its Application to the Investigation of Water Removal Potential*. Institute of Paper Science and Technology; :13.

233. T 425 om-16 Opacity of paper (15/d geometry, illuminant A/2°, 89% reflectance backing and paper backing).

234. Chandran S, Batra RK, Lawrence B. Is Seeing Believing? Consumer Responses to Opacity of Product Packaging. *Advances in Consumer Research*. 2009;36:970-970.

235. Wang W, Sabo RC, Mozuch MD, Kersten P, Zhu JY, Jin Y. Physical and Mechanical Properties of Cellulose Nanofibril Films from Bleached Eucalyptus Pulp by Endoglucanase Treatment and Microfluidization. *J Polym Environ*. 2015;23(4):551-558. doi:10.1007/s10924-015-0726-7

236. Tajik M, Resalati H, Hamzeh Y, Torshizi HJ, Kermanian H, Kord B. Improving the Properties of Soda Bagasse Pulp by Using Cellulose Nanofibers in the Presence of Cationic Polyacrylamide. *BioResources*. 2016;11(4):9126-9141.

237. Hobisch MA, Bossu J, Mandlez D, et al. Localization of cellulosic fines in paper via fluorescent labeling. *Cellulose*. 2019;26(11):6933-6942. doi:10.1007/s10570-019-02556-0

238. Feber D, Granskog A, Lingqvist O, Nordigården D. Sustainability in packaging: Inside the minds of US consumers. Published online 2020.

239. Sabri O, Doan HV, Malek F, Bachouche H. When is transparent packaging beneficial? *International Journal of Retail & Distribution Management*. 2020;48(8):781-801. doi:10.1108/IJRDM-03-2019-0097

240. Simmonds G, Woods AT, Spence C. 'Show me the goods': Assessing the effectiveness of transparent packaging vs. product imagery on product evaluation. *Food Quality and Preference*. 2018;63:18-27. doi:10.1016/j.foodqual.2017.07.015

241. Wolsink M. Contested environmental policy infrastructure: Socio-political acceptance of renewable energy, water, and waste facilities. *Environmental Impact Assessment Review*. 2010;30(5):302-311. doi:10.1016/j.eiar.2010.01.001

242. Clark J, Sheldon R, Raston C, Poliakoff M, Leitner W. 15 years of Green Chemistry. *Green Chem*. 2014;16(1):18-23. doi:10.1039/C3GC90047A

243. Zimmerman JB, Anastas PT, Erythropel HC, Leitner W. Designing for a green chemistry future. *Science*. 2020;367(6476):397-400. doi:10.1126/science.aay3060

244. Erythropel HC, Zimmerman JB, de Winter TM, et al. The Green ChemisTREE: 20 years after taking root with the 12 principles. *Green Chem*. 2018;20(9):1929-1961. doi:10.1039/C8GC00482J

245. Sheldon RA. The E factor 25 years on: the rise of green chemistry and sustainability. *Green Chem*. 2017;19(1):18-43. doi:10.1039/C6GC02157C

246. Meneses GD, Palacio AB. Recycling Behavior: A Multidimensional Approach. *Environment and Behavior*. 2005;37(6):837-860. doi:10.1177/0013916505276742

247. Anna Granskog, Eric Hannon, Solveigh Hieronimus, Marie Klaeyle, Angela Winkle. *How Companies Capture the Value of Sustainability: Survey Findings*. McKinsey and Company; 2021:9.

248. Karl Haller, Jim Lee, Jane Cheung. *Meet the 2020 Consumers Driving Change - Why Brands Must Deliver on Omnipresence, Agility, and Sustainability*. IBM Institute for Business Value; :20.

249. Kulkarni S, Arnaud Lefebvre. *How Can Sustainability Enhance Your Value Proposition?* Nielson

250. Portell G, Carlson C, Chafin C. *Consumer Support Still Strong as Earth Day Celebrates Its 50th Birthday*. Kearney; :11. kearney.com

251. Walker TR, McGuinty E, Charlebois S, Music J. Single-use plastic packaging in the Canadian food industry: consumer behavior and perceptions. *Humanit Soc Sci Commun*. 2021;8(1):80. doi:10.1057/s41599-021-00747-4

252. Martinho G, Pires A, Portela G, Fonseca M. Factors affecting consumers' choices concerning sustainable packaging during product purchase and recycling. *Resources, Conservation and Recycling*. 2015;103:58-68. doi:10.1016/j.resconrec.2015.07.012

253. Yamaguchi K, Takeuchi K. Consumer preferences for reduced packaging under economic instruments and recycling policy. *Waste Management*. 2016;48:540-547. doi:10.1016/j.wasman.2015.11.015

254. Steenis ND, van Herpen E, van der Lans IA, Ligthart TN, van Trijp HCM. Consumer response to packaging design: The role of packaging materials and graphics in sustainability perceptions and product evaluations. *Journal of Cleaner Production*. 2017;162:286-298. doi:10.1016/j.jclepro.2017.06.036

255. Wilson C, Dowlatabadi H. Models of Decision Making and Residential Energy Use. *Annu Rev Environ Resour*. 2007;32(1):169-203. doi:10.1146/annurev.energy.32.053006.141137

256. Phil Riebel. *U.S. Packaging Preferences 2020: A Study of Consumer Preferences, Perceptions, and Attitudes toward Packaging*. Two Sides North America, Inc.; 2020.

257. Bagozzi RP, Dabholkar PA. Consumer recycling goals and their effect on decisions to recycle: A means-end chain analysis. *Psychology & Marketing*. 1994;11(4):313-340. doi:10.1002/mar.4220110403

258. Langley J, Turner N, Yoxall A. Attributes of packaging and influences on waste: ATTRIBUTES OF PACKAGING. *Packag Technol Sci*. 2011;24(3):161-175. doi:10.1002/pts.924

259. Klaiman K, Ortega DL, Garnache C. Consumer preferences and demand for packaging material and recyclability. *Resources, Conservation and Recycling*. 2016;115:1-8. doi:10.1016/j.resconrec.2016.08.021

260. Klaiman K, Ortega DL, Garnache C. Perceived barriers to food packaging recycling: Evidence from a choice experiment of US consumers. *Food Control*. 2017;73:291-299. doi:10.1016/j.foodcont.2016.08.017

261. Wikström F, Williams H, Venkatesh G. The influence of packaging attributes on recycling and food waste behaviour – An environmental comparison of two packaging alternatives. *Journal of Cleaner Production*. 2016;137:895-902. doi:10.1016/j.jclepro.2016.07.097

262. *Advancing Sustainable Materials Management: 2018 Tables and Figures*. Environmental Protection Agency; 2020:84. https://www.epa.gov/sites/default/files/2021-01/documents/2018_tables_and_figures_dec_2020_fnl_508.pdf

263. Paper and paperboard production top countries 2020. Statista. Published 2020. Accessed June 24, 2022. https://www.statista.com/statistics/240598/production-of-paper-and-cardboard-in-selected-countries/

264. *Pulp and Paper Industry in the U.S.* Statista; 2020.

265. Elia V, Gnoni MG, Tornese F. Measuring circular economy strategies through index methods: A critical analysis. *Journal of Cleaner Production*. 2017;142:2741-2751. doi:10.1016/j.jclepro.2016.10.196

266. Van Ewijk S, Stegemann JA, Ekins P. Global Life Cycle Paper Flows, Recycling Metrics, and Material Efficiency: Global Paper Flows, Recycling, Material Efficiency. *Journal of Industrial Ecology*. 2018;22(4):686-693. doi:10.1111/jiec.12613

267. Smook GA. *Handbook for Pulp and Paper Technologists*. 4th ed.; 2015. Accessed June 24, 2022. https://www.semanticscholar.org/paper/Handbook-for-pulp-and-paper-technologists-smook-pdf-Smook/020a892c47902521909dca9837a2adc322300f29

268. Kirchherr J, Reike D, Hekkert M. Conceptualizing the circular economy: An analysis of 114 definitions. *Resources, Conservation and Recycling*. 2017;127:221-232. doi:10.1016/j.resconrec.2017.09.005

269. Wang K, Nakakubo T. Strategy for introducing sewage sludge energy utilization systems at sewage treatment plants in large cities in Japan: A comparative assessment. *Journal of Cleaner Production*. 2021;316:128282. doi:10.1016/j.jclepro.2021.128282

270. Deng R, Chang N, Green M. Peer behaviour boosts recycling. *Nat Energy*. 2021;6(9):862-863. doi:10.1038/s41560-021-00905-7

271. Walzberg J, Carpenter A, Heath GA. Role of the social factors in success of solar photovoltaic reuse and recycle programmes. *Nat Energy*. 2021;6(9):913-924. doi:10.1038/s41560-021-00888-5

272. Dhar P, M RK, Bhasney SM, Bhagabati P, Kumar A, Katiyar V. Sustainable Approach for Mechanical Recycling of Poly(lactic acid)/Cellulose Nanocrystal Films: Investigations on Structure–Property Relationship and Underlying Mechanism. *Ind Eng Chem Res*. 2018;57(43):14493-14508. doi:10.1021/acs.iecr.8b02658

273. Yue L, Ke K, Amirkhosravi M, Gray TG, Manas-Zloczower I. Catalyst-Free Mechanochemical Recycling of Biobased Epoxy with Cellulose Nanocrystals. *ACS Appl Bio Mater*. 2021;4(5):4176-4183. doi:10.1021/acsabm.0c01670

274. Zhou Y, Fuentes-Hernandez C, Khan TM, et al. Recyclable organic solar cells on cellulose nanocrystal substrates. *Sci Rep*. 2013;3(1):1536. doi:10.1038/srep01536

275. Henriksson M, Berglund LA, Isaksson P, Lindström T, Nishino T. Cellulose Nanopaper Structures of High Toughness. *Biomacromolecules*. 2008;9(6):1579-1585. doi:10.1021/bm800038n

276. *2007 Comprehensive Procurement Guidelines*. Environmental Protection Agency; 2007. www.epa.gov/osw

277. *National Source Reduction Characterization Report For Municipal Solid Waste in the United States*. Environmental Protection Agency; 1999.

278. Allen LH, Polverari MS. Dendrimeric polymers for the production of paper and board. Published online October 22, 2002. Accessed June 24, 2022. https://patents.google.com/patent/US6468396B2/en?oq=US6468396

279. Sutman F, Harrington J, Gelman R. Retention and drainage in the manufacture of paper. Published online November 13, 2012. Accessed June 24, 2022. https://patents.google.com/patent/US8308902B2/en?oq=US8308902

280. Kamleitner B, Thürridl C, Martin BAS. A Cinderella Story: How Past Identity Salience Boosts Demand for Repurposed Products. *Journal of Marketing*. 2019;83(6):76-92. doi:10.1177/0022242919872156

281. Trudel R, Argo JJ, Meng MD. The Recycled Self: Consumers' Disposal Decisions of Identity-Linked Products. *Journal of Consumer Research*. 2016;43(2):246-264. doi:10.1093/jcr/ucw014

282. Peña C, Civit B, Gallego-Schmid A, et al. Using life cycle assessment to achieve a circular economy. *Int J Life Cycle Assess*. 2021;26(2):215-220. doi:10.1007/s11367-020-01856-z

283. Tóth Szita K. THE APPLICATION OF LIFE CYCLE ASSESSMENT IN CIRCULAR ECONOMY. *HAE*. 2017;(31):5-9. doi:10.17676/HAE.2017.31.5

284. Plevin RJ, Delucchi MA, Creutzig F. Using Attributional Life Cycle Assessment to Estimate Climate-Change Mitigation Benefits Misleads Policy Makers: Attributional LCA Can Mislead Policy Makers. *Journal of Industrial Ecology*. 2014;18(1):73-83. doi:10.1111/jiec.12074

285. Linder M, Sarasini S, van Loon P. A Metric for Quantifying Product-Level Circularity. *Journal of Industrial Ecology*. 2017;21(3):545-558. doi:10.1111/jiec.12552

286. Gazibaric. A Method for Evaluating Human Observer's Perception of Color Differences. *Teh vjesn*. 2021;28(6). doi:10.17559/TV-20201027193639

287. Schanda J, International Commission on Illumination, eds. *Colorimetry: Understanding the CIE System*. CIE/Commission internationale de l'eclairage ; Wiley-Interscience; 2007.